

**Synthesis and Molecular Docking of Bioactive Natural
Products Containing (6*H*-Dibenzo[*b,d*]pyran-6-one)
Framework**

6*H*-Dibenzo[*b,d*]Pyran-6-one 骨格を有する生物活性天然物の合成と分子ド
ッキングに関する研究

A thesis submitted to
The University of Toyama

For the Degree of
Doctor of Philosophy

In the faculty of
**Advanced Nano and Bio Sciences,
Graduate School of Innovative Life Science**

Ishtiaq Jeelani

September 2021

1. Abstract

A variety of natural products, which possess the *6H*-dibenzo[*b,d*]pyran-6-one core have attracted our interest because of their unique biological activities. Among them, Hyalodendriol C was isolated from endophytic fungus associated with the hybrid 'Neva of *Populus deltoides*', *P. nigra* L along with hyalodendriol A and B. A variety of biological activities have been stated for hyalodendriol A-C, but only hyalodendriol C has shown significant antibacterial, larvicidal, and anti-fungal properties as mentioned previously in the literature. The interesting structural feature of this compound is the aromatic ring bearing chlorine atom on it. Natural products comprising a halogen on an olefinic, aromatic, heteroaromatic moieties as a substituent have gained considerable interest because of their multiple biological activities. Conversely, hyalodendriol A and B which do not possess chloro substituent, exhibited weaker activities than hyalodendriol C. Therefore, it was suspected that the presence of a chlorine atom was essential for the cytotoxicity of hyalodendriol C. In addition, urolithin is a metabolite of a class of compounds known as polyphenols which are found in various fruits, including pomegranates, nuts, and strawberries. In recent years, research on urolithins has mainly focused on the first metabolite consisting of Uro-A and Uro-B, but we are interested in the second metabolite of urolithins that can reach systemic tissues. Uro-A glucuronide (Uro-A glur) and Uro-B glucuronide (Uro-B glur) have already been chemically synthesized by Villapharma Research S. L. (Parque Tecnológico de Fuente Alamo, Murcia, Spain). On the other hand, the chemical synthesis of Urolithin C 3-glucuronide (Uro-C 3-glur) has not been achieved, and the bioavailability of Uro-A glur and Uro-B glur is shown to be higher than that of Uro-C 3-glur. Therefore, we decided to synthesize Urolithin C 3-glucuronide, which needs to pursue beneficial health benefits.

Urolithin is a biologically active compound that has anti-inflammatory, antioxidant, and anticancer properties. Urolithins, which are hydroxylated dibenzo[*b,d*]pyran-6-one derivatives, contain urolithin A (uro-A), urolithin B (uro-B), urolithin C (uro-C) and urolithin D (uro-D) derivatives which are produced *in vivo* by the gastrointestinal microbiota of humans and different animals upon intaking ellagitannins (ETs), which are high molecular weight polyphenols and ellagic acids (EAs). There are many different phenolic antioxidants such as ETs and EAs in walnuts and pomegranates, which have been linked to potential preventive effects against chronic diseases like diabetes, cancer, cardiovascular diseases, and neurodegenerative diseases.

A palladium-mediated intramolecular aryl-aryl coupling reaction was applied to the total synthesis of the bioactive natural products, Hyalodendriol C, and Urolithin C 3-Glucuronide. Keeping in view, the indispensable biological values of these compounds, we took the advantage of our established strategy to chemically synthesize hyalodendriol C and Urolithin C 3-Glucuronide. The total synthesis of hyalodendriol C got accomplished in 10 steps beginning with the preparation of phenol derivative from the commercially available 5-methylbenzene-1,3-diol and synthesis of the corresponding benzoic acid derivative. On the other hand, the total synthesis of Urolithin C 3-Glucuronide has been accomplished in 11 steps starting from commercially available 3,4-dimethoxybenzaldehyde. Our group has reported several natural product syntheses using the Pd-mediated intramolecular biaryl coupling reaction with phenyl benzoate derivatives for forming the 6*H*-dibenzo[*b,d*]pyran-6-one ring system. Utilizing this transformation, we achieved the efficient total syntheses of hyalodendriol C and urolithin C 3-glucuronide. Molecular docking of the synthesized compounds was also performed against **CYP1B1** and **BCL2** protein.

Synthesis and Molecular Docking of Bioactive Natural Products Containing (6*H*-Dibenzo[*b,d*]pyran-6-one) Framework

Contents

1.	General Introduction	1
1.1	Dibenzo- α -Pyrone	2
1.2.	Occurrence.	3
1.2.1	Dibenzo- α -pyrones from Fungi.	3
1.2.2.	Dibenzo- α -pyrones from Plants.	4
1.2.3	Transformation of intestinal bacteria produces dibenzo-pyrone.	5
1.2.4	Biological activities and functions.	6
2.	Synthesis and characterization of hyalodendriol C	8
2.1	Introduction.	8
2.2	synthesis of phenol derivative.	10
2.3	Synthesis of benzoic acid derivative.	11
2.4	Pd catalyzed intramolecular biaryl coupling reaction.	13
2.5	Significance of Pd catalyzed coupling reaction.	14
2.6	Experimental Section.	17
3	Synthesis and characterization of urolithin C 3 Glucuronide.	27
3.1	Introduction.	27
3.2.1	Synthesis of carboxylic acid derivative.	34
3.2.2	Synthesis of monobenzyl derivative.	34
3.2.3	Intramolecular coupling reaction.	35
3.3	Experimental Section.	37
4	Molecular docking.	49
4.1	Protein-ligand complex structure by docking.	50
4.2	Results and discussion	55
4.3	Procedure.	56
4.4	Molecular docking of synthesized compounds.	57
4.5	Docking results with CYP1B1.	73
4.6	Docking in BCL2.	74
4.7	Docking results with BCL2.	84

5.1 Acknowledgements.	85
5.2 References.	86

Abbreviations

In the text following terms and reagents are abbreviated as follows

Ac	acetyl
Bn	benzyl
Bu	butyl
DBDMH	1,3-dibromo-5,5-dimethylhydantoin
DBU	1,8-diazabicyclo[5.4.0]undec-7-ene
DIPEA	diisopropylethylamine
DMA	<i>N, N</i> -dimethylacetamide
DMAP	<i>N, N</i> -dimethyl-4-aminopyridine
DMF	<i>N, N</i> -dimethylformamide
EDC.HCl	1-ethyl-3-(3-dimethylaminopropyl) carbodiimide hydrochloride
Et	ethyl
Me	methyl
MOM	methoxymethyl
NBS	<i>N</i> -bromosuccinimide
NMR	nuclear magnetic resonance spectrometry
PDC	pyridinium dichromate
Ph	phenyl
PPTS	pyridinium <i>p</i> -toluenesulfonate
Pr	propyl
TBAF	tetrabutylammonium fluoride
TBS	tert-butyltrimethylsilyl
TFA	trifluoroacetic acid
THF	tetrahydrofuran
TLC	thin-layer chromatography
TMS	trimethylsilyl

Chapter 1

1. General Introduction

This thesis will describe new approaches to the total synthesis of natural dibenzo- α -pyrones and molecular docking studies of synthesized compounds. We used the Pd-catalyzed intramolecular biaryl coupling reaction of phenyl benzoate derivative to make the (6*H*-dibenzo[*b,d*]pyran-6-one) ring system to synthesize such compounds.

1.1 Dibenzo- α -Pyrones

Dibenzo-pyrones (also known as dibenzo-pyranones, 6*H*-benzo[*c*]chromen-6-ones, and 6*H*-dibenzo[*b,d*]pyran-6-ones) are heptaketide coumarin derivatives with a fused tricyclic nucleus. Fungi¹, plants⁴, mycobionts^{2,3}, and animal feces^{5,6} are the most common sources of Dibenzo- α -Pyrones. These compounds are biosynthesized via polyketide route in microorganisms or through the metabolism of natural ellagic acid and ellagitannins by intestinal bacteria. The group includes compounds with a variety of biological properties, including cytotoxicity, anticancer antioxidant, anti-inflammatory, antiglycation, and antimicrobial activity. Dibenzo-pyrones are also important intermediates in the development of cannabinoids⁷ and other pharmaceutically important compounds including androgen, progesterone, endothelial proliferation inhibitors, glucocorticoid receptor agonists, and antidyslipidemic agents.^{8,9} The pharmaceutical community is very interested in the possible applications of dibenzo-pyrones as antitumor agents, antiallergics, antioxidants, and antimicrobials. A few bioactive dibenzo-pyrones have been chemically synthesized.

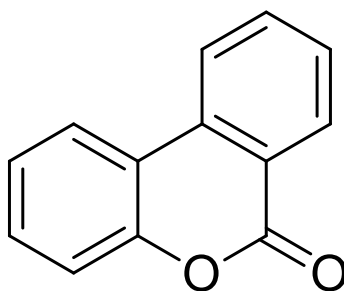
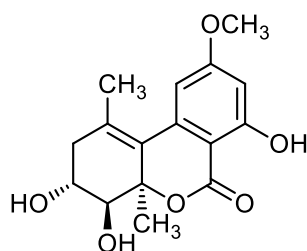


Figure 1. The basic skeleton of dibenzo- α -pyrones

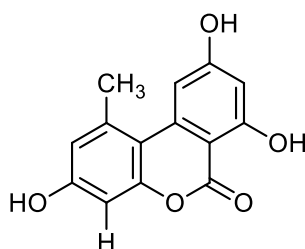
1.2. Occurrence

1.2.1 Dibenzo- α -pyrones from Fungi

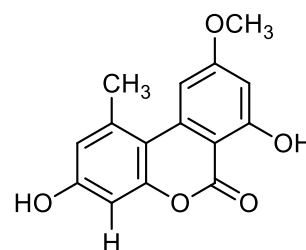
Alternaria species and mycobionts are the primary sources of dibenzo-pyrones. *Botrytis allii*, *Cephalosporium acremonium*, *Hyalodendriella* sp. Ponipode¹², *Microsphaeropsis olivacea*, *Penicillium verruculosum*, and *Phoma* sp. are among the dibenzo-pyrone-producing fungi. Some biologically important Dibenzo- α -pyrones from Fungi are Neoaltenuene, Altermenuol, Alternariol 9-methyl ether, Graphis lactone D, Alternariol, 4-Hydroxyalternariol 9-methyl ether, Graphis lactone A-C, Graphis lactone E-H, and Palmariol A-B.¹⁰⁻¹⁵



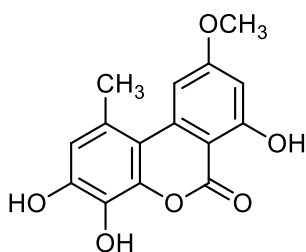
Neoaltenuene



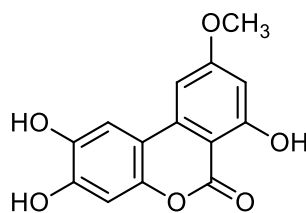
Alternariol



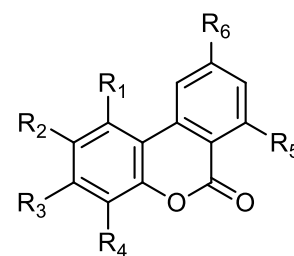
Alternariol 9-methyl ether



4-Hydroxyalternariol 9-methyl ether



Altermenuol



Graphis lactone A, R1 = CH₃, R2 = H, R3 = OCH₃, R4 = OH, R5 = OH, R6 = OCH₃.

Graphis lactone B, R1 = CH₃, R2 = H, R3 = OCH₃, R4 = OH, R5 = OCH₃, R6 = OCH₃

Graphis lactone C, R1 = CH₂OH, R2 = H, R3 = OCH₃, R4 = OH, R5 = OH, R6 = OCH₃

Graphis lactone E, R1 = OH, R2 = H, R3 = OCH₃, R4 = OH, R5 = OH, R6 = OCH₃

Graphis lactone F, R1 = OH, R2 = H, R3 = OCH₃, R4 = OH, R5 = OH, R6 = OH

Graphis lactone G, R1 = CH₃, R2 = Cl, R3 = OCH₃, R4 = H, R5 = OH, R6 = OCH₃

Graphislactone H, R1 = CH₃, R2 = H, R3 = OCH₃, R4 = OCH₃, R5 = OH, R6 = OCH₃

Palmariol A, R1 = CH₃, R2 = H, R3 = OH, R4 = Cl, R5 = OH, R6 = OCH₃

Palmariol B, R1 = CH₃, R2 = Cl, R3 = OH, R4 = H, R5 = OH, R6 = OCH₃

Figure 2. Structures of dibenzo- α -pyrones isolated from fungi.

1.2.2. Dibenzo- α -pyrones from Plants

Some dibenzo- α -pyrones from plants are listed as Autumnariniol, Autumnariol, Fasciculiferol, Lysilactone A, Lysilactone A, Lysilactone A, Sabilactone, and many more.¹⁶⁻¹⁹

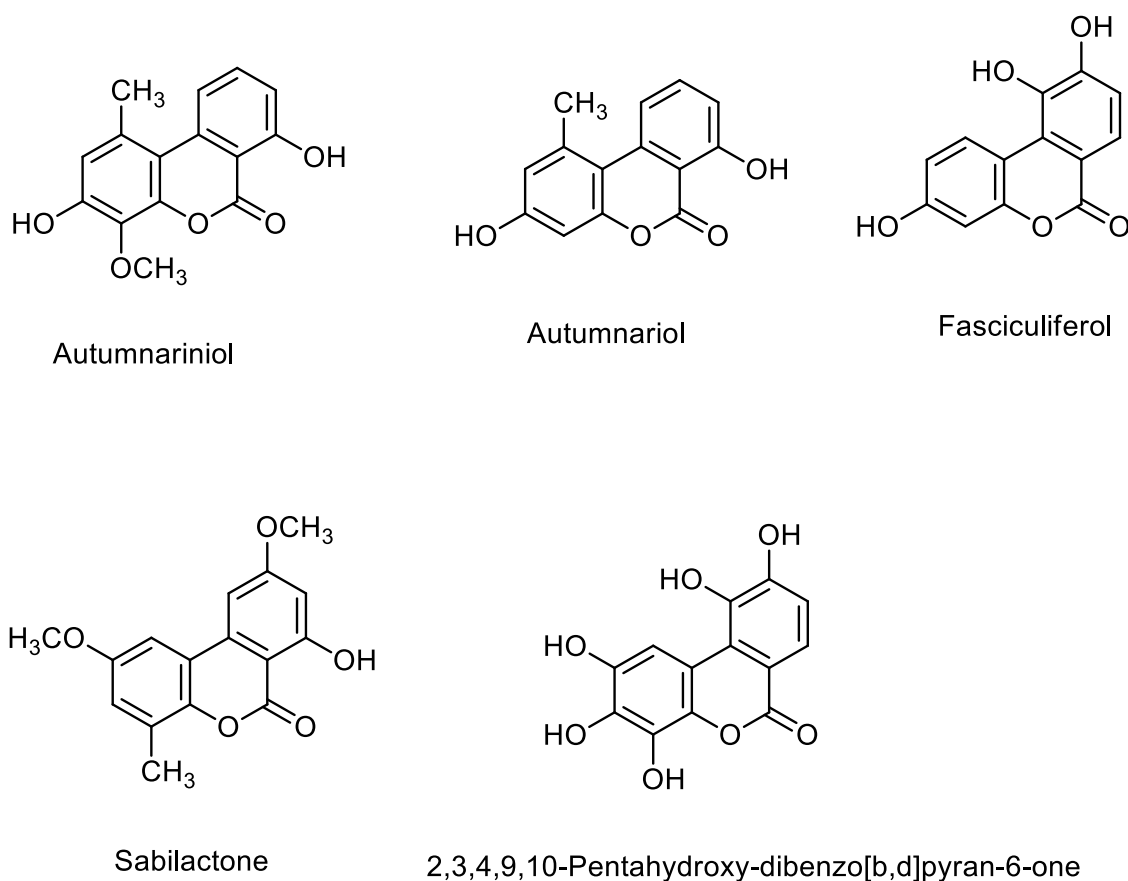
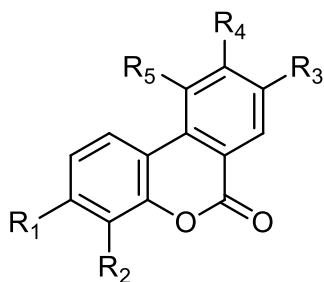


Figure 3. Structures of the dibenzo- α -pyrones from plants

1.2.3 Transformation of intestinal bacteria produces dibenzo-pyrones.

From animal manure, a group of dibenzo-pyrone known as urolithins with various phenolic hydroxylation patterns have been isolated. These dibenzo-pyrone can be present in pomegranates, nuts, oak-aged wines, berries, muscadine grapes, medicinal plants, and tisanes, among other foods. They are not consumed in the intestine and are instead metabolized in vivo by intestinal bacteria to create urolithins, a group of metabolites.^{5,6,20}



Urolithin A	R1=OH, R2=H, R3=OH, R4= H, R5=H
Urolithin B	R1=OH, R2=H, R3=H, R4= H, R5= H
Urolithin C	R1=OH, R2=H, R3=OH, R4= OH, R5= H
Urolithin D	R1= OH, R2=OH, R3=OH, R4=OH, R5=H
Urolithin E	R1=OH, R2=OH, R3=OH, R4=H, R5=OH
Urolithin M-5	R1=OH, R2= OH, R3= OH, R4=OH, R5=OH
Urolithin M-6	R1= OH, R2=H, R3=OH, R4= OH, R5=OH
Urolithin M-7	R1=OH, R2=H, R3= OH, R4= H, R5=OH
Isourolithin A	R1= OH, R2= H, R3=H, R4=OH, R5= H
Isourolithin B	R1=H, R2= H, R3=H, R4= OH, R5=H

Figure 3. Structures of Urolithins

1.2.4 Biological Activities and Functions

The chemical properties of dibenzo-pyrones and their derivatives have been explained widely. Some of them affect humans and animals as mycotoxins, while others affect plants as phytotoxins. They've been studied for their cytotoxic, antioxidant, antiallergic, antimicrobial, antinematodal, and acetylcholinesterase inhibitory properties.

1.2.4.1 Toxicity on Human and Animals

Mycotoxins produced by *Alternaria* fungi have long been associated with human and animal health. Toxins from *Alternaria* have been linked to a variety of negative effects on human and animal health (e.g., genotoxic, mutagenic, and carcinogenic).²¹

1.2.4.2 Cytotoxic Activity

Alternariol (10) was the most active metabolite in *Alternaria* dibenzo-pyrones, with cytotoxic activity on L5178Y mouse lymphoma cells²², as well as inhibitory activity on xanthine oxidase and protein kinase. Alternariol was discovered to be a topoisomerase I and II toxin, which can lead to DNA integrity deficiency in human colon carcinoma cells. It triggered cell death in human colon carcinoma cells by activating the mitochondrial apoptosis pathway.²³

1.2.4.3 Antioxidant Activity

Antioxidant activity was found in urolithin A, isourolithin A, and urolithin B from *Trapa natans* fruits. Isourolithin A had the highest antioxidative effect, while urolithin B had a weak antioxidative effect. Since ellagic acid and ellagitannins are poorly processed in the intestine, urolithins tend to be responsible for ellagitannin-related biological activities. In a cell-based assay, the majority of urolithins (i.e., urolithins A, C, and D) showed antioxidant activity.⁵

1.2.4.4 Antiallergic Activity

Urolithin A, isourolithin A, and urolithin B, isolated from the feces of *Trogopterus xanthipes*, were found to have hyaluronidase inhibitory activities with IC₅₀ values of 1.33, 1.07, and 2.33 mM, indicating antiallergic activity.²⁴

1.2.4.5 Other Bioactivities

Antimicrobial, antinematodal, and antimalarial activities, as well as calmodulin-dependent, antiestrogenic and estrogenic, and acetylcholinesterase (AChE) inhibitory activities, are some of the other biological activities of dibenzo-pyrones.

Chapter 2

2 Synthesis, and Characterization of Hyalodendriol C

2.1 Introduction

Hyalodendriol C²⁵ as indicated in figure 1, chemically named as (2-chloro-7,9-dihydroxy-3-methoxy-1-methyl-6*H*-dibenzo[*b,d*]pyran-6-one), a naturally occurring dibenzo- α -pyrones²⁶ and possess a fused tricyclic nucleus. In 2016, Zhou and co-workers reported the isolation and structural elucidation of hyalodendriol A-C from endophytic fungus associated with the hybrid 'Neva of *Populus deltoides*', *P. nigra* L.²⁵ A variety of biological activities have been stated for hyalodendriol A-C, but only hyalodendriol C has shown significant antibacterial, larvicidal, and anti-fungal properties as mentioned previously in the literature¹). Particularly, it has shown strong antifungal effects with a value of IC₅₀ of 11.6 $\mu\text{g mL}^{-1}$ in opposition to the spore germination of *Magnaporthe oryzae*. It has also exhibited strong larvicidal activities in the case of the yellow fever mosquito that is known to spread severe diseases for instance zika fever, dengue fever, chikungunya, and many other health problems. Conversely, hyalodendriol A and B which do not possess chloro substituent, exhibited weaker activities than those of 1. The inhibitory actions of all three analogues were tested against four phytopathogenic bacteria. Only Hyalodendriol C inhibited *B. subtilis* and *X. vesicatoria* with MIC values of 25 and 50 μM , respectively, while compounds A and B did not inhibit the bacteria at the maximum measured concentration of 125 μM . Several natural products that possess (6*H* dibenzo[*b,d*]pyran-6-one) moiety are found to exhibit numerous biological activities.²⁷ Among the varied biological activities of these compounds, the most exciting bioactivity is the prominent effect of some of the compounds with 6*H*-dibenzo[*b,d*]pyran-6-one core against SW1116 cancer cells.

The interesting structural feature of this compound is the aromatic ring bearing chlorine atom on it. Natural products comprising a halogen on an olefinic, aromatic, heteroaromatic moieties as a substituent have gained considerable interest because of their multiple biological activities. Chlorine is one of the most requisite halogens and it has been well studied in medicinal chemistry as an important constituent in drugs to cure diverse illnesses such as meningitis, cholera, typhoid plague, fungal infections, bacterial skin infections, respiratory and

neural complications.²⁸ Therefore, it was suspected that the presence of a chlorine atom was essential for the cytotoxicity of hyalodendriol C. We have focused on the synthesis of hyalodendriol C by making use of Pd-catalyzed biaryl coupling reaction of phenyl benzoate derivative for making (6*H*-dibenzo[*b,d*]pyran-6-one) ring system. Since the palladium-catalyzed coupling reaction for such compounds was successful as our group has already described, we took advantage and planned the total synthesis of hyalodendriol C. The Pd catalyzed biaryl coupling reaction is one of the most convenient techniques for the formation of carbon-carbon bonds between two aromatic rings among the various provisions of this kind of ring system. The intramolecular biaryl coupling reaction of phenyl benzoate derivatives using the Pd reagent has been documented to be widely useful for synthesizing several of these types of natural products. Our group has synthesized several natural products possessing 6*H*-dibenzo[*b,d*]pyran-6-one ring system, by making use of palladium-catalyzed intramolecular biaryl coupling reaction with phenyl benzoate derivatives for forming the 6*H*-dibenzo[*b,d*]pyran-6-one framework.

The sequential transformation of esterification between the corresponding benzoic acid and phenol, followed by the Pd-mediated coupling reaction, is shown in Scheme 1, as our simple synthetic strategy.

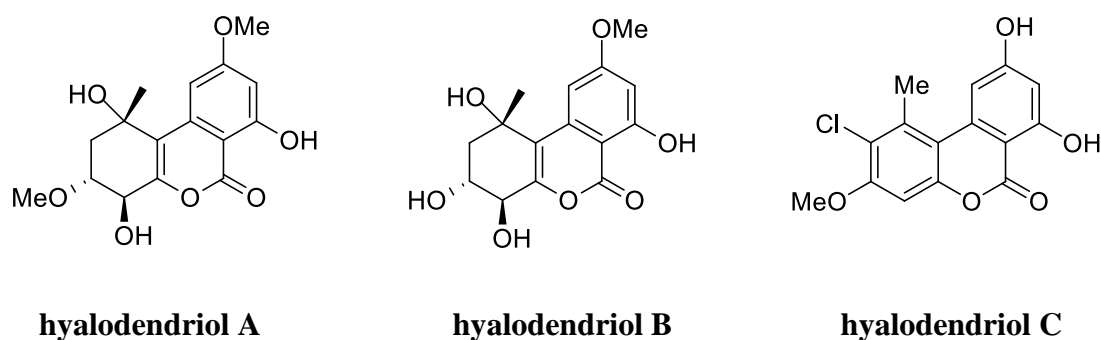
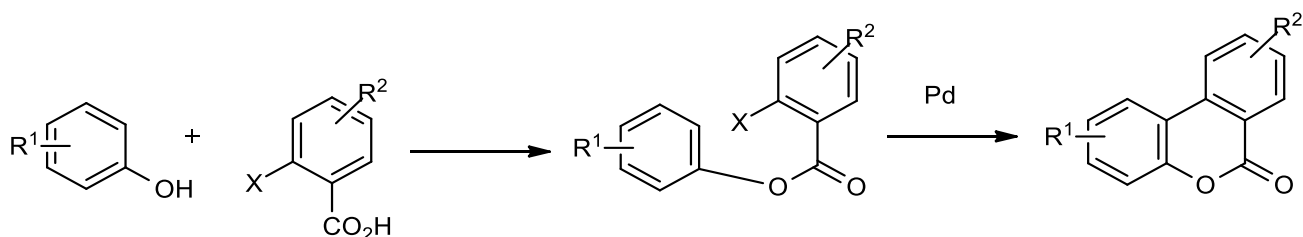


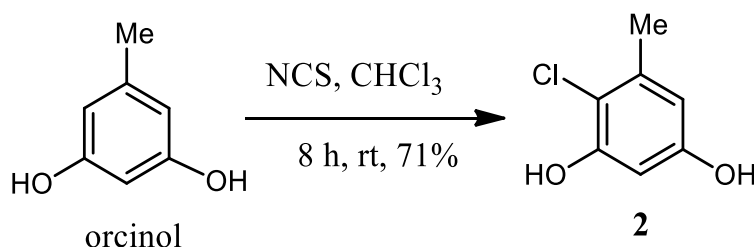
Figure 1. Structures of hyalodendriol A-C



Scheme 1. Synthetic outline of 6*H*-dibenzo[*b,d*]pyran-6-one ring system

2.2 Synthesis of phenol derivative

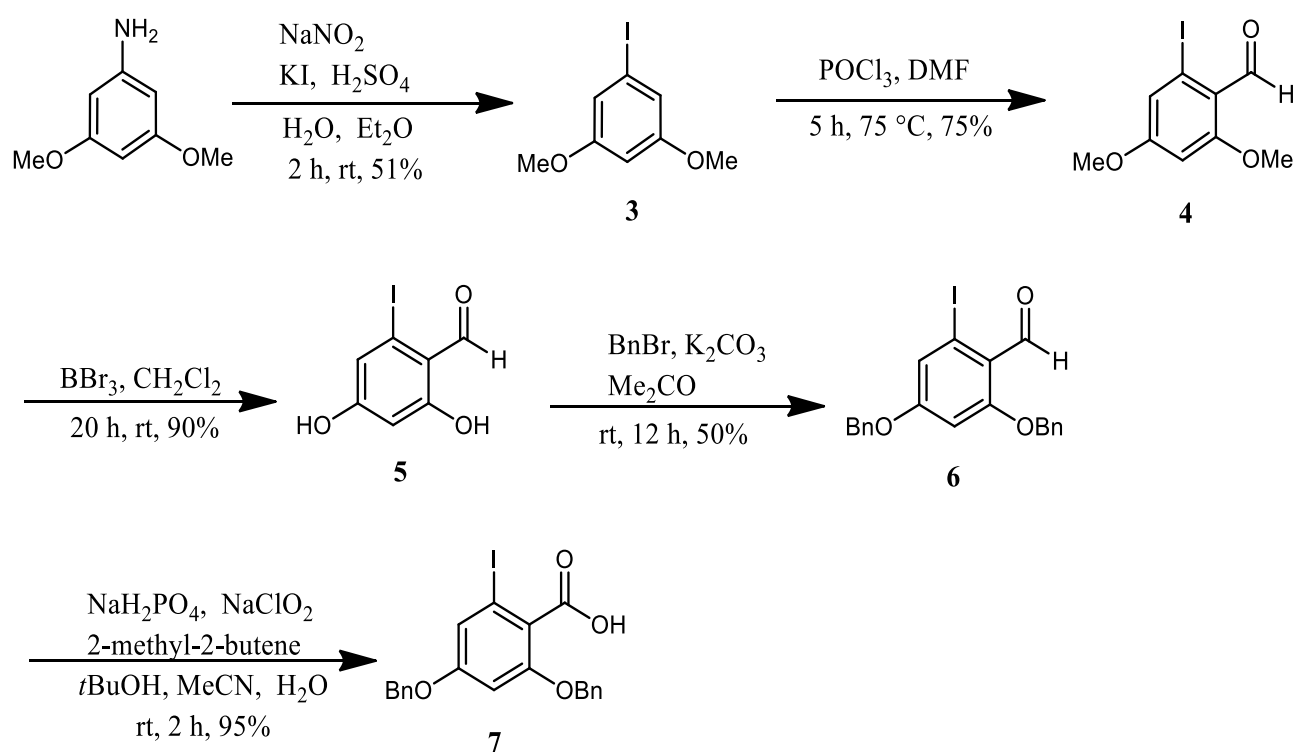
The synthetic investigation of hyalodendriol C (**1**) started with the preparation of 4-chloro-5-methylbenzene-1,3-diol by the known method, as an essential part of phenyl benzoate. Regioselective chlorination of commercially available orcinol to **2** using *N*-chlorosuccinimide (NCS) (scheme 2).²⁹



Scheme 2. Synthesis of phenol derivative **2**

2.3 Synthesis of benzoic acid derivative

On the other hand, through 5 step transformations, the corresponding benzoic acid was prepared as an important precursor for the esterification reaction. First, 3,5-dimethoxyaniline was iodinated to 3, 5-Dimethoxyiodobenzene (**3**) with the substitution of the amino group into iodide via Sandmeyer reaction in presence of potassium iodide,³⁰ which was eventually subjected to Vilsmeier conditions for the introduction of formyl group to produce 6-Iodo-2, 4-dimethoxybenzaldehyde (**4**).³¹ Then demethylation using BBr₃ was carried out to obtain 2, 4-Dihydroxy-6-iodobenzaldehyde (**5**).³² The dihydroxyl group of compound **5** must be tentatively protected by the benzyl group using benzyl bromide to yield 2, 4-Dibenzyloxy-6-iodobenzaldehyde (**6**)^{32,33} before it was allowed for Pinnick oxidation to obtain the corresponding benzoic acid **7**. Compounds **2** and **7** were prepared as per the methods already reported by our research group and results were found to be exactly matching including the spectroscopic data *e.g.*, ¹H-NMR, ¹³C-NMR, Mass (HRMS (EI) *m/z*), and IR.

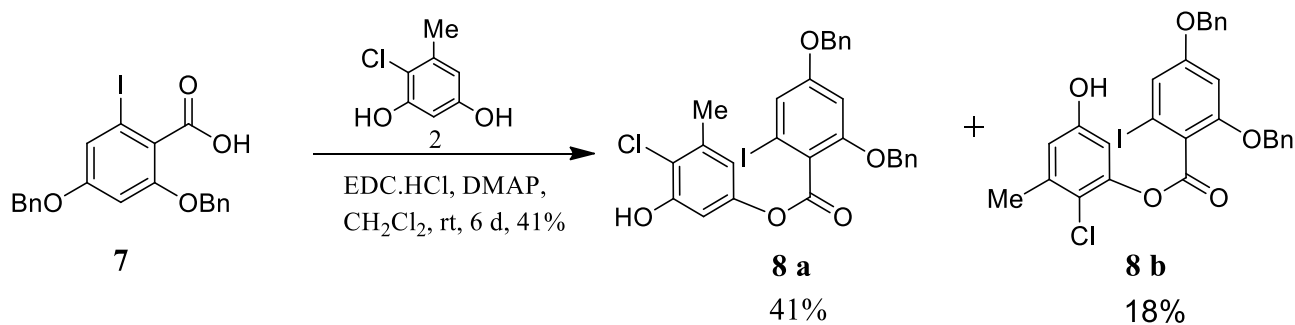


Scheme 3. Synthetic route of acid derivative **7**

Esterification reaction

Esterification between phenol derivative and corresponding benzoic acid derivative by using 1-ethyl-3-(3dimethylaminopropyl)carbodiimide hydrochloride (EDC.HCl) and 4-dimethylaminopyridine (DMAP) as a base was successful to yield the key precursor, 4-Chloro-3-hydroxy-5-methylphenyl 2, 4-dibenzyloxy-6-iodobenzoate (**8**)³⁴ in a moderate yield for the palladium mediated biaryl coupling reaction³⁵ (scheme 4). Despite several attempts, the low yield continued to remain a concern, but almost 41% yield was observed via entry **6** when 2 equivalent phenol was used and the reaction was performed at room temperature for 6 days. (Table 1). The low yield of the desired product was caused due to the condensation at both hydroxy groups. To find optimum reaction conditions, various variations were employed, such as a change in solvent, temperature, time, reagents, and equivalent weight of both substrates. Compound **9** was successfully achieved from compound **8** using MeI and K₂CO₃ as a base³⁶ and this step was pleasingly found to offer a 74% yield.

Table 1. Reaction conditions for the esterification between **7** and **2**

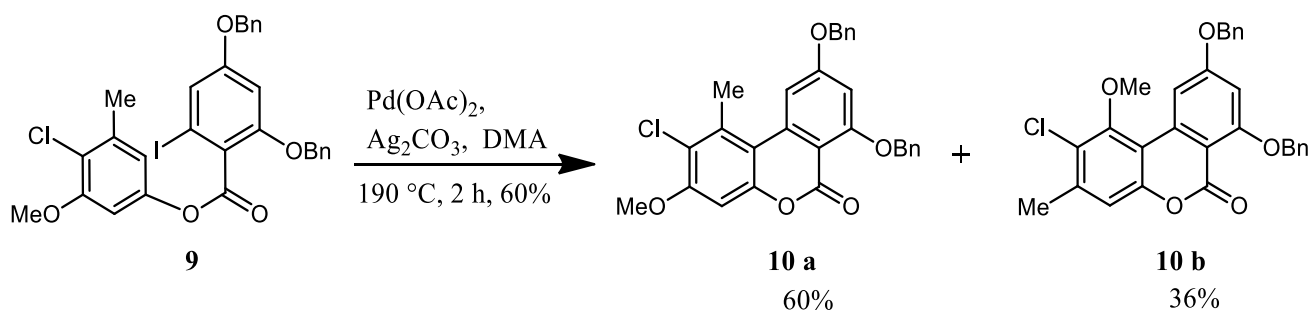


Entry	Reagent	base	solvent	phenol eq	time	yield % of 8 a
1	EDC (3 eq)	DMAP	DCM	1.05	10 h	15
2	DCC (3 eq)	DMAP	DCM	1.05	24 h	20
3	DCC (3 eq)	DMAP	CHCl ₃	0.8	24 h	trace
4	DCC (3 eq)	DMAP	DMF	1.5	5 d	25
5	EDC (2 eq)	Et ₃ N (5 eq)	DCM	1	5 d	trace
6	EDC (1.15 eq)	DMAP	DCM	2	6 d	41

2.4 Pd catalyzed intramolecular biaryl coupling reaction

The all-important intramolecular biaryl coupling reaction using Pd reagent was a significant potential for application to the construction of 2-Chloro-7,9-dibenzyloxy-3-methoxy-1-methyl-6*H*-dibenzo[*b,d*]pyran-6-one (**10**). As shown in the table below the bi aryl intramolecular coupling reaction was observed in different conditions to achieve the maximum yield. We examined the intramolecular biaryl coupling reaction using Pd(OAc)₂ and NaOAc as base, in DMF at 150 °C with Triphenylphosphine (PPh₃) as ligand which produced **10** in 56% yield. In the second run Ag₂CO₃ was used as base with PPh₃ but produced **10** in low yield as compare to the one with NaOAc being used as base. Combination of Pd(OAc)₂ with NaOAc as base, with and without phosphine ligand produced the product in almost same percentage yield. However, Pd(OAc)₂ in presence of Ag₂CO₃ at high temperature (190 °C) lead to an improvement in the yield of **10**. Finally, deprotection using 10% Pd/C in presence of H₂³⁷ produced hyalodendriol C (**1**) successfully in a modest yield. The spectral data of the synthetic compound is in line with the data provided in the literature.

Table 2. Pd catalyzed cyclisation of **9**



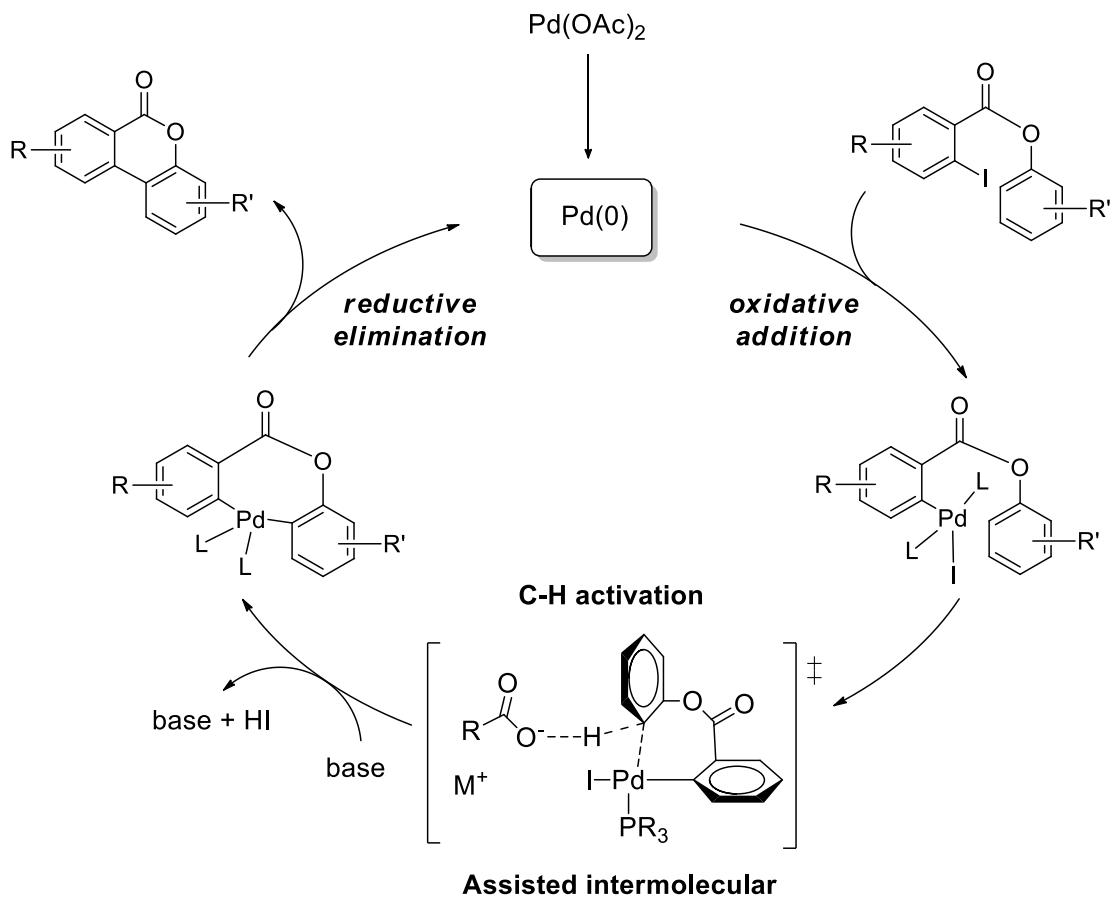
Run	Catalyst	Ligand	Base	Time (h)	Temp.	Yield (%) of 10 a
1	Pd(OAc) ₂	PPh ₃	NaOAc	2	130	56%
2	Pd(OAc) ₂	PPh ₃	Ag ₂ CO ₃	20	reflux	29%
3	Pd(OAc) ₂	None	NaOAc	2	130	57%
4	Pd(PPh ₃) ₄	None	NaOAc	5	130	32%
5	Pd(OAc) ₂	PPh ₃	NaOAc	2	reflux	11%
6	Pd(OAc) ₂	None	Ag ₂ CO ₃	2	190	60%

In each case, the coupling reaction proceeded smoothly, producing the lactone compounds 10a and 10b in moderate to good yield. The product ratio of 10a and 10b changed dramatically with the reaction conditions. When Pd(OAc)₂ with and without ligand was used, high regioselectivity was observed especially at high temperature (run 1 and 6), generating the product 10a, which was reacted at the position ortho to the methyl group

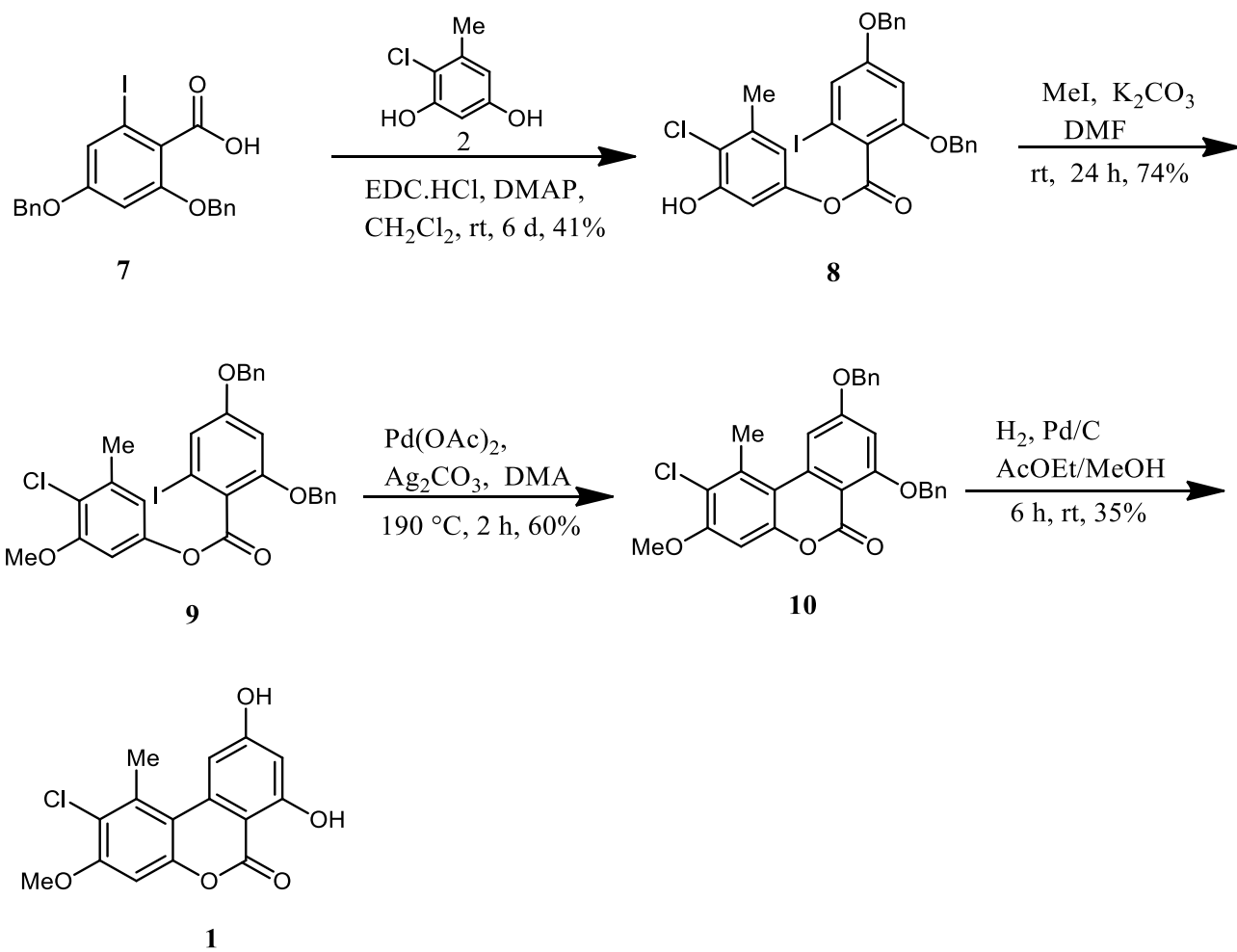
2.5 Significance of Palladium-Catalyzed coupling reaction

One of the most effective methods for forming carbon-carbon bonds is through palladium-catalyzed coupling reactions. Palladium's remarkable ability to form C-C bonds between properly functionalized substrates has allowed synthetic organic chemists to perform transformations that were previously impossible or only possible through multi-step processes. As a result, these coupling methodologies have changed the way people think about synthetic organic chemistry, and they're now widely used in organic synthesis and material science, as well as in the pharmaceutical, agrochemical, and fine chemical industries. In this context, the Nobel Prize in Chemistry awarded in 2010 to Richard F. Heck, Ei-ichi Negishi, and Akira Suzuki for their outstanding contributions to Pd-catalyzed cross-couplings in organic synthesis was well-deserved. In our opinion, the most important and elegant application of the coupling reactions is the synthesis of pharmaceuticals.

The generally accepted mechanism for Pd-catalyzed C-C coupling reactions is summarized below. First, Pd (II) is reduced to Pd (0) by a ligand or solvent, and Pd (0) is oxidatively added to the substrate. Next, at the reaction point on the phenoxy side, activation of the C-H bond occurs via the transition state of the intermolecular assisted intermolecular mechanism, and the C-Pd bond is formed by the base abstracting the proton. Finally, reductive elimination forms a biaryl bond, constructing a 6*H*-dibenzo [*b,d*] pyran-6-one backbone and regenerating Pd (0). However, Scheme 4 is used for this intramolecular biaryl coupling reaction.



Scheme 4. The mechanism of Pd catalyzed coupling reaction

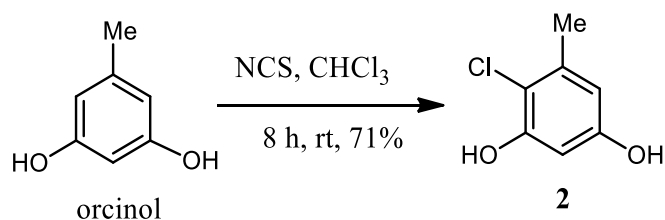


Scheme 5. Synthesis of hyalodendriol C (**1**)

2.6 Experimental Section

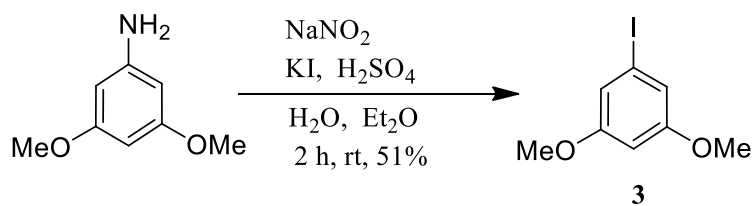
General: All reactions were executed under N₂ atmosphere. Reaction solvents were used after purification by the standard methods. Reaction progress was observed with the help of thin-layer chromatography by making use of silica gel (70 F₂₅₄) TLC plates and UV light as an agent for visualizing. Silica gel (particle size: 100–200 and 230–400 mesh). Melting points (mp) were obtained using the Yanaco micro melting point apparatus and are uncorrected. With the Shimadzu FTIR 8400 spectrophotometer, the IR spectra were acquired. The JOEL α -400 MHz instrument was utilized for obtaining ¹H and ¹³C NMR spectra with the couplings being shown in Hertz and chemical shift being expressed as δ ppm. Silica gel column chromatography was accomplished using Wakogel 60N, 63~212 μ m.

Experimental Procedures



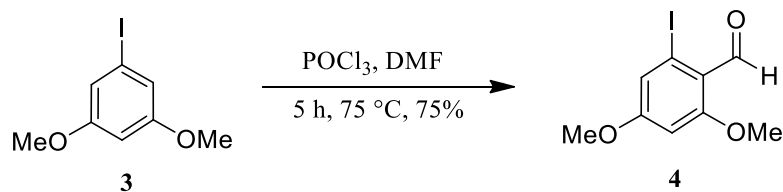
4-Chloro-1,3-dihydroxy-5-methylbenzene (**2**)

A 500-mL, single-necked, round-bottomed flask, equipped with a 3-cm, egg-shaped, magnetic stir bar was charged with a solution of 5-methylbenzene-1,3-diol, (5 g, 50.3 mmol) in CHCl₃ (200 mL). The reaction mixture was cooled to 0 °C by using an ice bath. To the resulting solution, was added N-Chlorosuccinimide (NCS) (6.4 g, 48.35 mmol) with stirring over a period of 5 min before bringing it back to room temperature. A TLC analysis using ethyl acetate:hexane (1:5) indicated the reaction was complete. The solution was decanted into water (120 mL) after being stirred at room temperature for 8 h and stirred for 5 more min. The mixture was transferred to a 500 mL separatory funnel. The organic layer was separated, and the remaining aqueous layer was extracted with CH₂Cl₂ (3 × 100 mL). The combined organic extracts were washed with saturated brine (100 mL), dried over anhydrous MgSO₄, and concentrated using a rotary evaporator to yield a white solid which was collected and dried under vacuum. Recrystallization from EtOAc obtained a white solid of **2** in 71% yield.



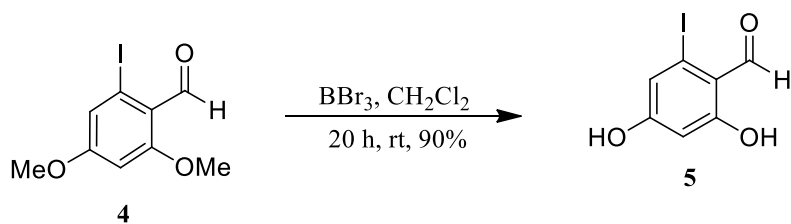
3, 5-Dimethoxyiodobenzene (3)

A 300-mL, single-necked, round-bottomed flask, equipped with a 3-cm, egg-shaped, magnetic stir bar was charged with an ice-cooled solution of 3,5-dimethoxyaniline 5 g (32.6 mmol) in 55 mL water, H₂SO₄ (5 mL) was added drop wise to the solution. After the solution had cooled down to -10 to -15 °C, a solution of NaNO₂ (2.635 g, 38.2 mmol) in 10 mL water was added accompanied by the addition of Et₂O 25 mL. To limit the evolution of N₂, a solution of potassium iodide (KI) (16.42 g, 98.9 mmol) in water (15 mL) was added gently and kept at stirring at room temperature. A TLC analysis using ethyl acetate:hexane (1:2) indicated the reaction was complete. The mixture was transferred to a 500 mL separatory funnel. The organic layer was separated, and the remaining aqueous layer was extracted with diethyl ether (3 × 100 mL). The combined organic layer was washed with Na₂S₂O₃·5H₂O (aq) (3×30 mL), 1M HCl (50 mL), 2M NaOH (50 mL). The combined organic extracts were washed with saturated brine (100 mL), dried over anhydrous MgSO₄, and concentrated using a rotary evaporator to yield a white solid which was collected and dried under vacuum. Two times recrystallization from EtOAc yielded yellow-colored solid product in 51% yield.



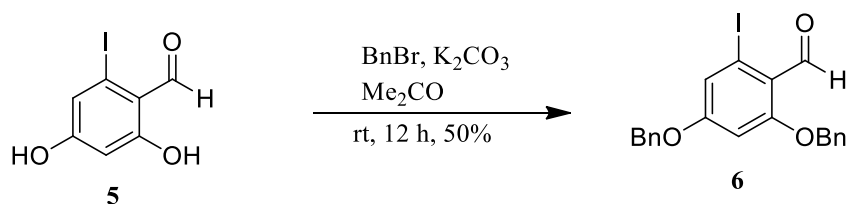
6-Iodo-2,4-dimethoxybenzaldehyde (**4**)

To a 200-mL, three-necked, round-bottomed flask, equipped with a 4.0-cm, egg-shaped stir bar and fitted with an addition funnel and a condenser (nitrogen inlet) was charged with a solution of 3,5-Dimethoxyiodobenzene (**3**) (4.42 g, 17.04 mmol) in DMF (16 mL), and stirring was begun to dissolve the solid. POCl₃ (5.5 mL, 59.64 mmol) was added dropwise *via* the addition funnel with stirring over a period of 20 min. The reaction flask was then placed in a pre-heated oil bath at 75 °C for 4 hours. During this time change in colour from yellowish to brownish was observed. A TLC analysis of the solution using Ethyl Acetate: hexane (3:2) indicated the reaction was complete. After cooling for 10 min, the reaction mixture was poured into a 300-mL Erlenmeyer flask containing crushed ice (50 g). The resulting mixture was cooled in an ice bath with continuous stirring for 10 min. The mixture was transferred to a 500 mL separatory funnel using ethyl acetate (100 mL). The organic layer was separated, and the remaining aqueous layer was extracted with ethyl acetate (4 × 150 mL). The combined organic extracts were washed with saturated aqueous NaHCO₃ (50 mL), dried over anhydrous MgSO₄, and concentrated using a rotary evaporator to yield a yellow solid. Purification of this material by column chromatography (25-cm × 4-cm column), eluted with (hexane/EtOAc, 5/2), gave **5** in 75% yield.



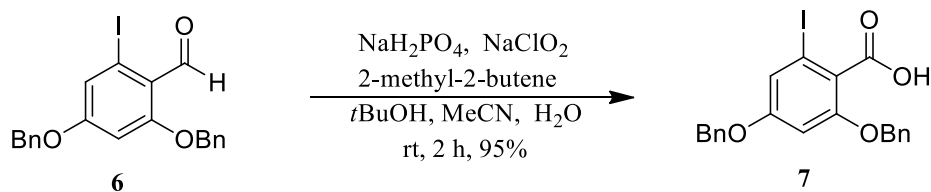
2, 4-Dihydroxy-6-iodobenzaldehyde (5)

To a 200-mL, three-necked, round-bottomed flask, equipped with a 2.5-cm, egg-shaped stir bar and fitted with an addition funnel and a condenser (nitrogen inlet) was charged with BBr_3 (38.8 mL, 38.808 mmol), a solution of 6-Iodo-2, 4-dimethoxybenzaldehyde (**4**) (2.70 g, 9.24 mmol) in dry CH_2Cl_2 (50 mL) was slowly added to the mixture *via* the addition funnel with stirring continued for 20 h. [*Caution*: BBr_3 was handled very carefully]. During the addition process, the color of the reaction mixture changed from yellow to red. A TLC analysis of the solution using ethyl acetate:hexanes (1:3) indicated the reaction was complete. Later, iced water (60 mL), was added very slowly with continued stirring, a precipitate began to form during the addition of water. The reaction mixture was acidified with 1 M aq HCl (28 mL). The precipitate was filtered to obtain a pure brown solid product. Whereas the filtrate was transferred to a 500-mL separatory funnel and the aqueous layer was extracted with EtOAc (3×50 mL). The combined organic extracts were washed with saturated aqueous brine (60 mL), dried over anhydrous MgSO_4 , and concentrated using a rotary evaporator to yield a brown oil. Purification of this material was achieved by column chromatography (15-cm × 2-cm column), eluted with (hexane/EtOAc, 3/1), and gave **5** in 90% yield.



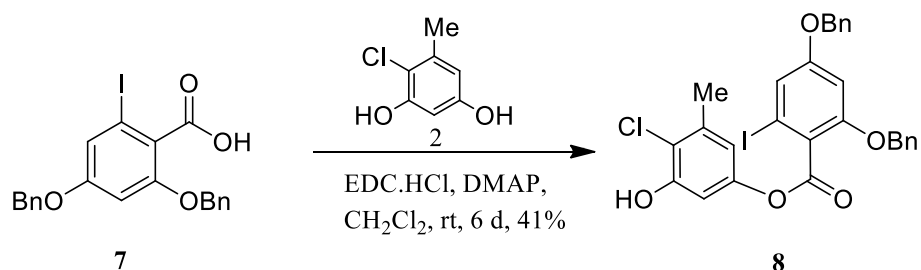
2, 4-Dibenzyloxy-6-iodobenzaldehyde (6)

To a 200-mL, three-necked, round-bottomed flask, equipped with a 3.0-cm, egg-shaped stir bar and fitted with an addition funnel and a condenser (nitrogen inlet) was charged with a solution of 2, 4-Dihydroxy-6-iodobenzaldehyde (**5**) (1.65 g, 7.83 mmol) in acetone (34 mL) and stirring was begun to dissolve the solid. K_2CO_3 (2.165 g, 15.66 mmol) was then added and stirring was continued for 10 min. Benzyl bromide (2.21 ml, 18.79 mmol) was slowly added to the mixture *via* the addition funnel with stirring continued at room temperature. During the addition process, the color of the reaction mixture changed from brown to yellow. After 13 h a TLC analysis of the solution using ethyl acetate:hexanes (1:3) indicated the reaction was complete. The reaction mixture was quenched by the slow addition of water (30 mL) and diluted with EtOAc (100 mL). Then the reaction mixture was filtered and the solid part was discarded. The mixture was transferred to a 500-mL separatory funnel and proceeded with extractive workup with EtOAc (3×50 mL), the organic layer was washed with saturated brine (50 mL), dried over anhydrous MgSO_4 , and concentrated to get oil like crude. The residue was twice recrystallized from EtOAc to get a yellow solid product in 50% yield.



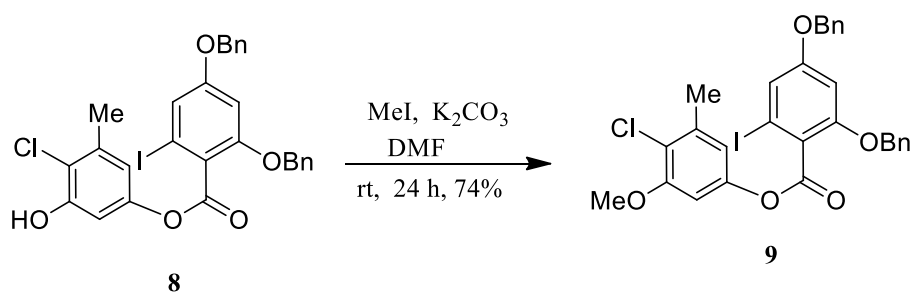
2, 4-Dibenzoyloxy-6-iodobenzoic acid (7)

A 300-mL, single-necked, round-bottomed flask, equipped with a 2.5-cm, egg-shaped, magnetic stir bar was charged with a solution of 2, 4-dibenzoyloxy-6-iodobenzaldehyde **6** (930 mg, 2.09 mmol) in *t*-BuOH (27 mL), and stirring was begun to dissolve the solid. MeCN (7.75 mL), NaH₂PO₄·2H₂O (2.6 g, 16.74 mmol) and 2-methyl-2-butene (5.09 mL, 48.14 mmol) were added. The solution was cooled to 0 °C and NaClO₂ (1.5 g, 16.74 mmol) dissolved in water (12 mL) was dropwise added and kept on stirring at room temperature. A TLC analysis of the solution using ethyl acetate: hexane (1:3) indicated the reaction was complete. After stirring for 2 h, EtOAc (100 mL) water (20 mL) was added and stirred for 5 more min. The mixture was transferred to a 500-mL separatory funnel and the organic layer was separated. The aqueous phase was extracted with EtOAc (3×50 mL), and the combined organic layer was washed with saturated brine (50 mL), dried over anhydrous MgSO₄, and concentrated under reduced pressure. Two times recrystallization from EtOAc yielded white-colored solid product in 95% yield.



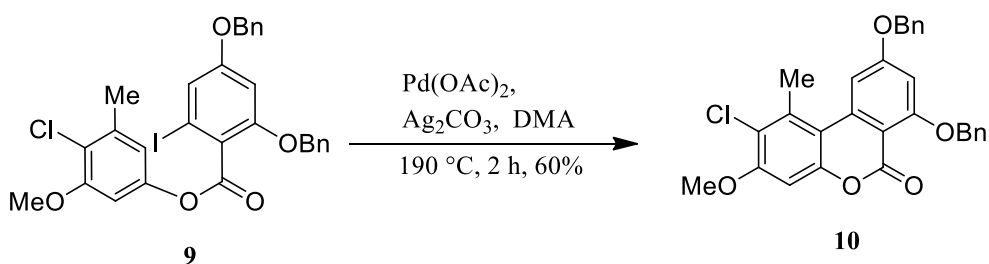
4-Chloro-3-hydroxy-5-methylphenyl 2, 4-dibenzyloxy-6-iodobenzoate (**8**)

To a 100-mL, three-necked, round-bottomed flask, equipped with a 1.0-cm, egg-shaped stir bar and fitted with an addition funnel and a condenser (nitrogen inlet) was charged with a solution of 2, 4-Dibenzyloxy-6-iodobenzoic acid (**7**) (500 mg, 1.087 mmol) in DCM (16 ml) and stirring was begun to dissolve the solid. N-(3-Dimethylaminopropyl)-N'-ethylcarbodiimide hydrochloride (EDC.HCl) (245 mg, 1.08 mmol), 4-Dimethylaminopyridine (DMAP) (65 mg, 0.54 mmol) and 4-Chloro-1,3-dihydroxy-5-methylbenzene (**substrate 2**) (345 mg, 1.17 mmol) were added. The reaction mixture was stirred for 6 days at room temperature. A TLC analysis of the solution using (hexane/EtOAc/ CH₂Cl₂, 3/1/0.25) indicated the reaction was complete. The reaction mixture was then poured into water and then aqueous layer was extracted with CH₂Cl₂ (3×30 mL). The organic layer was washed with saturated brine (50 mL), dried over anhydrous MgSO₄, and concentrated under reduced pressure to give a residue that was subjected to column chromatography (silica gel) (hexane/EtOAc/ CH₂Cl₂, 3/1/0.25). White solid product was obtained (269 mg, 41%) yield, mp 162.9-164.2 °C; IR KBr/cm : 3384, 1732, 1589, 910, 762, 611; ¹H-NMR (400 MHz, CDCl₃) δ 7.41-7.35 (m, 10H), 7.08 (d, *J* = 7.3 Hz, 1H), 6.72 (d, *J* = 2.7 Hz, 1H), 6.62 (d, *J* = 2.3 Hz, 1H), 6.58 (d, *J* = 2.7 Hz, 1H), 5.66 (s, 1H), 5.08 (s, 2H), 5.04 (s, 2H), 2.31 (s, 3H); ¹³C-NMR (100 MHz, CDCl₃) δ 165.9, 161.1, 157.3, 152.0, 149.6, 137.6, 135.9, 135.8, 128.8, 128.8, 128.5, 128.4, 127.7, 127.6, 122.9, 118.0, 116.8, 115.9, 107.5, 101.0, 92.8, 77.4, 77.1, 76.8, 70.9, 70.6, 20.3; HRMS (EI) *m/z* [M⁺] calculated for C₂₈H₂₂O₅ICl 600.0200, found 600.0247.



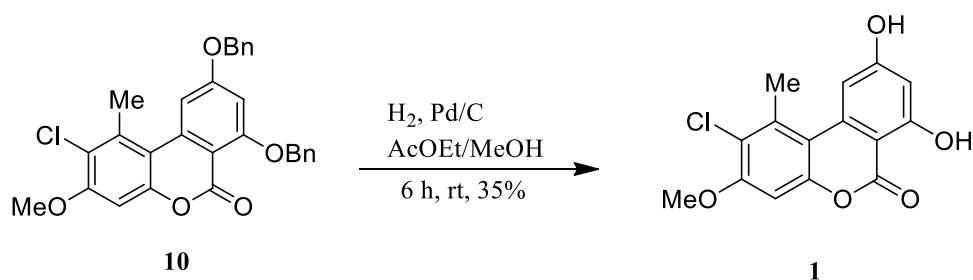
4-Chloro-3-methoxy-5-methylphenyl 2, 4-dibenzyloxy-6-iodobenzoate (9)

To a 100-mL, three-necked, round-bottomed flask, equipped with a 1.0-cm, egg-shaped stir bar and fitted with an addition funnel and a condenser (nitrogen inlet) was charged with a solution of to a solution of 4-Chloro-3-hydroxy-5-methylphenyl 2, 4-dibenzyloxy-6-iodobenzoate (**8**) (240 mg, 0.39 mmol) in DMF (2.4 mL) and stirring was begun to dissolve the solid. K_2CO_3 (82 mg, 0.60 mmol) and methyl iodide (0.025 mL) were added to the reaction mixture. A TLC analysis of the solution using EtOAc:hexanes (1:3) indicated the reaction was complete After 24 hours of stirring at room temperature, the reaction mixture was poured into the water accompanied by layer separation. The aqueous layer was extracted with EtOAc (3×30 mL) whereas, the washing of the combined organic layer was done with additional water (3×20 mL) and one time with sodium chloride solution, dried over anhydrous $MgSO_4$, and evaporated to give a residue. Two times recrystallization from EtOAc yielded white coloured solid product (180 mg, 74%), mp 94.4-95.5 °C ; IR KBr/cm :1745, 1696, 831, 736; 1H -NMR (400 MHz, $CDCl_3$) δ 7.43-7.35 (m, 10H), 7.09 (d, $J = 1.8$ Hz, 1H), 6.65 (d, $J = 5.5$ Hz, 2H), 6.53 (s, 1H), 5.06 (d, $J = 2.3$ Hz, 4H), 3.72 (s, 3H), 2.33 (s, 3H); ^{13}C -NMR (100 MHz, $CDCl_3$) δ 166.0, 161.1, 157.3, 155.6, 149.3, 138.4, 135.8, 128.9, 128.7, 128.5, 128.4, 127.8, 127.7, 122.9, 120.1, 116.8, 115.8, 103.7, 101.0, 92.8, 77.4, 77.1, 76.8, 71.0, 70.7, 56.3, 20.5; HRMS (EI) m/z [M^+] calculated for $C_{29}H_{24}O_5ICl$ 614.0399, found 614.0357.



2-Chloro-7,9-dibenzyloxy-3-methoxy-1-methyl-6*H*-dibenzo[*b,d*]pyran-6-one (**10**)

To a 100-mL, three-necked, round-bottomed flask, equipped with a 1.0-cm, egg-shaped stir bar and fitted with an addition funnel and a condenser (nitrogen inlet) was charged with a solution of 4-Chloro-3-methoxy-5-methylphenyl 2, 4-dibenzyloxy-6-iodobenzoate (**9**) (154 mg, 0.24 mmol) in DMA (3 mL), Pd(OAc)₂ (5.60 mg, 0.46 mmol) and Ag₂CO₃ (138.09 mg, 0.50 mmol) were added. The reaction mixture was then stirred for 5 min at rt and subsequently heated at 190 °C for 2 h. Later, at room temperature, the reaction mixture was cooled down, diluted with EtOAc, filtered to remove undissolved materials and then the filtrate was poured into 10 ml water and extracted with EtOAc (3×20 mL). The organic layer was washed with water and sodium chloride solution, dried over anhydrous MgSO₄ and evaporated to give a brown mixture. Column chromatography (silica gel) (hexane/EtOAc, 3/1) was employed to yield **10** as white powder (74 mg, 60%), mp 187.1-188.3 °C; IR KBr/cm : 1720, 1600, 823, 734; ¹H-NMR (400 MHz, CDCl₃) δ 7.59 (d, *J* = 6.9 Hz, 2H), 7.44-7.36 (m, 8H), 7.14 (d, *J* = 1.8 Hz, 1H), 6.76 (s, 1H), 6.67 (d, *J* = 1.8 Hz, 1H), 5.29 (s, 2H), 5.17 (s, 2H), 3.94 (s, 3H), 2.70 (s, 3H); ¹³C-NMR (100 MHz, CDCl₃) δ 163.5, 162.6, 157.3, 156.1, 151.7, 139.7, 136.3, 135.8, 134.9, 128.9, 128.7, 128.5, 127.9, 127.4, 126.8, 120.6, 112.4, 104.8, 104.6, 100.4, 98.4, 77.4, 77.1, 76.8, 71.0, 70.5, 56.5, 21.2; HRMS (EI) *m/z* [M⁺] calculated for C₂₉H₂₃O₅Cl 486.1261, found 486.1234.



Hyalodendriol C (2-Chloro-7,9-dihydroxy-3-methoxy-1-methyl-6H-dibenzo[*b,d*]pyran-6-one) (1)

To a 25-mL, two-necked, round-bottomed flask, equipped with a 0.5-cm, egg-shaped stir bar and fitted with an addition funnel and a condenser (hydrogen inlet) was charged with a solution of 2-Chloro-7,9-dibenzyloxy-3-methoxy-1-methyl-6H-dibenzo[*b,d*]pyran-6-one (**10**) (42 mg, 0.086 mmol) in 1:1 MeOH/EtOAc (1 mL) followed by the addition of 10% Pd/C (52 mg). The resulting mixture was stirred for 6 h at rt under H₂ atmosphere. A TLC analysis of the solution using EtOAc:hexanes (1:2) indicated the reaction was complete after which the mixture was filtrated to remove the catalyst and eluted with EtOAc. The volatiles were evaporated to provide the crude which was subjected to column chromatography (hexane/EtOAc, 2:1) to yield hyalodendriol C (**1**) as brown solid, (10 mg, 35%), mp 235 °C-237 °C. IR KBr/cm :3284, 2362, 1652, 1070, 983; ¹H-NMR (400 MHz, DMSO-D6) δ 7.21 (d, *J* = 1.8 Hz, 1H), 7.16 (s, 1H), 6.42 (d, *J* = 1.8 Hz, 1H), 3.94 (s, 3H), 2.81 (s, 3H); ¹³C-NMR (100 MHz, DMSO-D6) δ 163.9, 150, 132.2, 129.2, 67.9, 40.6, 40.4, 40.2, 40.0, 39.8, 39.6, 39.4, 38.6, 30.3, 29.5, 28.9, 22.9; HRMS (EI) *m/z* [M⁺] calcd for C₁₅H₁₁O₅Cl 306.0253, found 306.0295.

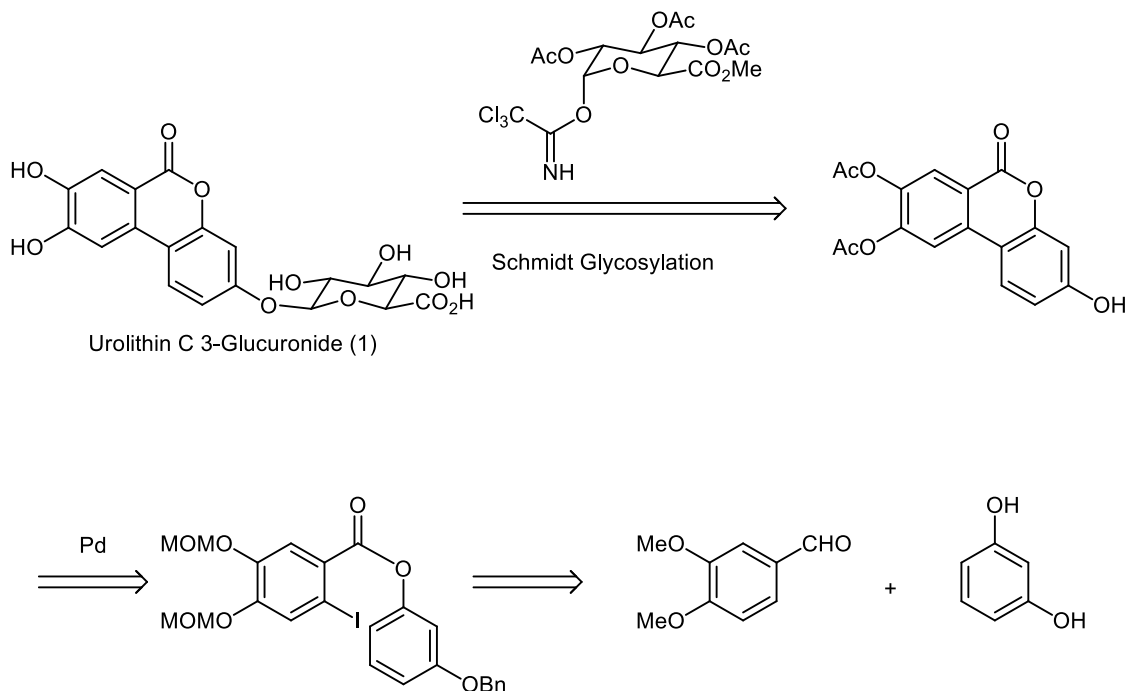
Chapter 3

3 Synthesis and characterization of urolithin C 3-glucuronide

3.1 Introduction

Over recent years, it has been reported that gastrointestinal microbiota metabolize xenobiotics, which are produced from natural products⁵⁷ Urolithins, which are hydroxylated dibenzo[*b,d*]pyran-6-one derivatives, contain urolithin A (uro-A), urolithin B (uro-B), urolithin C (uro-C) and urolithin D (uro-D) derivatives which are produced *in vivo* by the gastrointestinal microbiota of humans and different animals upon intaking ellagitannins (ETs), which are high molecular weight polyphenols and ellagic acids (EAs).⁵⁸⁻⁶³ There are many different phenolic antioxidants such as ETs and EAs in walnuts and pomegranates, which have been linked to potential preventive effects against chronic diseases like diabetes, cancer, cardiovascular diseases, and neurodegenerative diseases.⁶⁴⁻⁶⁵ The bioavailability of ETs and EAs is much lower than transformed urolithins. Glucuronides of uro-A, uro-B, uro-C, and sulfate conjugates are formed by urolithins which circulate in the plasma. Total concentrations of these metabolites can reach a range of 0.2-20 μM .⁶² Although it is suggested that positive health effects are arising from the metabolism of ETs, there is not enough *in vivo* research. So, a clear evaluation in terms of the *in vivo* biological effects of these metabolites is necessary.⁶⁴ In addition to these reports, it is shown that phase-II metabolites of urolithins, which are primarily glucuronide and sulfate conjugates, can reach systemic human tissues⁶⁶. In recent years, research regarding urolithins has concentrated on phase-I metabolites which are composed of mainly uro-A and uro-B, whereas we have been interested in phase-II metabolites of urolithins. Uro-A glucuronide (uro-A glur) and uro-B glucuronide (uro-B glur) were already chemically synthesized and purified by Villapharma Research S. L. (Parque Tecnológico de Fuente Alamo, Murcia, Spain)⁶⁸⁻⁶⁹. On the other hand, the chemical synthesis of Uro-C 3-glur has not been completed and the bioavailability of uro-A glur and uro-B glur has been shown to be much more than uro-C 3-glur⁷⁰. Thus, we have decided to synthesize Urolithin C 3-Glucuronide which is needed to pursue the advantageous health effects. Our retrosynthetic analysis to form Uro-C 3-glur is outlined in Scheme 1. Firstly, we aimed at forming the 6*H*-dibenzo[*b,d*]pyran-6-one skeleton of urolithin as an intermediate with a palladium catalyst so that the final product can be generated *via* a Schmidt Glycosylation⁷⁰⁻⁷². Secondly, we assumed that the precursor of

the coupling compound could be derived from the commercially available starting materials 3,4-dimethoxybenzaldehyde and resorcinol.



Scheme 1. Retrosynthetic Analysis

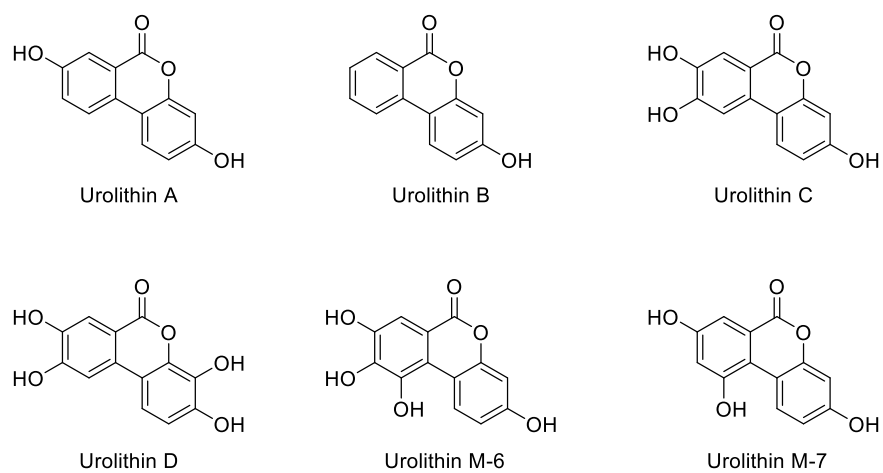


Figure 1. Structures of Urolithin A-D and Urolithin M6-Urolithin M7

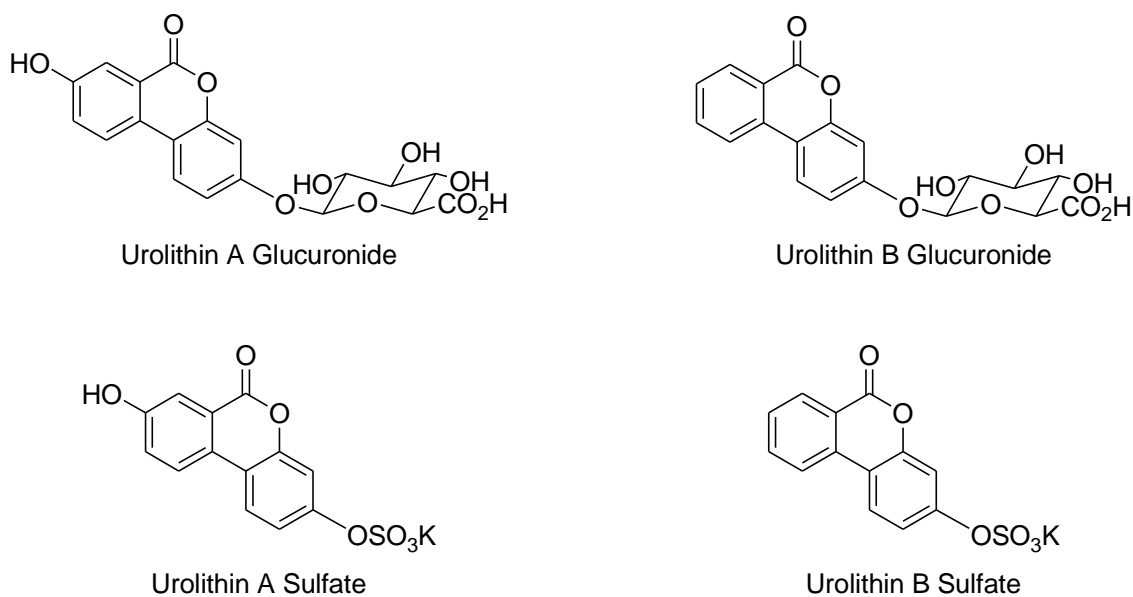


Figure 3. Structures of Urolithin A and B Glucuronide, Urolithin A and B Sulphate.

Synthetic example and synthetic plan of Urolithins through intramolecular biaryl coupling reaction

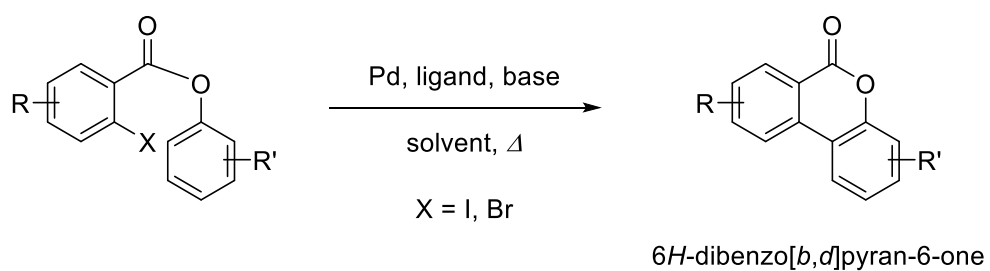
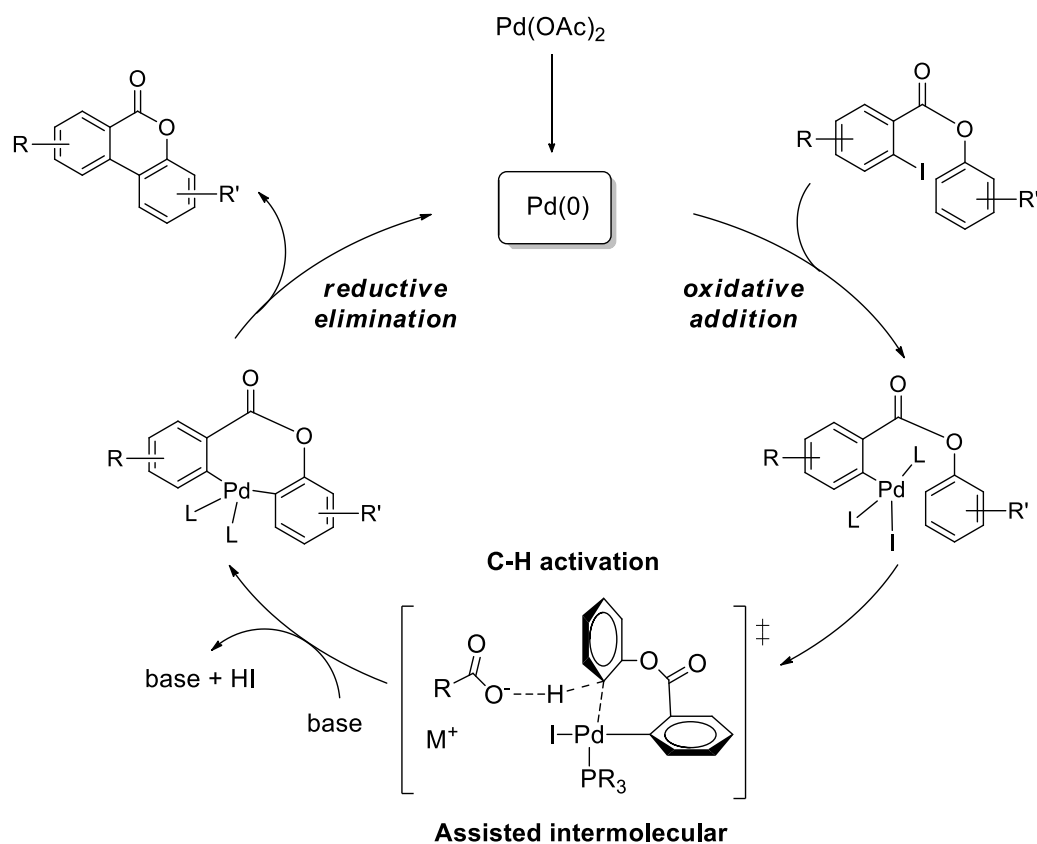


Figure 4. Intramolecular biaryl coupling reaction

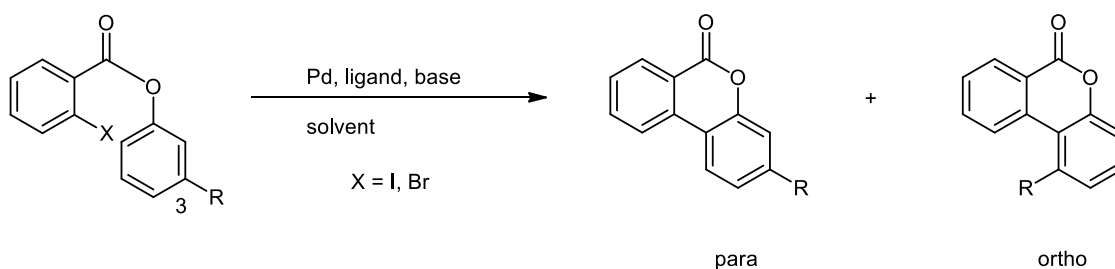
The reaction mechanism of the intramolecular biaryl coupling reaction is estimated as follows

22-25

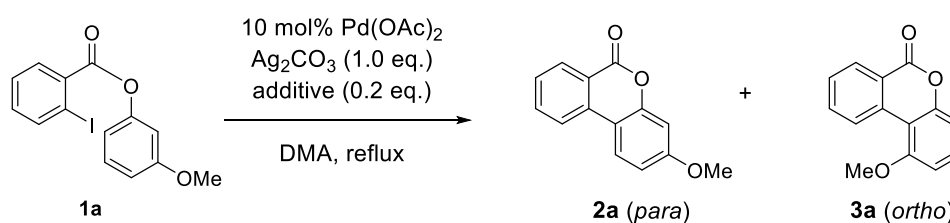


Scheme 2. Mechanism of the intramolecular biaryl coupling reaction.

First, Pd (II) is reduced to Pd (0) by a ligand or solvent, and Pd (0) is oxidatively added to the substrate. Next, at the reaction point on the phenoxy side, activation of the C-H bond occurs via the transition state of the intermolecular assisted intermolecular mechanism, and the C-Pd bond is formed by the base abstracting the proton. Finally, reductive elimination forms a biaryl bond, constructing a 6*H*-dibenzo [b, d] pyran-6-one backbone and regenerating Pd (0). However, this intramolecular biaryl coupling reaction has a problem of regioselectivity than the estimation mechanism shown in Scheme 4. That is, if a substituent is present at the 3-position of the phenoxy site, two positional isomers (para and ortho) may be generated.



In order to investigate the regioselectivity in this reaction, experiments were conducted using a phenyl benzoate derivative having a methoxy group (Table 1).⁸¹⁻⁸²



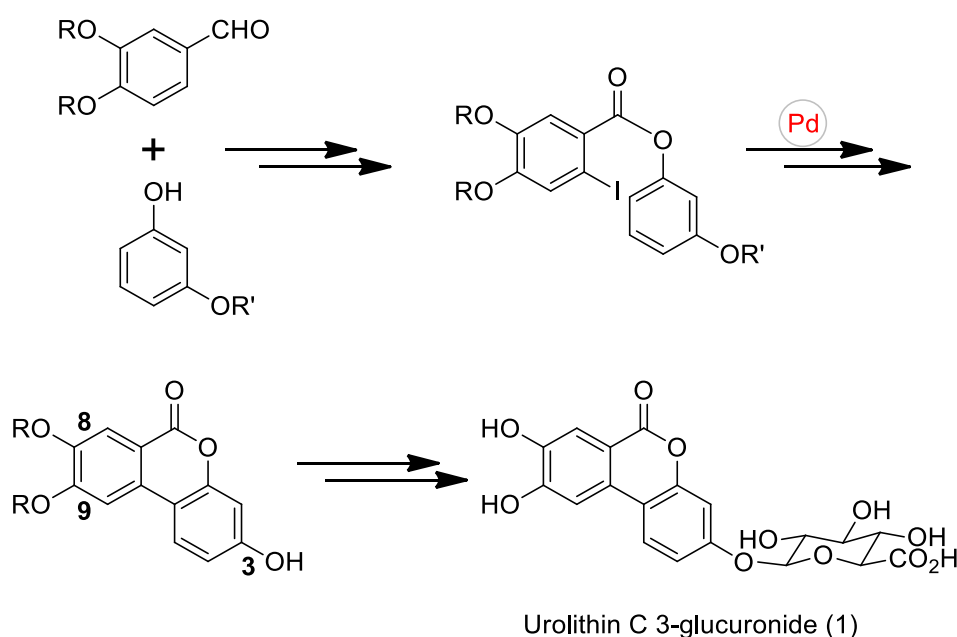
entry	base	ligand	yield (%)	<i>para</i> : <i>ortho</i> ^{a)}
1	K ₂ CO ₃	-	93	2 : 1
2	K ₂ CO ₃	<i>n</i> Bu ₃ P	73	1.4 : 1
3	Ag ₂ CO ₃	-	92	4.5 : 1
4	Ag ₂ CO ₃	<i>n</i> Bu ₃ P	81	0.5 : 1

a) Determined by ¹H-NMR analysis.

In Entry 1 and 2, K₂CO₃ is used as the base, and the conditions with and without the ligand are examined. The production ratios of 2a and 3a were slightly different with and without the ligand. In Entry 3 and 4, the base was changed to Ag₂CO₃ for examination. The 2a production ratio was highest in the absence of the ligand, entry 3. The 2a and 3a production ratios were reversed in the presence of the ligand, entry 4. From this, it was clarified that the regioselectivity was reversed depending on the presence or absence of the ligand in the reaction using Ag₂CO₃ as the base.

Our Synthetic Plan

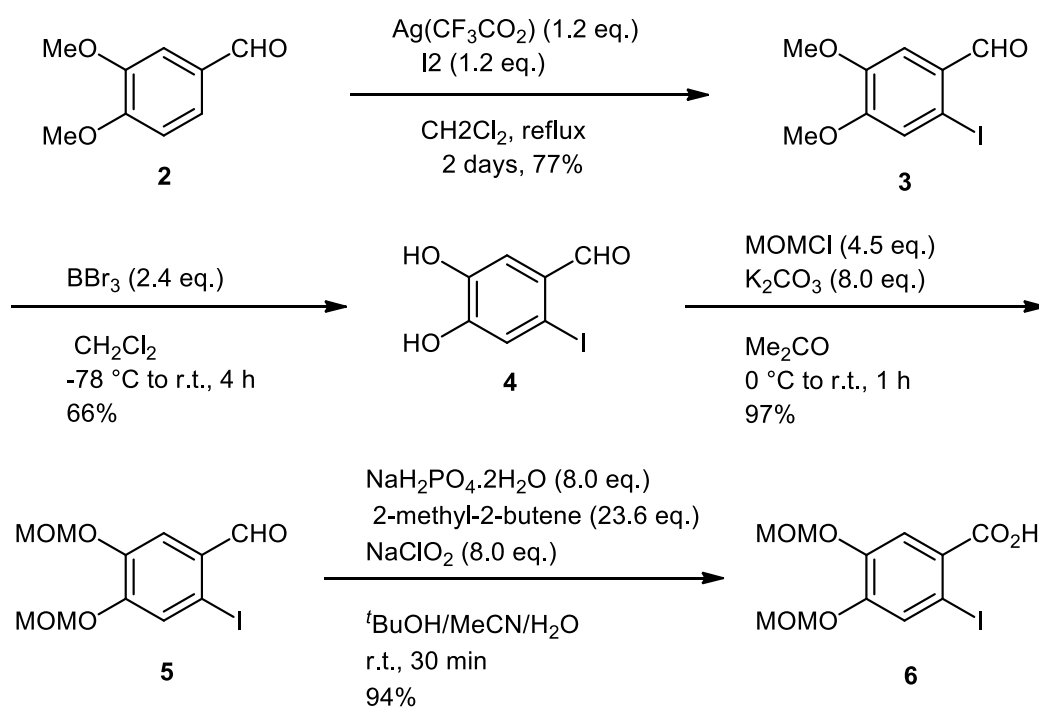
As shown in Scheme 1, Uro-C is chemically synthesized but Uro-C 3-glucur is not yet synthesized^{62,67}. Since Uro-C has three hydroxyl groups at the reaction site, the Uro-C derivative can be obtained by intramolecular biaryl coupling reaction by using a protecting group different from the hydroxyl group at the 8-position and the 9-position. Then, we realized that Urolithin C 3-glucuronide could be synthesized by removing only one protecting group from the Uro-C derivative (Scheme 3).



Scheme 3.

3.2.1 Synthesis of carboxylic acid derivative

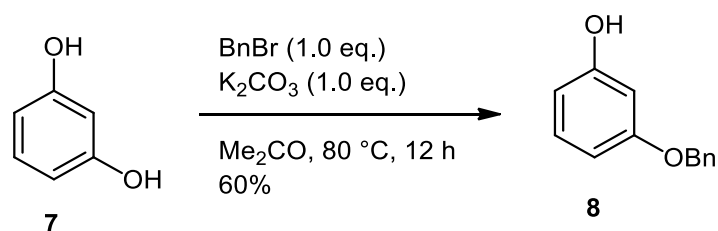
According to the retrosynthetic analysis we chose 3,4-dimethoxybenzaldehyde **2** as the first substrate. Starting material **2** was converted into iodine compound **3**, with reference to a published paper⁷³, followed by demethylation using BBr_3 . As depicted in Scheme 4, the iodine compound **3** was transformed into its MOM ether **5**.⁷⁴ The substrate **5** was subjected to Pinnick oxidation to yield carboxylic acid **6**.⁷⁵



Scheme 4. Synthesis of carboxylic acid derivative

3.2.2 Synthesis of monobenzyl derivative

For Esterification, commercially available resorcinol **7** was monobenzylated with benzyl bromide to give a monobenzyl derivative **8** (Scheme 5).⁸⁷⁻⁸⁸

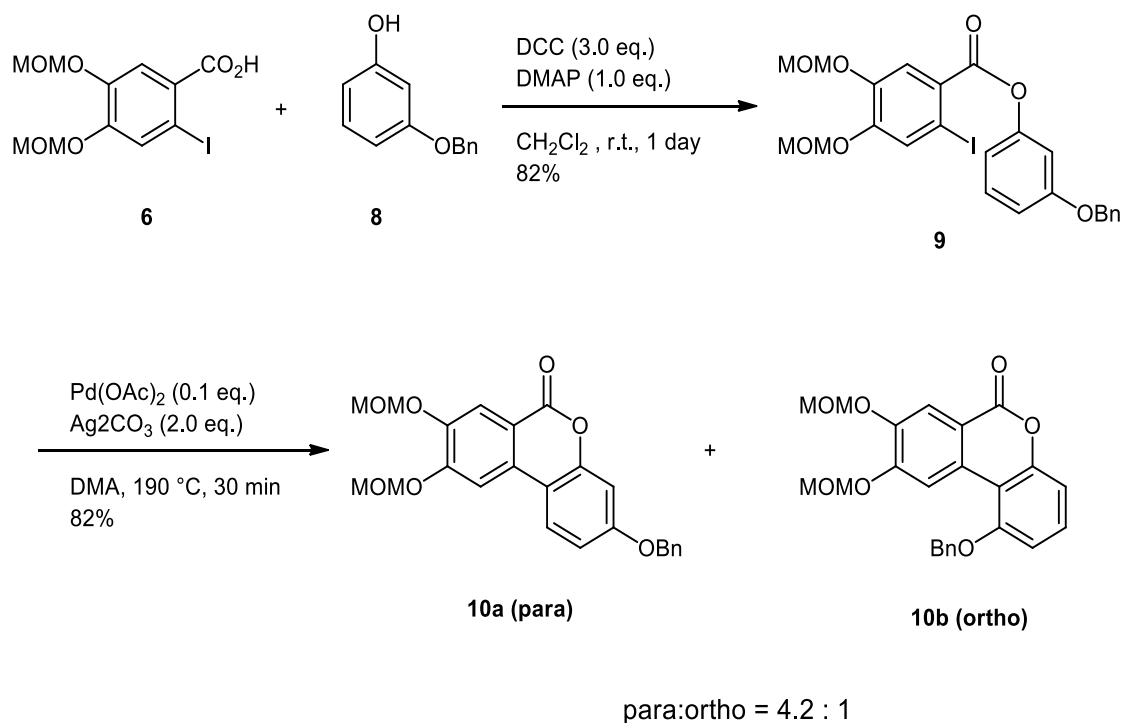


Scheme 5. Synthesis of monobenzyl derivative

3.2.3 Intramolecular coupling reaction for 10a and 10b

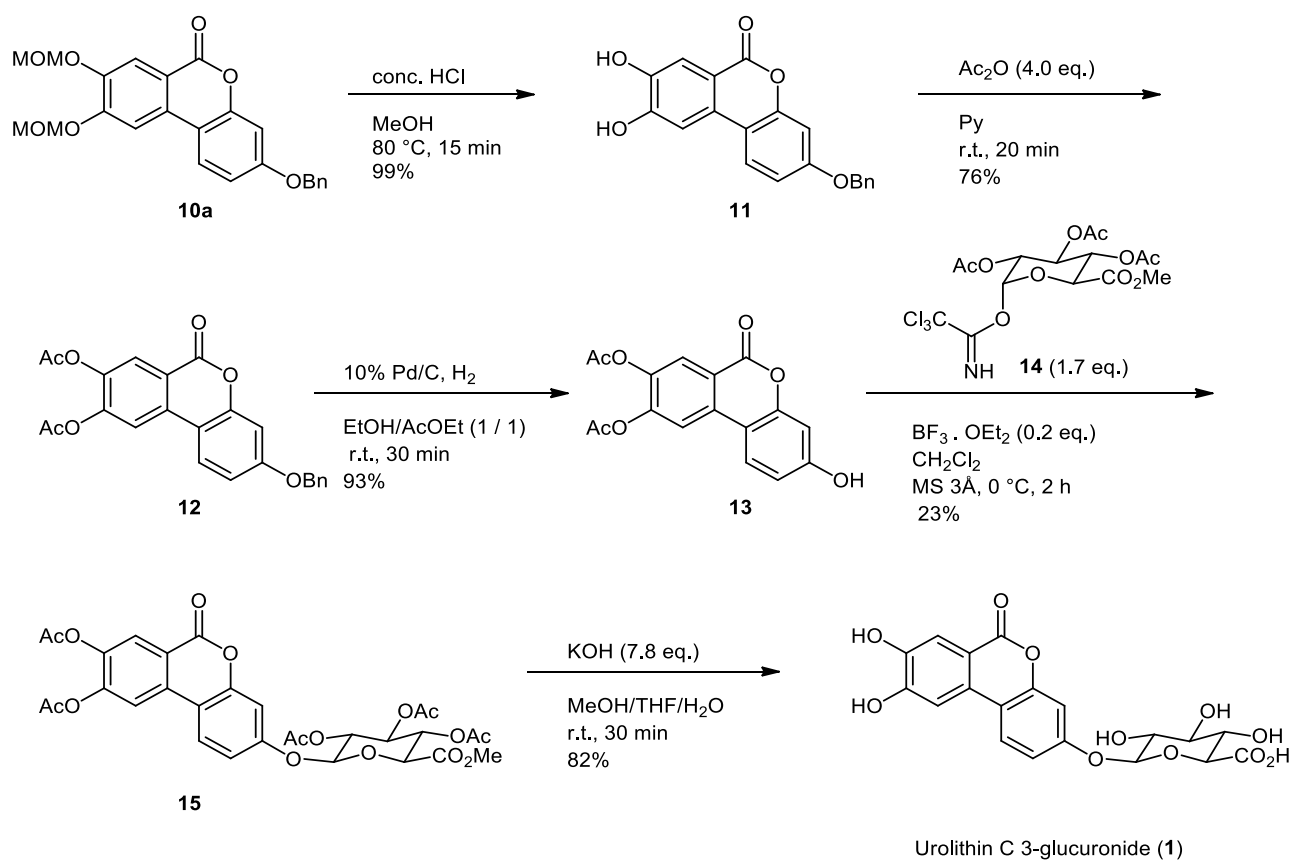
Treating carboxylic acid **6** with prepared monobenzyl derivative **8**, using *N,N'*-dicyclohexylcarbodiimide (DCC) gave the coupling precursor **9** through condensation.⁷⁸⁻⁷⁹ Exposure of the resulting compound **9** on the use of a palladium-catalyzed intramolecular

biaryl coupling reaction afforded a mixture of compound **10a** and its regioisomer **10b** in the ratio 4.2:1.0 (Scheme 6).⁸⁰⁻⁸²



Scheme 6. Intramolecular coupling reaction for **10a** and **10b**

Next, glucuronide which is a moiety of the urolithin C 3-glucuronide was constructed following a known procedure.⁸³⁻⁸⁴ The desired product **10a** was isolated from the regioisomers (**10a** and **10b**), and these MOM groups were deprotected by concentrated hydrochloric acid (HCl) to give Uro-C derivative **11** without further purification. The resulting compound was reacted with acetic anhydride (Ac₂O) to obtain the protected compound **12**.⁸⁵⁻⁸⁶ Hydrogenation of the compound **12** with 10% Pd/C under H₂ yielded the hydroxyl compound **13** as a crude mixture.³¹ The glycosylation reaction of the compound **13** and the already prepared trichloroacetoimidate **14** was performed based on the conditions described in scheme 7 to yield the precursor **15** of Uro-C 3-glucur.⁶⁴ Finally, the synthesis of Urolithin C 3-glucuronide (**1**) was achieved by hydrolysis of the precursor **15** using potassium hydroxide (KOH) in MeOH/THF/H₂O (Scheme 7).⁸⁸



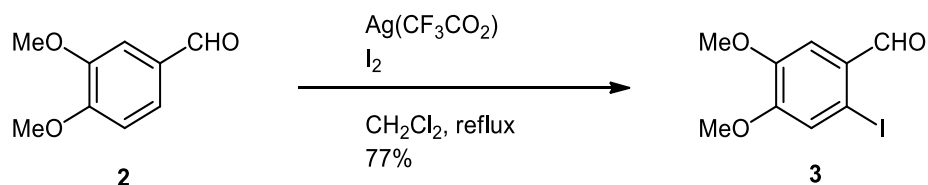
Scheme 7. Synthesis of urolithin C 3-glucuronide (uro-C 3-glur) (**1**)

3.3 Experimental Section

General: All reactions were executed under N₂ atmosphere. Reaction solvents were used after purification by the standard methods. Reaction progress was observed with the help of thin-layer chromatography by making use of silica gel (70 F₂₅₄) TLC plates and UV light as an agent for visualizing. Silica gel (particle size: 100–200 and 230–400 mesh). Melting points (mp) were obtained using the Yanaco micro melting point apparatus and are uncorrected. With the Shimadzu FTIR 8400 spectrophotometer, the IR spectra were acquired. The JOEL α -400 MHz instrument was utilized for obtaining ¹H and ¹³C NMR spectra with the couplings being shown in Hertz and chemical shift being expressed as δ ppm. Silica gel column chromatography was accomplished using Wakogel 60N, 63~212 μ m.

Experimental Procedures

2-Iodo-4,5-dimethoxybenzaldehyde (**3**)

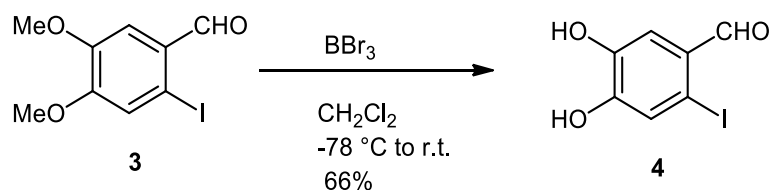


Under N₂, 3,4-dihymethoxybenzaldehyde (**2**) (4.0 g, 24.0 mmol) was dissolved in DCM (180 mL) followed by the addition of AgTFA (6.38 g, 28.8 mmol) and slow addition of I₂ (7.34 g, 28.8 mmol) using a dropping funnel and kept at stirring at 55 ° C for 2 days. The reaction mixture was filtered, transferred into a separatory funnel, washed with sat. Na₂S₂O₃ aq. (200 mL \times 3), washed with Brine (200 mL), dried with MgSO₄, concentrated, and the solvent was evaporated under reduced pressure to leave a brown solid residue. Obtain (10.0 g). The obtained solid residue was subjected to open column chromatography (ϕ = 4.8 cm, l = 7 cm, H: A = 5: 1) with Hexane: AcOEt = 6: 1 to 5: 1 to yield **3** (5.40 g, 77%)

White solid: mp 138-140 °C (lit. mp 137-139 °C)

¹H NMR (400 MHz, CDCl₃) δ 9.87 (s, 1H), 7.42 (s, 1H), 7.31 (s, 1H), 3.96 (s, 3H), 3.92 (s, 3H).

4,5-dihydroxy-2-iodobenzaldehyde (**4**)

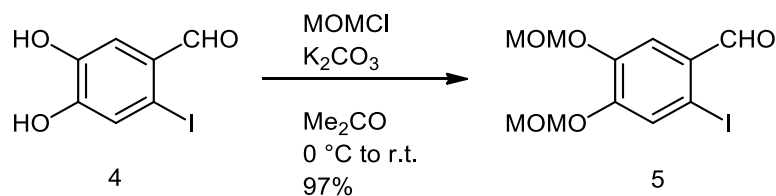


Under a nitrogen atmosphere, 2-Iodo-4,5-dimethoxybenzaldehyde (**3**) (9.9 g, 34 mmol) was dissolved in DCM (100 mL) and stirred at -78 °C for 10 minutes. BBr₃ (17% in DCM, 81 mL, 81 mmol) was added dropwise using a dropping funnel, and the mixture was returned to room temperature and stirred for 4 hours. The reaction was quenched with ice H₂O (200 mL) followed by the addition of 1M HCl. The aqueous layer was extracted with EtOAc 3 times, once with brine, dried over MgSO₄, and concentrated under reduced pressure. Black residue **4** was obtained (5.87 g, 66%).

Black solid: mp 169-171 °C (lit. mp 169-171 °C)

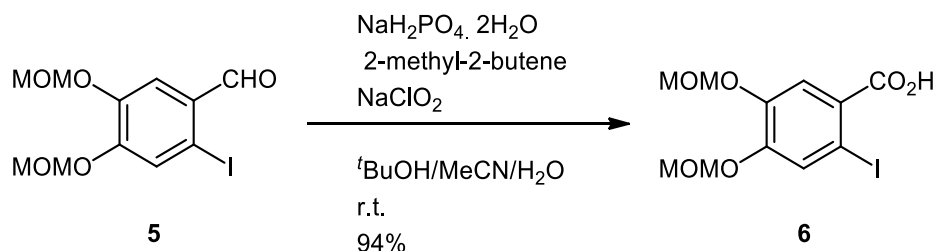
¹H NMR (400 MHz, Acetone-*d*₆) δ 9.80 (s, 1H), 7.43 (s, 1H), 7.38 (s, 1H).

2-Iodo-4,5-dimethoxymethoxybenzaldehyde (**5**)



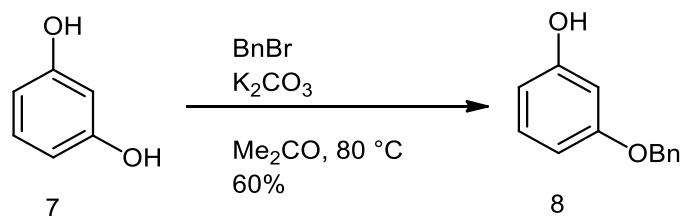
K₂CO₃ (122 mg, 0.88 mmol) was added to a solution of substrate **4** (31 mg, 0.11 mmol) in acetone (2 mL), which was stirred until the temperature reached 0 °C under an N₂ atmosphere. MOMCl (0.045 mL, 0.51 mmol) was slowly poured into the mixture over a period of 15 mins, keeping the temperature at 0 °C. After adding all the reagents, the temperature increased to room temperature. The reaction mixture was stirred for another 1 h at room temperature. The reaction mixture was then quenched with saturated aqueous NH₄Cl at 0 °C and extracted with CHCl₃ (3 × 10 mL). The combined extracts were washed with saturated aqueous NaHCO₃ (2 × 10 mL) and saturated brine (1 × 10 mL). The combined organic layer was dried over MgSO₄, filtered, and concentrated under reduced pressure. The residue was purified using silica gel column chromatography (hexane/ethyl acetate = 6:1) to afford **5** (39.8 mg, 97%) as a yellow solid: mp 79.2-80.7 °C; ¹H NMR (400 MHz, CDCl₃) δ 9.88 (s, 1H), 7.68 (s, 1H), 7.66 (s, 1H), 5.31 (s, 2H), 5.27 (s, 2H), 3.53 (s, 3H), 3.50 (s, 3H); ¹³C NMR (100MHz, CDCl₃) δ 194.6, 152.6, 147.4, 129.3, 126.1, 116.6, 95.1, 95.0, 93.2, 56.6, 56.4; IR (KBr) ν 2955, 2360, 1682, 1576, 1414, 1257, 923, 744, 613 cm⁻¹; HRMS (EI) *m/z* [M⁺] calcd for C₁₁H₁₃O₅I 351.9808, found 351.9795.

2-iodo-4,5-dimethoxymethoxybenzoic acid (**6**)



To a solution of the **5** (9.2 g, 26.1 mmol) in *t*-BuOH (350 mL) and MeCN (85 mL) were added $\text{NaH}_2\text{PO}_4 \cdot 2\text{H}_2\text{O}$ (32.7 g, 209 mmol) and 2-methyl-2-butene (64 mL, 601 mmol). The solution was cooled to 0 °C and NaClO_2 (19 g, 209 mmol) dissolved in H_2O (175 mL) was slowly added. After stirring for 30 min, AcOEt and H_2O were added. The organic layer was separated, and the aqueous layer was extracted with AcOEt (3 × 200 mL). The combined organic layer was washed with saturated brine (1 × 100 mL) and dried over MgSO_4 . The combined organic layer was filtered and concentrated under reduced pressure. The crude residue was purified by recrystallization from AcOEt to afford **6** (9.0 g, 94%) as a white powder: mp 163.8-165.0 °C; ^1H NMR (400 MHz, CDCl_3) δ 7.87 (s, 1H), 7.77 (s, 1H), 5.28 (s, 2H), 5.26 (s, 2H), 3.52 (s, 6H); ^{13}C NMR (100MHz, $\text{DMSO}-d_6$) δ 166.8, 149.5, 146.2, 128.3, 126.1, 118.8, 94.8, 94.6, 85.8, 56.6, 55.9; IR (KBr) ν 2991, 2511, 1693, 1587, 1434, 1330, 1157, 1074, 716 cm^{-1} ; HRMS (EI) m/z [M^+] calcd for $\text{C}_{11}\text{H}_{13}\text{O}_6\text{I}$ 367.9757, found 367.9722.

3-Benzyloxy-phenol (**8**)

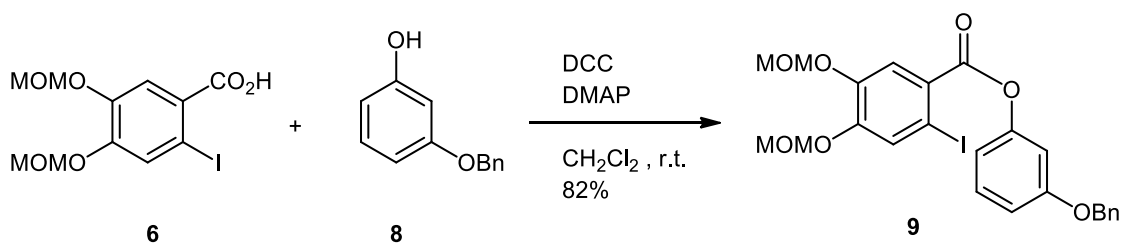


Acetone (44 ml) was added to **7** (5.3 g, 48.1 mmol) and K₂CO₃ (3.33 g, 24.0 mmol), and the mixture was stirred under a nitrogen atmosphere. BnBr (2.85 mL, 24.0 mmol) was added dropwise to the reaction solution over 10 minutes, and the mixture is stirred at 80 °C. After 12 hours, K₂CO₃ is filtered and washed with AcOEt, washed with water (20 mL × 2), and Brine (20 mL), dried with MgSO₄ and concentrated to obtain a brown oily residue (9.6 g). The obtained oily residue was subjected to open column chromatography (φ = 4.8 cm, l = 5 cm, Hexane: AcOEt = 9: 1 to 4: 1 to obtain **8** as a pale-yellow (2.89 g, 60%).

(Lit. mp 52 °C)^{31, 32}

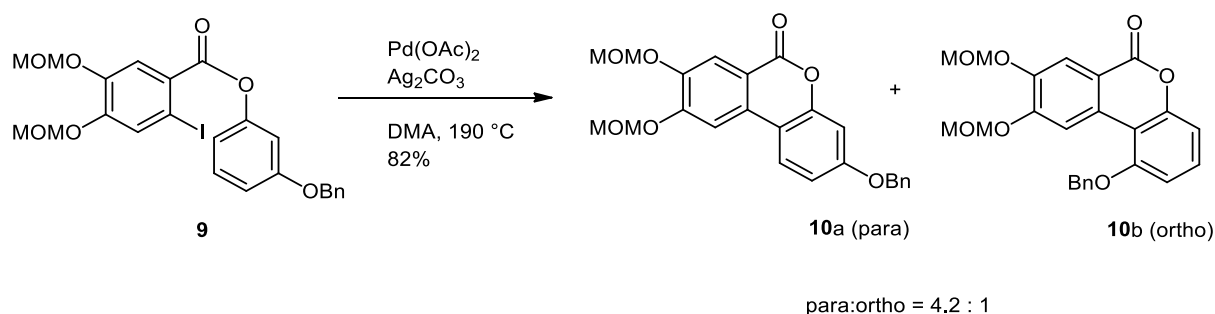
¹H NMR (400 MHz, CDCl₃) δ : 7.45-7.30 (m, 5H), 7.14 (t, *J* = 8.0 Hz, 1H), 6.57 (dd, *J* = 8.0 Hz, *J* = 2.0 Hz, 1H), 6.49 (t, *J* = 2.0 Hz, 1H), 6.44 (dd, *J* = 8.0 Hz, *J* = 2.0 Hz, 1H), 5.04 (s, 2H), 4.86 (s, 1H).

3-(Benzyloxy)phenyl 2-iodo-4,5-dimethoxymethoxybenzoate (**9**)



6 (2.4 g, 6.5 mmol) and DCC (4.0 g, 19.5 mmol) were dissolved in DCM (25 mL). To the solution, **8** (1.3 g, 6.8 mmol) dissolved in DCM (25 mL) and DMAP (0.79 g, 6.5 mmol) were added, then the mixture was stirred for 1 day at room temperature. After the reaction, the mixture was filtered, and the solvent was removed in vacuo. The crude residue was purified by silica gel column chromatography (hexane/ethyl acetate/ dichloromethane = 5:1:1) to afford **9** (2.9 g, 82%) as a yellow solid: mp 61.2-62.2 °C; ¹H NMR (400 MHz, CDCl₃) δ 7.90 (s, 1H), 7.79 (s, 1H), 7.45-7.30 (m, 6H), 6.90-6.85 (m, 3H), 5.30 (s, 2H), 5.28 (s, 2H), 5.07 (s, 2H), 3.53 (s, 6H); ¹³C NMR (100MHz, CDCl₃) δ 163.8, 159.7, 151.6, 150.7, 146.7, 136.6, 129.8, 128.6, 128.4, 128.0, 127.5, 126.7, 119.6, 114.2, 112.6, 108.7, 95.4, 95.1, 86.7, 70.2, 60.4, 56.6, 56.5; IR (KBr) ν 1678, 1284, 976 cm⁻¹; HRMS (EI) *m/z* [M⁺] calcd for C₂₄H₂₃O₇I 550.0488, found 550.0457.

3-(benzyloxy)-8,9-dimethoxymethoxy-6*H*-enzo[*b,d*]pyrane-6-one (9a) and 1-(benzyloxy)-8,9-dimethoxymethoxy-6*H*-benzo[*b,d*]pyrane-6-one (9b)



Under an N₂ atmosphere, **9** (1.4 g, 2.54 mmol), Ag₂CO₃ (1.4 g, 5.09 mmol), and Pd(OAc)₂ (57.0 mg, 0.25 mmol) were dissolved in DMA (32 mL), then the mixture was stirred at 190 °C for 30 min. After being stirred, the reaction mixture was cooled to room temperature and filtered. Water was added to the mixture, and the aqueous layer was extracted with AcOEt (3 × 100 mL). The combined organic layer was washed with water (5 × 20 mL), saturated brine (1 × 20 mL), and dried over MgSO₄. The combined organic layer was filtered and concentrated under reduced pressure. The crude residue was purified by silica gel column chromatography (hexane/ethyl acetate = 4:1) to afford a mixture of **10a** and **10b** (0.88 g, 82%) in the ratio 4.2:1 as a yellow solid.

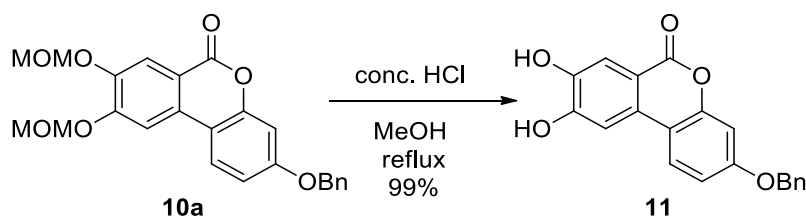
Major isomer (9a)

White solid: mp 121.7-122.4 °C; ¹H NMR (400 MHz, CDCl₃) δ 8.03 (s, 1H), 7.85 (d, *J* = 8.4 Hz, 1H), 7.71 (s, 1H), 7.47-7.33 (m, 5H), 6.99-6.92 (m, 2H), 5.43 (s, 2H), 5.34 (s, 2H), 5.13 (s, 2H), 3.57 (s, 3H), 3.54 (s, 3H); ¹³C NMR (100MHz, CDCl₃) δ 161.1, 160.0, 153.6, 152.2, 147.0, 136.1, 131.2, 128.7, 128.3, 127.5, 123.5, 116.1, 114.1, 112.9, 111.3, 106.8, 102.6, 95.4, 95.1, 70.4, 56.6, 56.5; IR (KBr) ν 1707, 1618, 1501, 1448, 1367, 1331, 1269, 1007 cm⁻¹; HRMS (EI) *m/z* [M⁺] calcd for C₂₄H₂₂O₇ 422.1365, found 422.1361.

Minor isomer (9b)

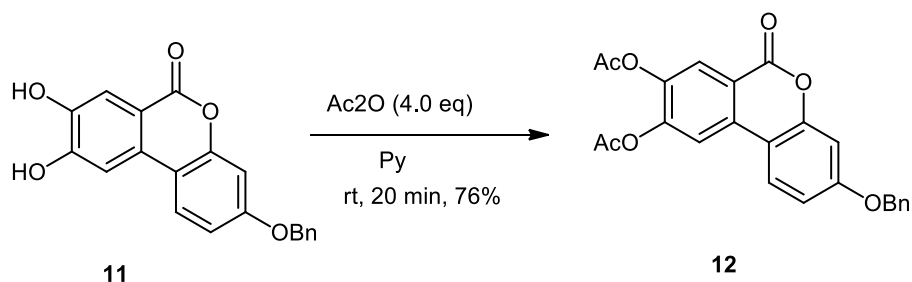
White solid: mp 114.0-114.9 °C; ¹H NMR (400 MHz, CDCl₃) δ 8.64 (s, 1H), 8.09 (s, 1H), 7.55-7.33 (m, 6H), 7.71 (s, 1H), 7.03 (d, *J* = 7.4 Hz, 1H), 6.94 (d, *J* = 8.2 Hz, 1H), 5.32 (s, 2H), 5.22 (s, 2H), 4.84 (s, 2H), 3.51 (s, 3H), 3.36 (s, 3H); ¹³C NMR (100MHz, CDCl₃) δ 160.9, 156.9, 152.4, 152.0, 146.8, 135.8, 130.3, 129.1, 128.8, 128.7, 128.6, 115.9, 115.3, 113.3, 110.6, 108.4, 107.7, 95.1, 94.3, 71.6, 56.6, 56.4 ; IR (KBr) ν 1711, 1603, 1506, 1462, 1359, 1283, 1070, 993 cm⁻¹; HRMS (EI) *m/z* [M⁺] calcd for C₂₄H₂₂O₇ 422.1365, found 422.1377.

3-(benzyloxy)-8,9-dihydroxy-6H-dibenzo[*b,d*]pyrane-6-one (11)



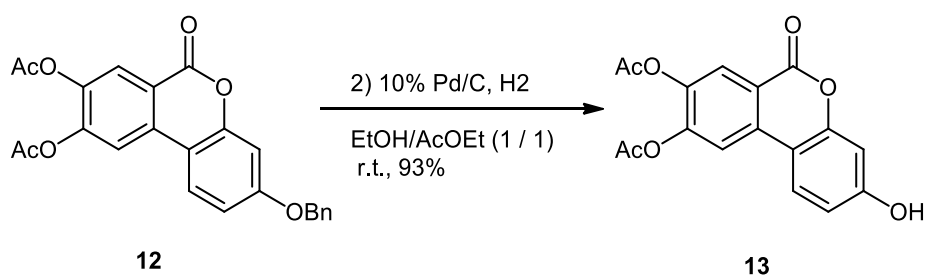
10a (210 mg, 0.50 mmol) was dissolved in MeOH (6.6 mL) and concentrated HCl (0.047 mL) was added. The mixture was heated to 80 °C, and stirred for 15 min. After reacting, the solvent was removed under reduced pressure, which gave a solid residue, and was dissolved in AcOEt. The organic layer was washed with saturated aqueous NaHCO₃ (2 × 5 mL) and saturated Brine (1 × 5 mL). The organic phase was dried over MgSO₄, filtered and concentrated under reduced pressure to afford the crude product **11** (164 mg, 99%) as a white solid and was used without further purification: mp 206.0-206.7 °C; ¹H NMR (400 MHz, Acetone-*d*₆) δ 7.95 (d, *J* = 8.8 Hz, 1H), 7.62 (s, 1H), 7.53 (s, 1H), 7.48 (d, *J* = 7.4 Hz, 2H), 7.39-7.28 (m, 3H), 6.97 (dd, *J* = 8.8 Hz, *J* = 2.5 Hz, 1H), 6.92 (d, *J* = 2.4 Hz, 1H), 5.20 (s, 2H); ¹³C NMR (100MHz, Acetone-*d*₆) δ 161.0, 160.7, 153.7, 153.0, 146.8, 137.8, 130.6, 129.5, 129.3, 129.0, 128.5, 124.5, 115.4, 114.8, 113.4, 112.4, 110.8, 107.8, 103.2, 70.9 ; IR (KBr) ν 3448, 3354, 1695, 1620, 1578, 1452, 1269, 1170 cm⁻¹; HRMS (EI) *m/z* [M⁺] calcd for C₂₀H₁₄O₅ 334.0841, found 334.0862.

8,9-diacetoxy-3-Benzyloxy-6*H*-dibenzo[*b,d*]pyran-6-one (**12**)



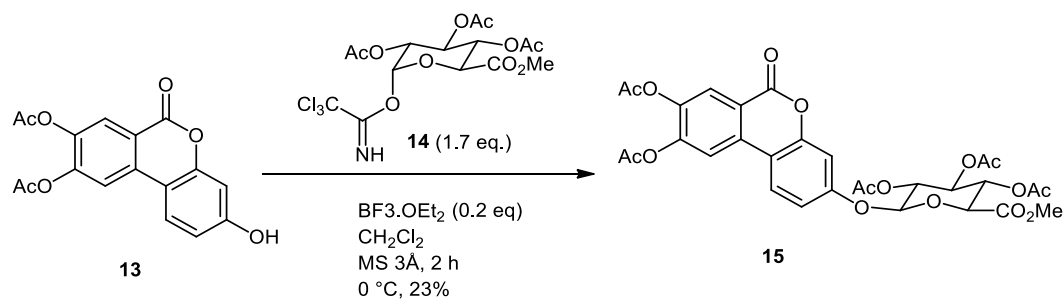
To a solution of **11** (200 mg, 0.60 mmol) in pyridine (0.8 mL), Ac₂O (0.22 mL, 2.4 mmol) was added. The reaction mixture was stirred at room temperature for 20 min and water was subsequently poured into the reaction mixture. The aqueous phase was acidified to pH 2 and extracted with AcOEt (3 × 3 mL). The combined organic phase was washed with 0.1 M HCl (3 × 3 mL), saturated brine (1 × 3 mL), and dried over MgSO₄. The combined organic phase was filtered and concentrated under reduced pressure. The crude residue was purified by recrystallization from AcOEt to afford **12** (190 mg, 76%) as a white solid: mp 182.3-183.0 °C; ¹H-NMR (400 MHz, CDCl₃) δ 8.16 (s, 1H), 7.84-7.81 (m, 2H), 7.46-7.34 (m, 5H), 7.00-6.93 (m, 2H), 5.14 (s, 2H), 2.37 (s, 3H), 2.35 (s, 3H); ¹³C-NMR (100 MHz, CDCl₃) δ 167.9, 167.5, 161.0, 160.1, 152.6, 148.1, 141.7, 135.9, 134.4, 128.7, 128.3, 127.6, 125.4, 124.0, 118.2, 116.2, 113.3, 110.4, 102.7, 70.5, 20.8, 20.5; IR (KBr) 1736, 1620 cm⁻¹; HRMS (EI) *m/z* [M⁺] calcd for C₂₄H₁₈O₇ 418.1052, found 418.1058.

8,9-diacetoxy-3-hydroxy-6*H*-dibenzo[*b,d*]pyran-6-one (13)



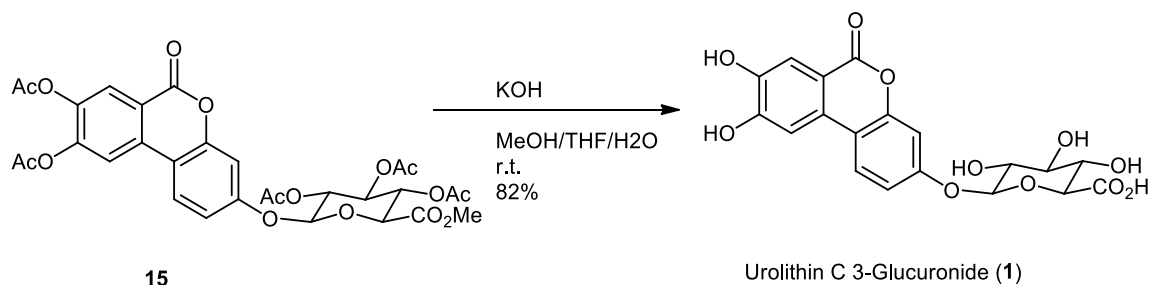
To a solution of **12** (174 mg, 0.41 mmol) in EtOH/AcOEt (3.6 mL/3.6 mL), 10% Pd-C (112 mg) was added. Under an H₂ atmosphere, the reaction mixture was stirred at room temperature for 30 min and hydrogenated. The mixture was filtered to remove the catalyst, then concentrated under reduced pressure to afford the crude product **13** (126 mg, 93%) as a white solid which was used without further purification: mp 180.9-182.7 °C; ¹H-NMR (400 MHz, acetone-*d*₆) δ 8.08 (dd, *J* = 12.4 Hz, *J* = 8.8 Hz, 3H), 6.92 (dd, *J* = 8.8 Hz, *J* = 2.4 Hz, 1H), 6.82 (d, *J* = 2.8 Hz, 1H), 2.36 (s, 3H), 2.35 (s, 3H); ¹³C-NMR (100 MHz, acetone-*d*₆) δ 132.4, 130.1, 128.8, 68.2, 38.7, 30.9, 30.3, 29.7, 28.9, 23.7, 23.0, 14.0, 10.9; IR (KBr) 3398, 1705, 1622, 1452, 1371.3, 1200, 923 cm⁻¹; HRMS (EI) *m/z* [M⁺] calcd for C₁₇H₁₂O₇ 328.0583, found 328.0577.

Urolithin C 3-(2,3,4-tri-O-acetylglucuronide) methyl ester (**15**)



Under an N_2 atmosphere, to a solution of **13** (115 mg, 0.35 mmol), MS3Å (150 mg) and trichloroacetoimidate **14** (290 mg, 0.59 mmol) in anhydrous DCM (7 mL) at 0 °C, $\text{BF}_3 \cdot \text{OEt}_2$ (0.07 mmol) were added. After 2 h, the reaction mixture was quenched with NEt_3 and concentrated in vacuo. The crude residue was purified by silica gel column chromatography (hexane/ethyl acetate = 3:1 to 1:1) to afford **15** (48.3 mg, 23%) as a white solid: mp 219.7-220.6 °C; ^1H NMR (400 MHz, CDCl_3) δ 8.18 (s, 1H), 7.87-7.83 (m, 2H), 6.99 (dd, $J = 7.8$ Hz, $J = 2.0$ Hz, 2H), 5.39-5.24 (m, 4H), 4.24 (q, $J = 3.2$ Hz, 1H) 3.75 (s, 3H), 2.37 (s, 3H), 2.35 (s, 3H), 2.08 (d, $J = 8.4$ Hz, 9H); ^{13}C NMR (100MHz, CDCl_3) δ 170.0, 169.3, 167.5, 166.6, 159.7, 158.3, 152.2, 148.2, 142.2, 133.8, 125.6, 124.2, 118.6, 116.6, 114.5, 112.6, 105.1, 98.5, 72.7, 71.6, 70.8, 68.9, 53.1, 20.8, 20.6, 20.5 ; IR (KBr) ν 1757, 1620, 1572, 1493, 1251, 1173, 1043 cm^{-1} ; $[\alpha]^{25.1}_{\text{D}} -35.1$ (c 0.5, CHCl_3); HRMS (EI) m/z [M^+] calcd for $\text{C}_{30}\text{H}_{28}\text{O}_{16}$ 644.1377, found 644.1343.

Urolithin C 3-Glucuronide (1)



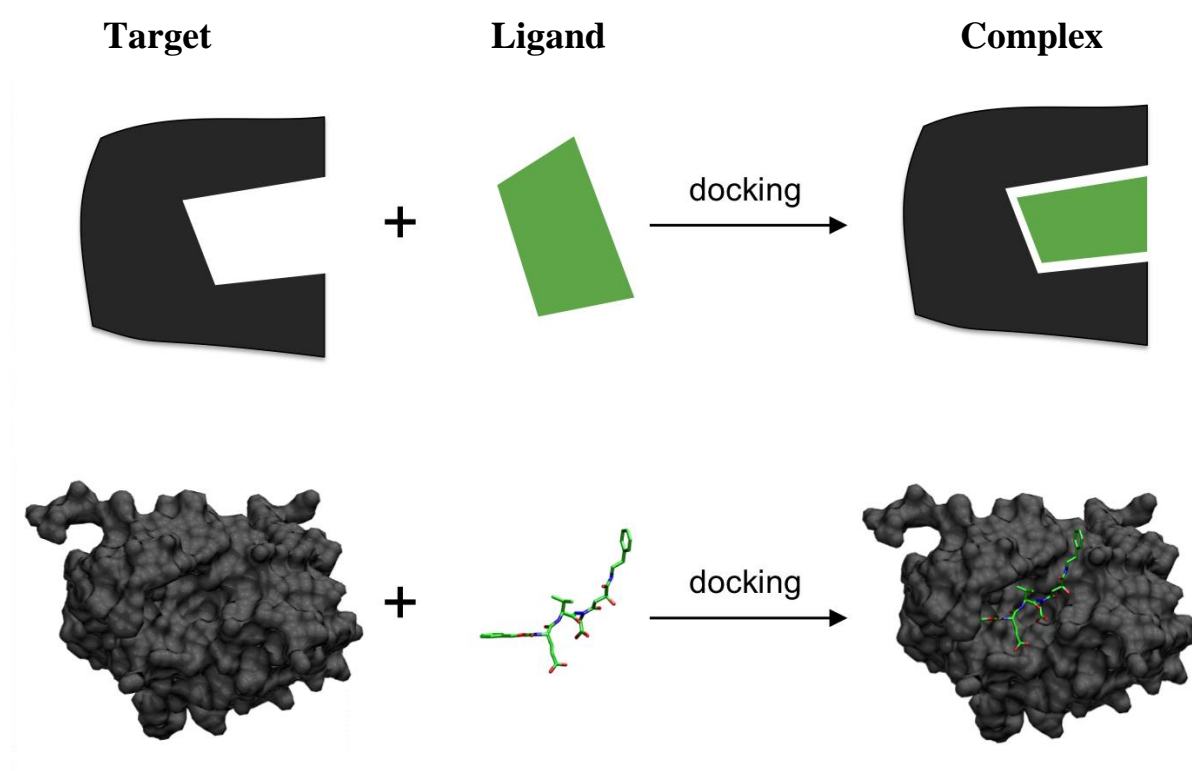
15 (20 mg, 0.03 mmol) was dissolved in MeOH/THF/H₂O (0.25 mL/0.5 mL/0.25 mL) and KOH (13.5 mg, 0.24 mmol) was added to the solution, then the reaction mixture was stirred at room temperature for 30 min. The mixture was quenched with Amberlite to pH 4, filtered and concentrated under reduced pressure. The crude residue was purified by silica gel column chromatography (MeOH/H₂O = 1:9) to afford **Urolithin C 3-glucuronide (1)** (11.6 mg, 82%) as a brown solid: mp 179.0-179.6 °C; ¹H NMR (400 MHz, MeOH-*d*₄) δ 7.89 (d, *J* = 8.8 Hz, 1H), 7.56 (s, 1H), 7.42 (s, 1H), 7.08-7.01 (m, 2H), 5.09 (dd, *J* = 5.6 Hz, 2.0 Hz, 1H), 4.07 (d, *J* = 9.6 Hz, 1H), 3.66-3.51 (m, 3H); ¹³C NMR (100MHz, MeOH-*d*₄) δ 161.9, 158.2, 153.6, 151.4, 146.6, 129.5, 123.2, 114.1, 113.6, 113.2, 111.9, 106.6, 104.5, 100.8, 76.0, 73.2, 71.7, 29.4; IR (KBr) ν 3321, 1718, 1620, 1506, 1267, 1038 cm⁻¹; HRMS (EI) *m/z* [M⁺] calcd for C₁₉H₁₆O₁₁ 420.0693, found 420.0705.

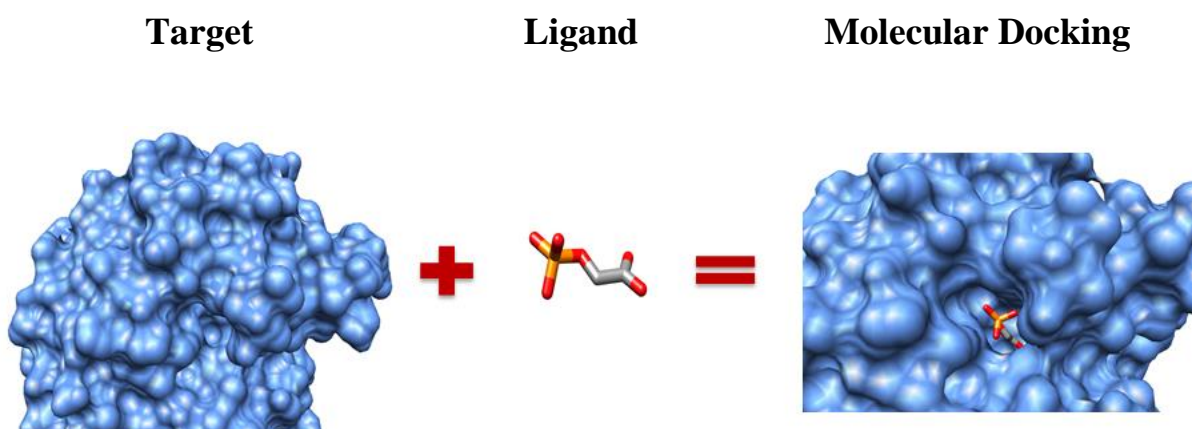
Chapter 4

Molecular docking

4 Introduction

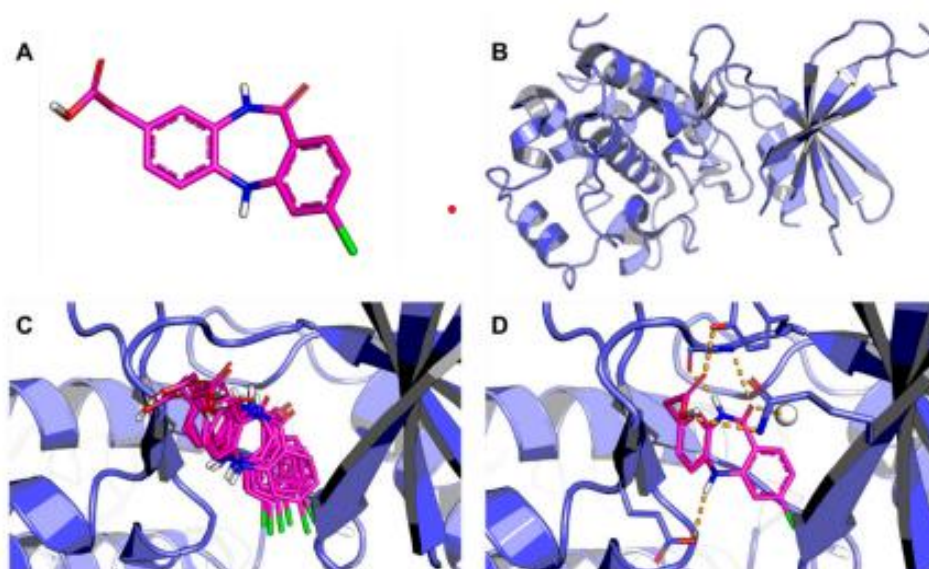
Finding active compounds from existing chemicals is typically the first step in a drug research and development project. While several pharmaceutical companies have their libraries with millions of compounds, maintaining the library and performing high-throughput screening are both expensive. Virtual scanning is a new way to complete the screening of millions of millions of compounds within a few days³⁸. When the 3D structure of the target protein is visible, molecular docking is one of the most commonly used virtual screening methods. This approach was able to predict the ligand-protein binding affinity as well as the structure of the protein-ligand complex, which is useful knowledge for lead optimization. Indeed, molecular docking has been used for more than three decades, and it has resulted in the discovery and development of a large number of new drugs.³⁹ Although it will undoubtedly continue to play an important role, molecular docking is still a long way from being a complete success in terms of success rate. This is also why high-throughput screening is still commonly used in many pharmaceutical firms today. The docking-based virtual screening will never have a chance to play an irreplaceable role in drug discovery and development until its success rate is essentially improved.





4.1 Protein-ligand complex structure by docking

The 3D structure of a protein-ligand complex provides atomic-level information on the ligand-target protein binding process, which is especially useful for lead optimization. Several studies have shown that the docked binding conformation of a ligand can vary significantly from the experimentally determined structure, especially, when the ligand is of high flexibility with a small energy barrier between different conformations.⁴⁰ Present docking techniques, for example, have difficulty treating ligands with long-chain or carbohydrate moieties with precision. If the binding pocket contains residues with flexible chains or is formed by flexible loops, the situation becomes even more difficult. Not only could the binding pocket be shifting on its own all the time, but ligand binding could also cause drastic changes in the pocket profile. There is currently no docking software that can accurately deal with the entire intrinsic versatility of the protein structure as well as the mediated transformation of the protein structure. During docking, the overall flexibility of the protein was seldom taken into account.



The molecular docking mechanism is depicted in this diagram. (A) The ligand's three-dimensional structure; (B) the receptor's three-dimensional structure; (C) The ligand is docked into the receptor's binding cavity and the putative conformations are explored; (D) The most probable binding conformation and the associated intermolecular interactions are established. In stick representation, the ligand (magenta carbon) and active site residues (blue carbon) are shown. Water is depicted as a white disk, with dotted lines indicating hydrogen bonds.

Binding thermodynamics & kinetics

If the drug has a higher binding affinity and a longer residence period in the binding pocket, it may have a better therapeutic effect. The Gibbs free energy (G), which is the amount of binding enthalpy (H) and entropy change (S), determines binding affinity. Both words are associated with atomic interactions, but striking a balance between them when optimizing drug candidates is difficult.⁴¹

We are still in the early stages of thermodynamically guided drug design, even though several efforts have been devoted to thermodynamic optimization and several methods have been published, such as enthalpic optimization, thermodynamic optimization plots, and the enthalpic efficiency index. Furthermore, the drug's kinetic residence period is measured by drug-target interaction and dissociation rates. In high-throughput virtual screening, however, no docking software for kinetic prediction is available.

Covalent binding

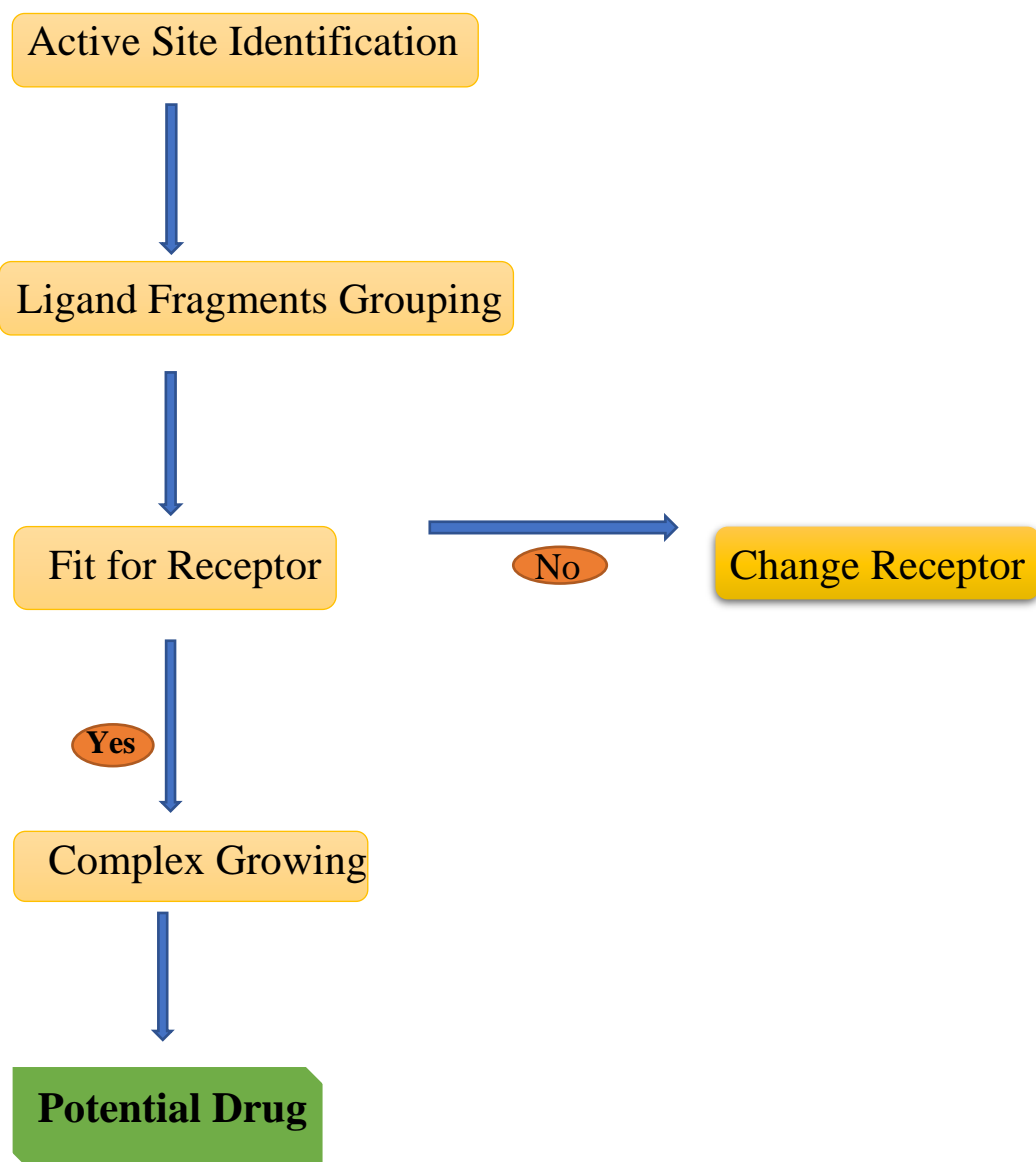
In addition to the expected behavior, molecular docking has a flaw in terms of covalent binding. If a weak covalent bond forms between the ligand and protein residues, such as cysteine, the situation becomes more complicated, as the complex structure undergoes intrinsic vibration. As a result, thermodynamic and kinetic calculations of weak covalent bonding between protein and ligand are difficult. Furthermore, due to the difficulty of disassociation, if off-target binding occurs, covalent ligands are more likely to be associated with toxicity than noncovalent ligands. While the US FDA has approved several covalent medications, mainly for the treatment of infections, cancer, gastrointestinal disorders, central nervous system, and cardiovascular indications, there is still a long way to go before covalent docking achieves a high success rate.⁴²

Nucleic acids

Drug designers and chemical biologists are becoming increasingly interested in the binding of ligands to nucleic acids (RNA or DNA). It is, however, a new challenge for molecular modelers. Given the unique 3D structure of nucleic acids, docking must contend with both the ribose moiety's high structural versatility and extremely anisotropic charge distributions compared to proteins, resulting in additional variability in predicted binding poses and affinity.⁴³ Because of the lack of suitable software and the 3D structure of nucleic acids, molecular docking may be of little use in the development of nucleic acid drugs.

Virtual screening through molecular docking, on the other hand, has already proven to be effective in a number of new drug development ventures and is now widely used in both academic institutions and the pharmaceutical industry. More and more structures will be possible as technology for evaluating the structures of biomacromolecules advances, and molecular docking will continue to play an important role in lead discovery and optimization. However, as previously said, this technology is still far from being a complete success. Future research should focus on accurately predicting binding thermodynamics and kinetics constants, as well as reproducing protein-ligand complex structure while accounting for overall protein versatility and solvent molecules, dealing with covalent binding as well as other biomacromolecule targets such as nucleic acids and protein machinery with precision.

Receptor/ Structure-based approach



Structure-Based Drug Design (SBDD)

In pharmaceutical research and development, understanding the concepts by which small-molecule ligands identify and interact with macromolecules is critical (R & D).⁴⁴ SBDD is the systematic use of structural data (e.g., macromolecular targets, also known as receptors) obtained either experimentally or by computational homology modeling.⁴⁵ The aim is to create ligands with unique electrostatic and stereochemical properties that will bind to receptors with high affinity. Since three-dimensional macromolecular structures are available, a thorough examination of the binding site topology, including the existence of clefts, cavities, and sub-pockets, is possible. Charge distribution and other electrostatic properties may also be closely examined. Current SBDD methods allow the development of ligands with the properties required for effective modulation of the target receptor. High-affinity ligands selectively modulate a validated drug target, interfering with particular cellular processes and resulting in the desired pharmacological and therapeutic results.⁴⁶ SBDD is a cyclic process that involves acquiring information in steps. *In silico* experiments are used to find possible ligands starting with a known target structure. Following these molecular simulation techniques, the most promising compounds are synthesized.⁴⁷ Following that, various experimental platforms are used to assess biological properties such as potency, affinity, and efficacy. The three-dimensional structure of the ligand-receptor complex can be solved once active compounds have been detected. The available structure allows for the observation of a number of intermolecular features that aid in the molecular recognition process. The study of binding conformations, characterization of key intermolecular interactions, characterization of unknown binding sites, mechanistic studies, and the elucidation of ligand-induced conformational changes all benefit from structural descriptions of ligand-receptor complexes. Biological activity data is combined with structural information once a ligand-receptor complex has been determined.^{47,48} As a result, the SBDD process is restarted with new steps to add molecular modifications that may improve the affinity of new ligands for the binding site. Since significant conformational change can occur upon ligand binding, the target receptor's flexibility is an important factor to consider in the modeling process. Techniques like flexible docking and MD are useful for dealing with the problem of versatility.^{49,50}

Protein-Protein Interaction Inhibitors and Molecular Docking

Interactions between various classes of proteins regulate a lot of cellular and biochemical processes.⁵⁴ Defective protein-protein interactions (PPIs) are linked to a variety of diseases, including cancer; as a result, this form of intermolecular occurrence is a highly appealing target in drug development.⁵⁵ The use of biochemical and biophysical data to direct the docking process is a unique technique. PPI interfaces have been established and the reciprocal orientation of the two binding partners determined using data from biomolecular NMR spectroscopy.⁵⁶

4.2 Results and Discussion

Structurally similar eight molecules synthesis is reported in our earlier papers. In this thesis we have explored the docking studies of these molecules in two proteins i.e., CYP1B1 and BCL2.

The docking results of the reported molecules with CYP1B1 protein are tabulated in table 1 and the docking images can be seen in below. All the reported molecules show high binding in CYP1B1 protein and the binding energy ranges from 7.3 to 10.6 Kcal/mole. The high values of binding energy attribute to higher inhibition of the protein and thus all these molecules can act as a potent inhibitor of CYP1B1 protein. Amongst the reported molecules Urolithin M 7-Glucuronide shows highest binding of -10.6 Kcal/mol in the protein cavity. Ligand molecules are stabilized in the protein cavity by hydrophobic interactions and hydrogen bonds. The number of hydrogen bonds explains the stable binding between ligand and protein and during the transport process the ligand gets least released due to external pressure. On an average one hydrogen bond is formed by this series in the protein pocket and the hydrogen bond with glycine is most prominently visible. CYP1B1 protein has a reported inhibitor and the energy of all the molecules is greater than the inhibitor reported. The docking images are shown in three different styles to better understanding the ligand protein binding. The first image shows only the ligand and the amino-acid involved in hydrogen bonding with it, second image shows cartoon view of protein showing the coiling of protein and the third image shows the protein in mesh form helping us understand the penetration of the ligand in the protein. On visualizing the protein in surface, the ligand was completely encapsulated in the cavity and hence mesh visualization is preferred. The entire series of molecules show similar behavior and hence all the images were visualized in mesh view. In ribbon view the protein primary and secondary

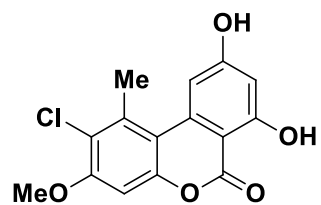
coiling is visible and how well the ligands occupy the cavity is seen. Thus, all the molecules reported in this paper show significant affinity towards CYP1B1 protein and they can prominently act on inhibition of its activity.

4.3 Procedure

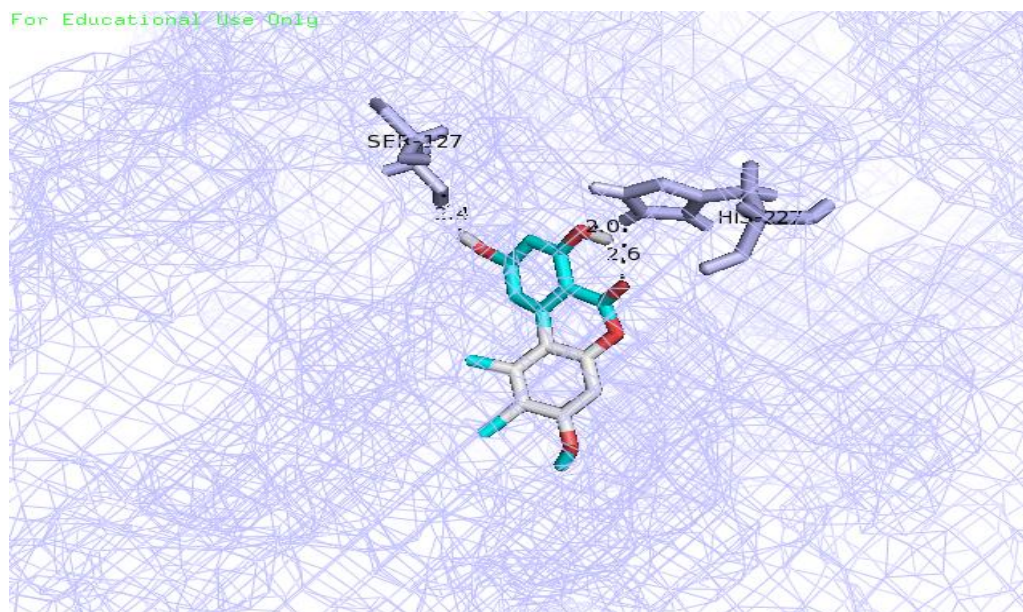
Molecular docking experiments were performed using Autodock vina software. All the chemical structures were drawn in ChemDraw and their 3D structures were procured from 3D corona software. A protein PDB file was obtained from an online depository of RCSB PDB. The protein was cleaned to remove water, heteroatoms, and ligand molecules. The cleaned protein was converted into pdbqt file using MGL Tools software. Docking experiments were performed by keeping protein rigid and allowing the ligand to occupy any place in the cavity. The best-fitted conformation amongst the ten confirmations was visualized using Pymol software.

4.4 Molecular Docking of synthesized compounds in CYP1B1.

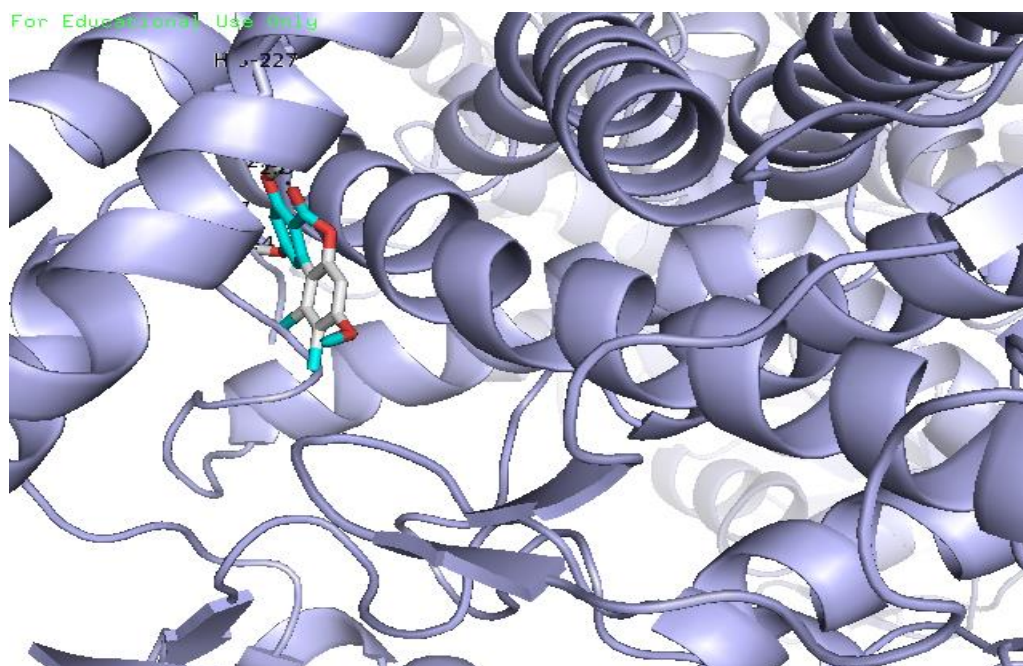
1. Hyalodendriol C



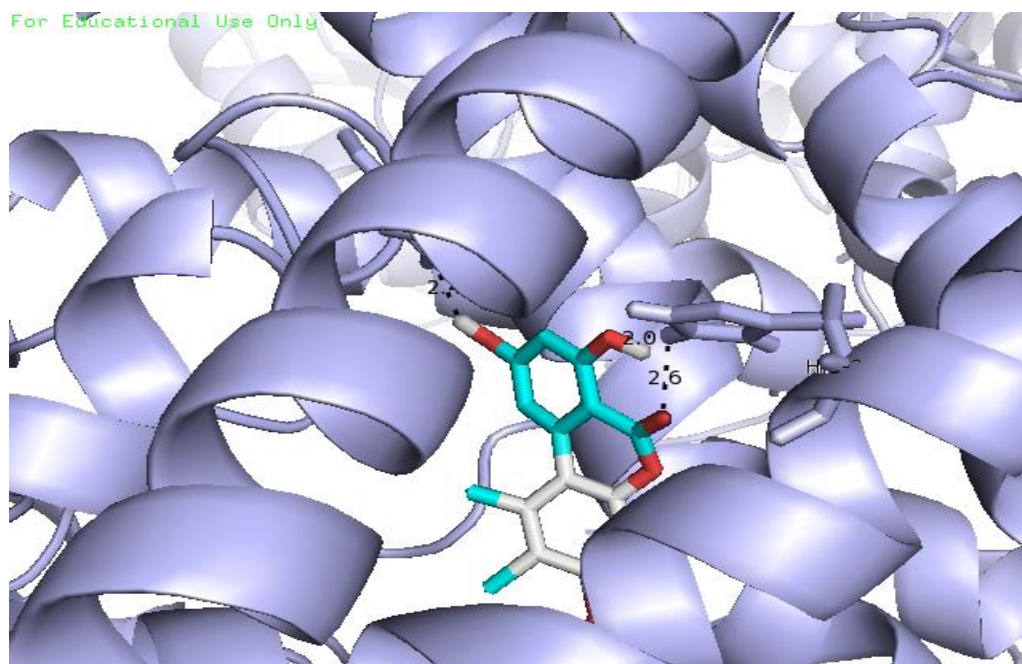
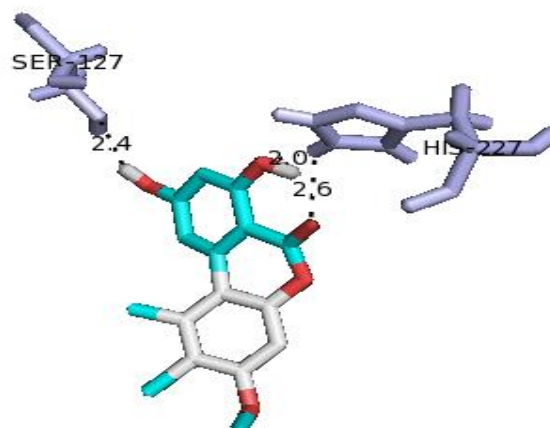
For Educational Use Only



For Educational Use Only

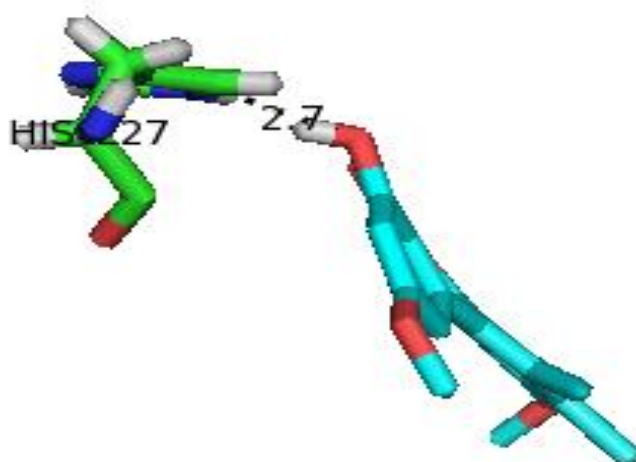
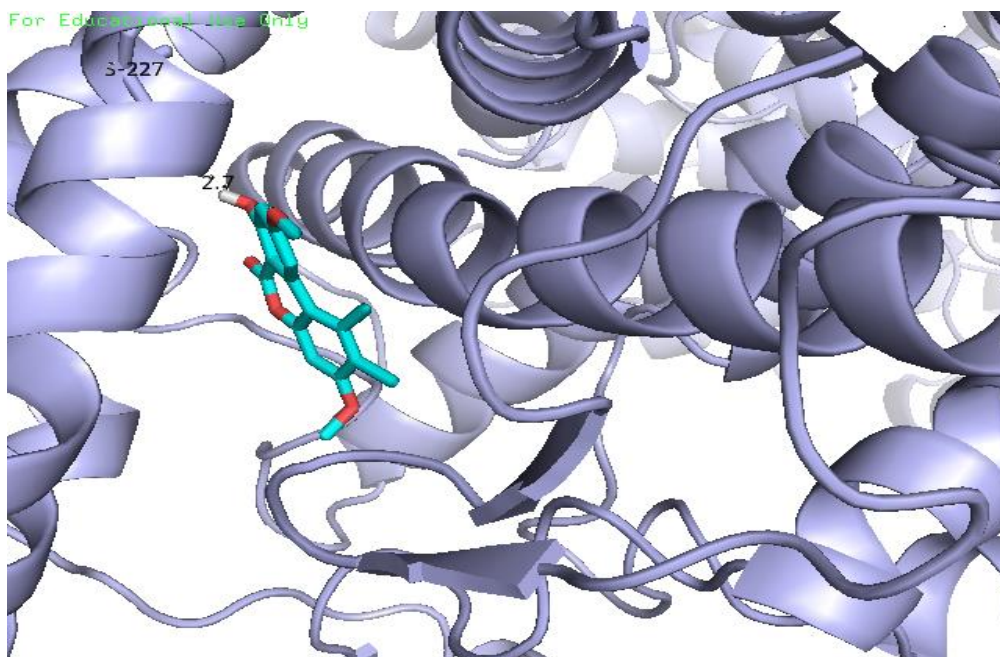
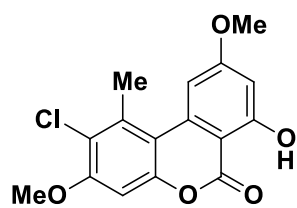


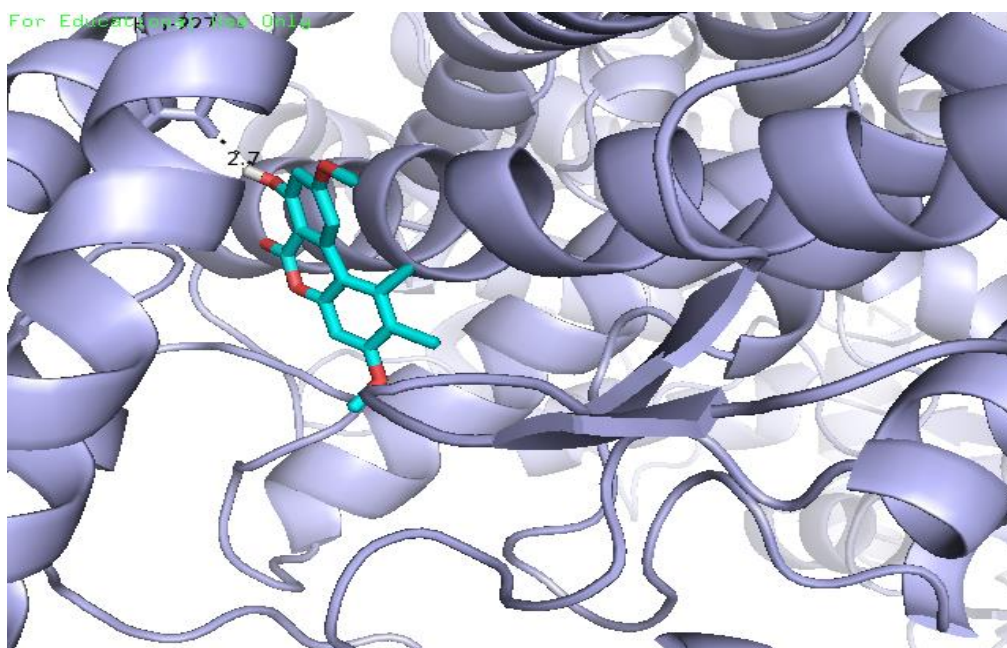
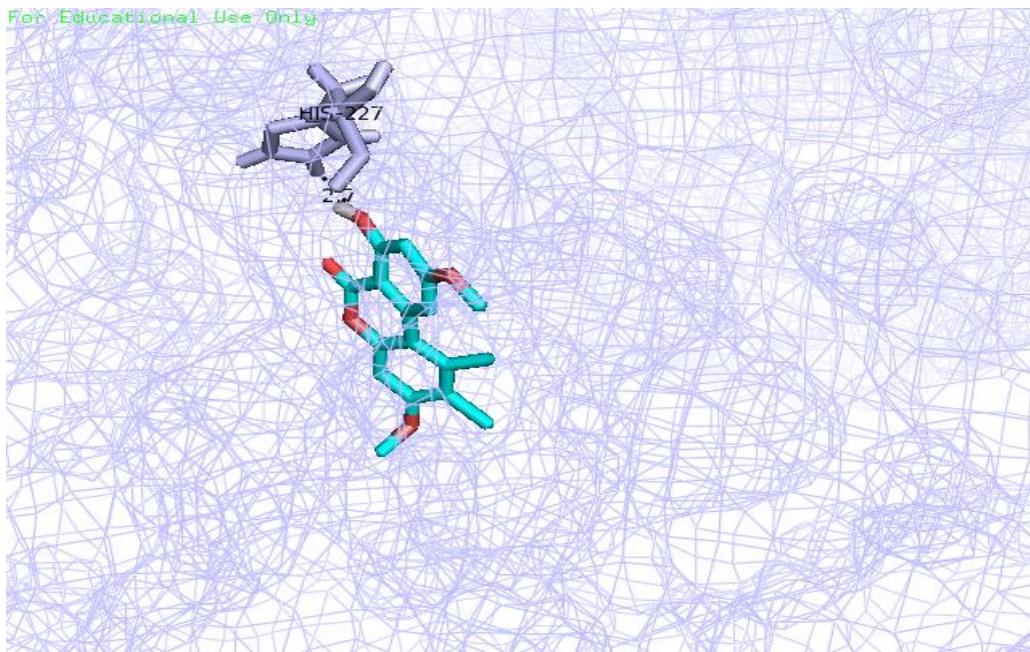
For Educational Use Only



Binding energy [Kcal/mol]	Number of H bonds	Bond distance[Å]	Amino acid residue involved in bonding
-9.3	3	2.0,2.6,2.4	SER-127,HIS-227

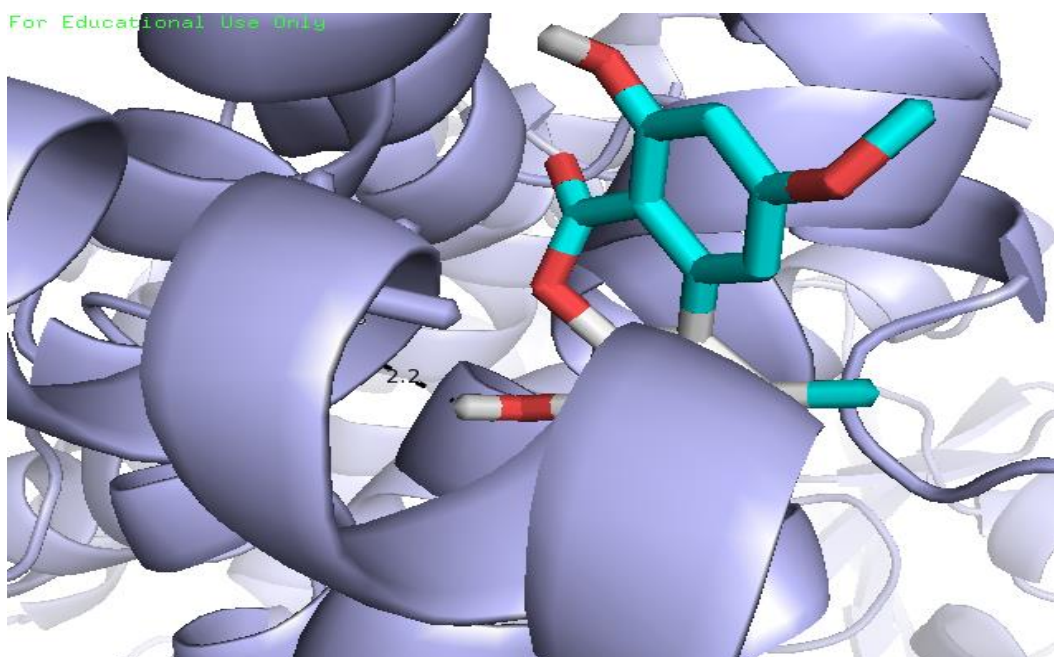
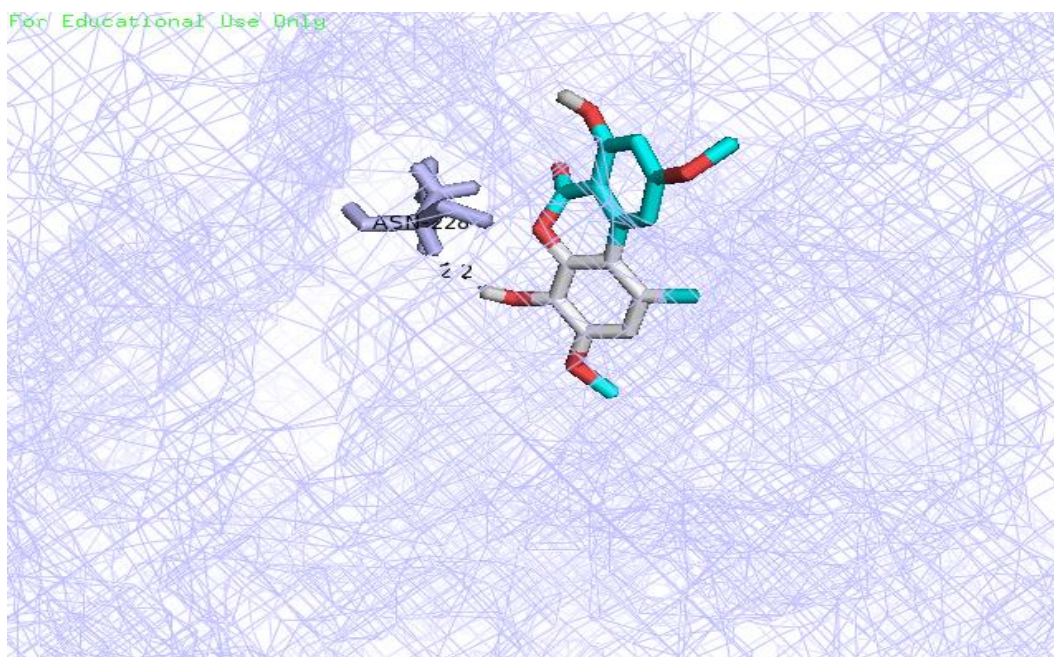
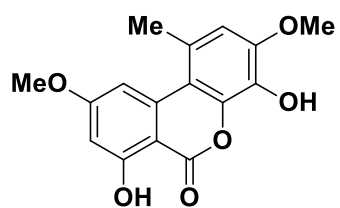
2. Graphis lactone G



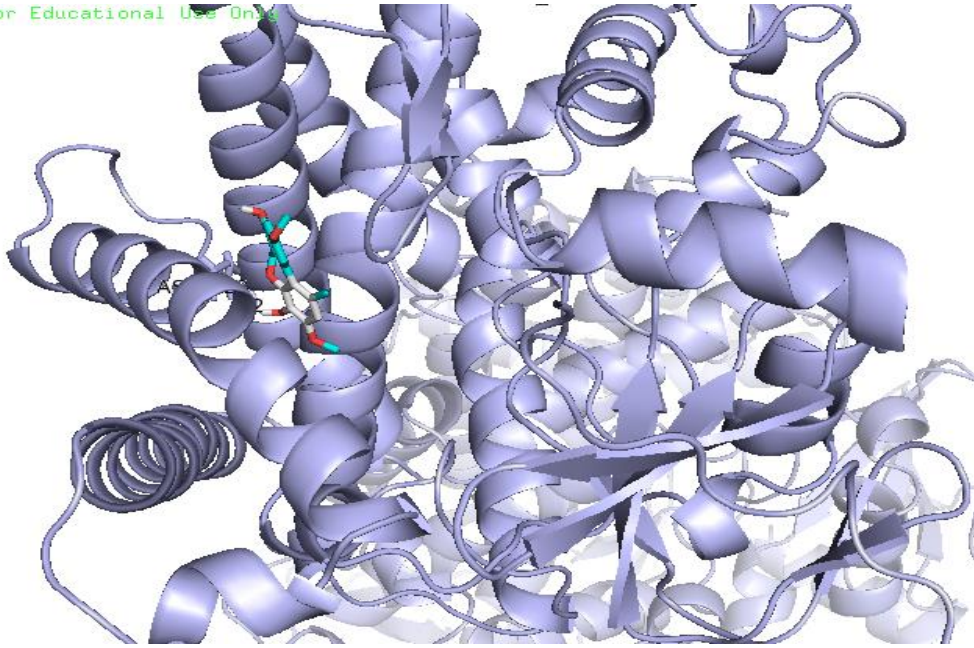


Binding energy [Kcal/mol]	Number of H bonds	Bond distance[Å]	Amino acid residue involved in bonding
-9.2	1	2.7	HIS-227

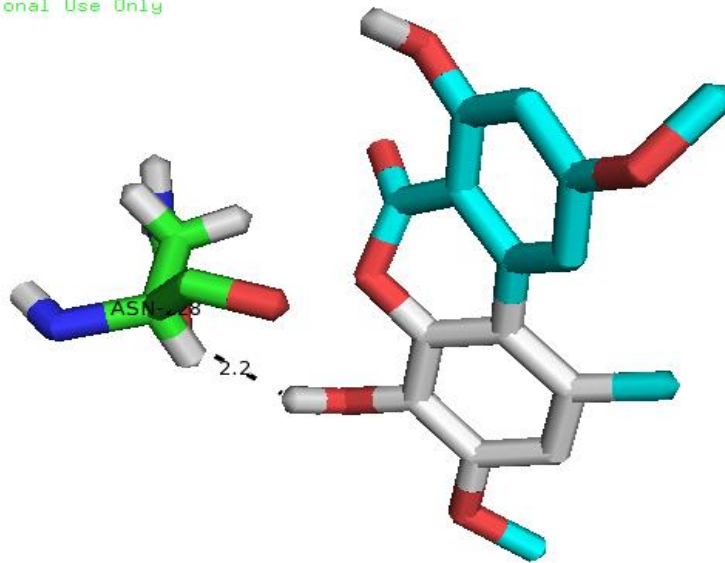
3. Graphislactone A



For Educational Use Only

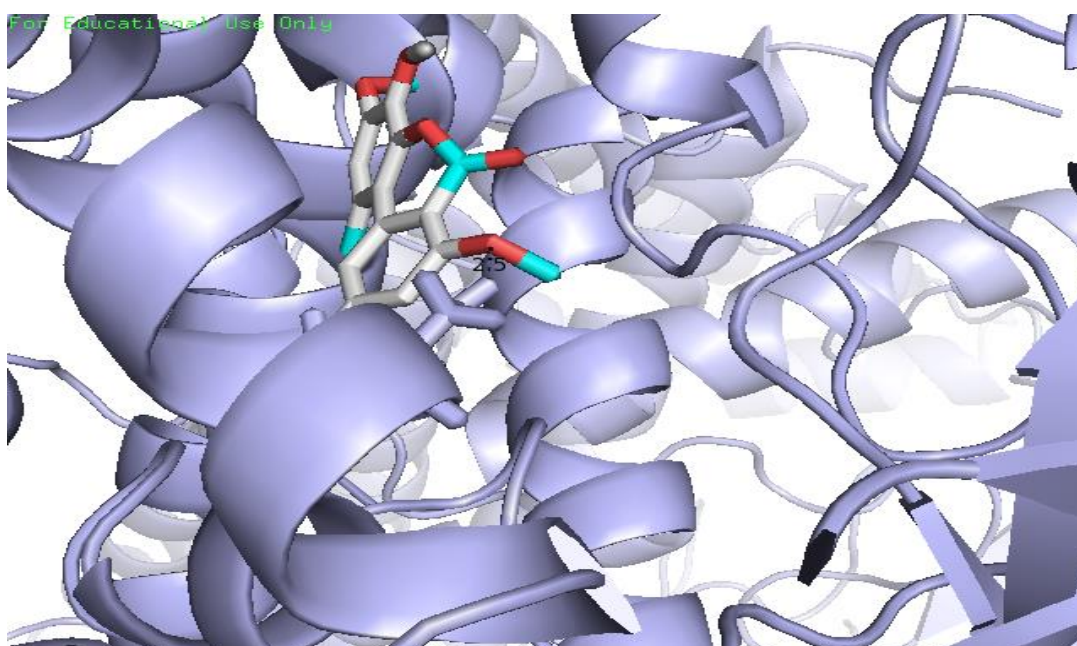
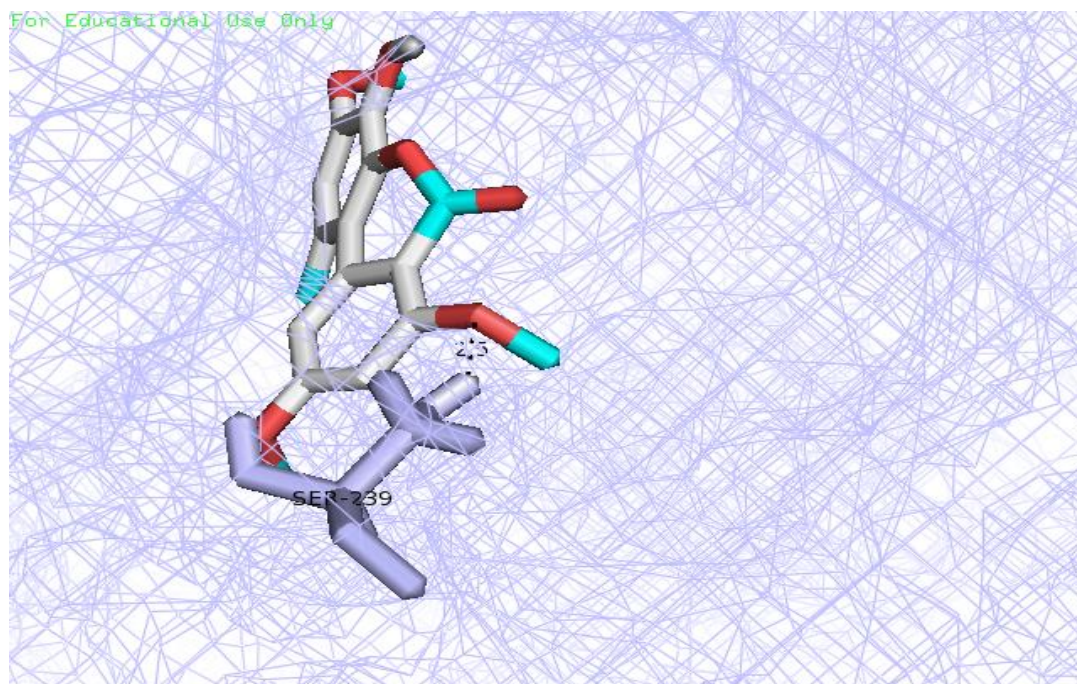
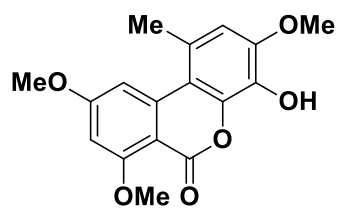


For Educational Use Only

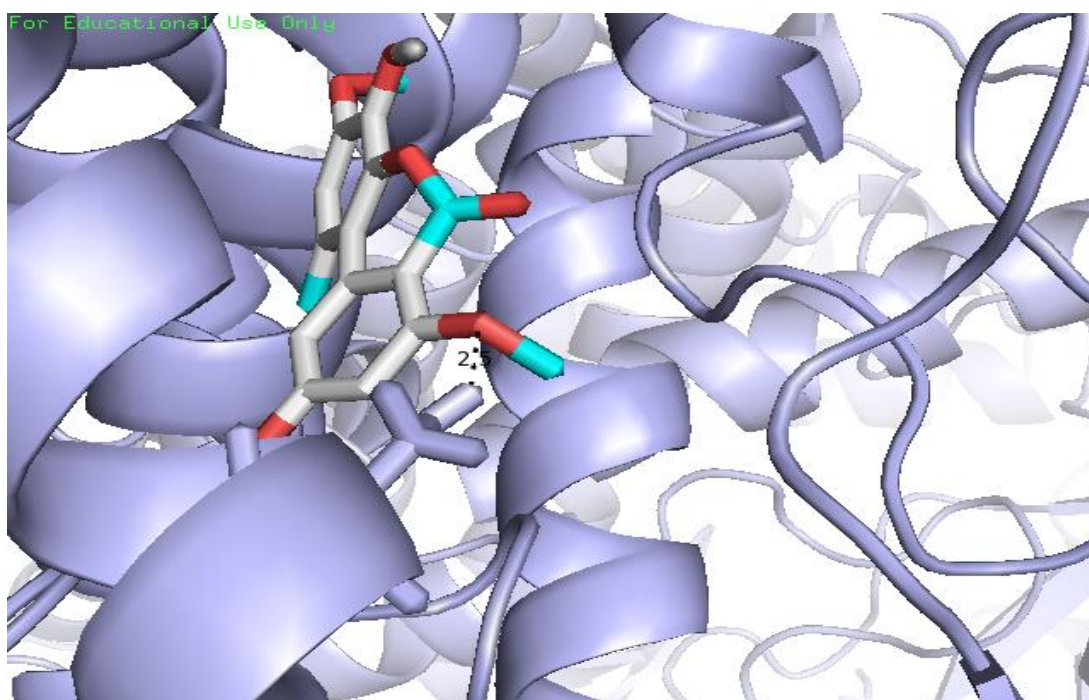
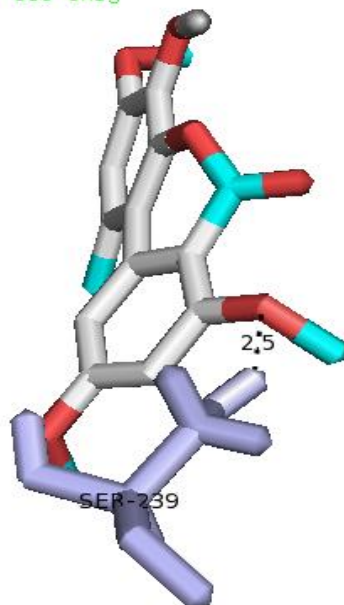


Binding energy [Kcal/mol]	Number of H bonds	Bond distance[Å]	Amino acid residue involved in bonding
-7.5	1	2.2	ASN-228

4. Graphis lactone B

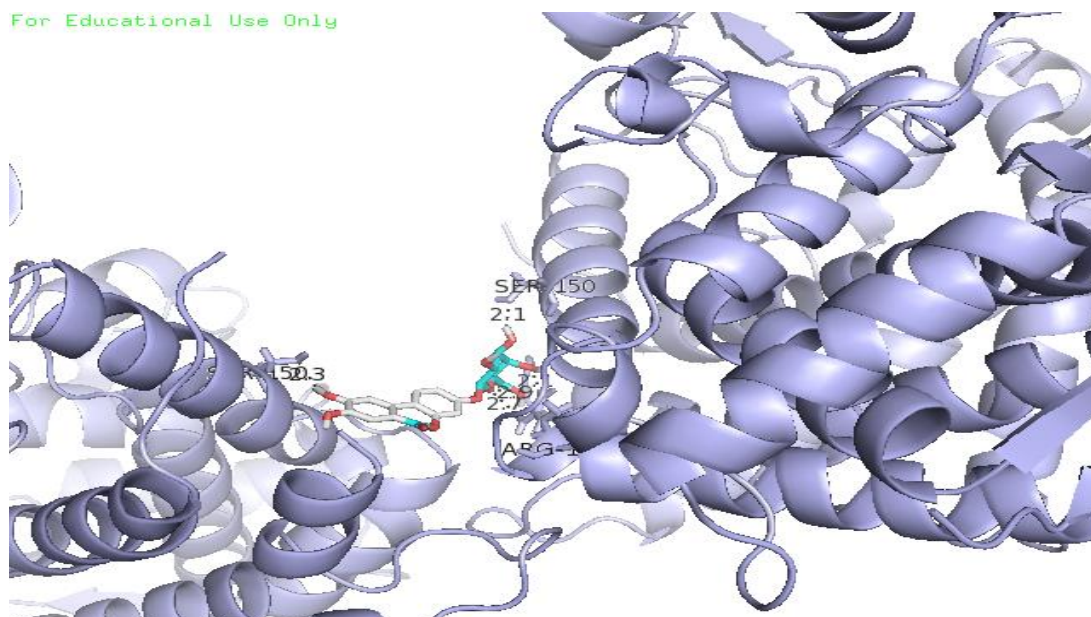
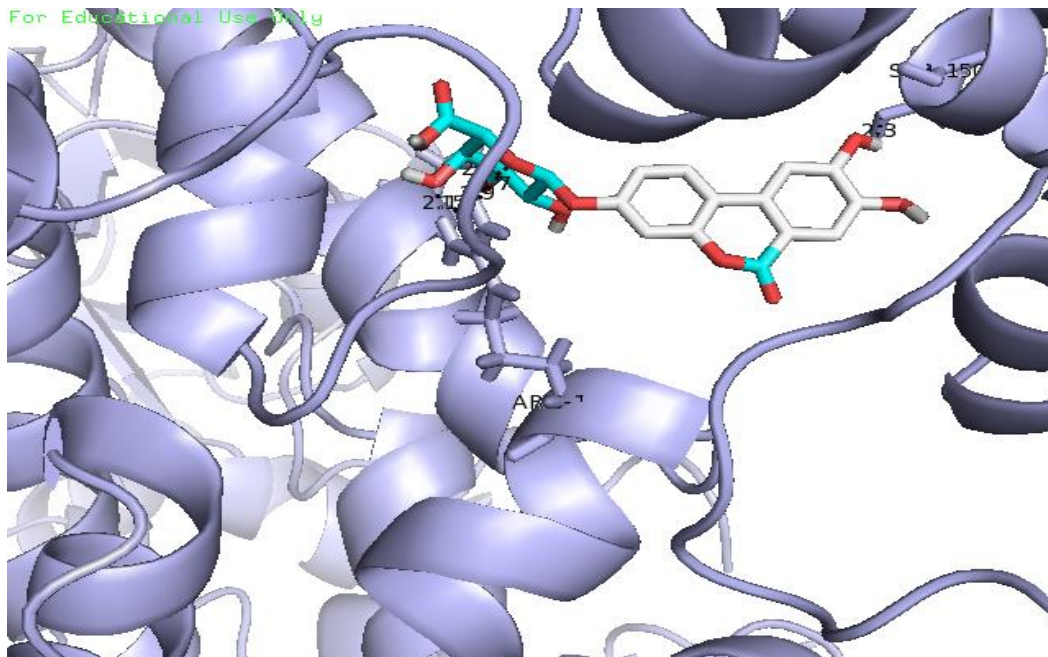
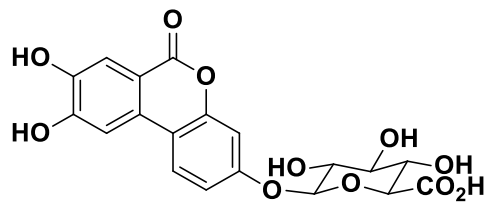


For Educational Use Only

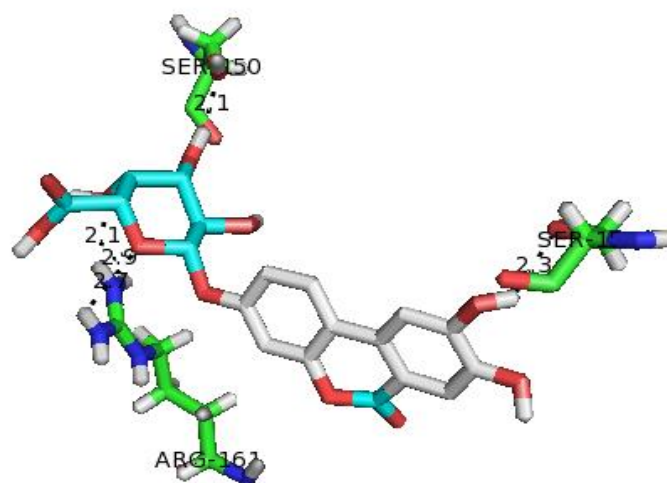


Binding energy [Kcal/mol]	Number of H bonds	Bond distance[Å]	Amino acid residue involved in bonding
-7.1	1	2.5	SER-239

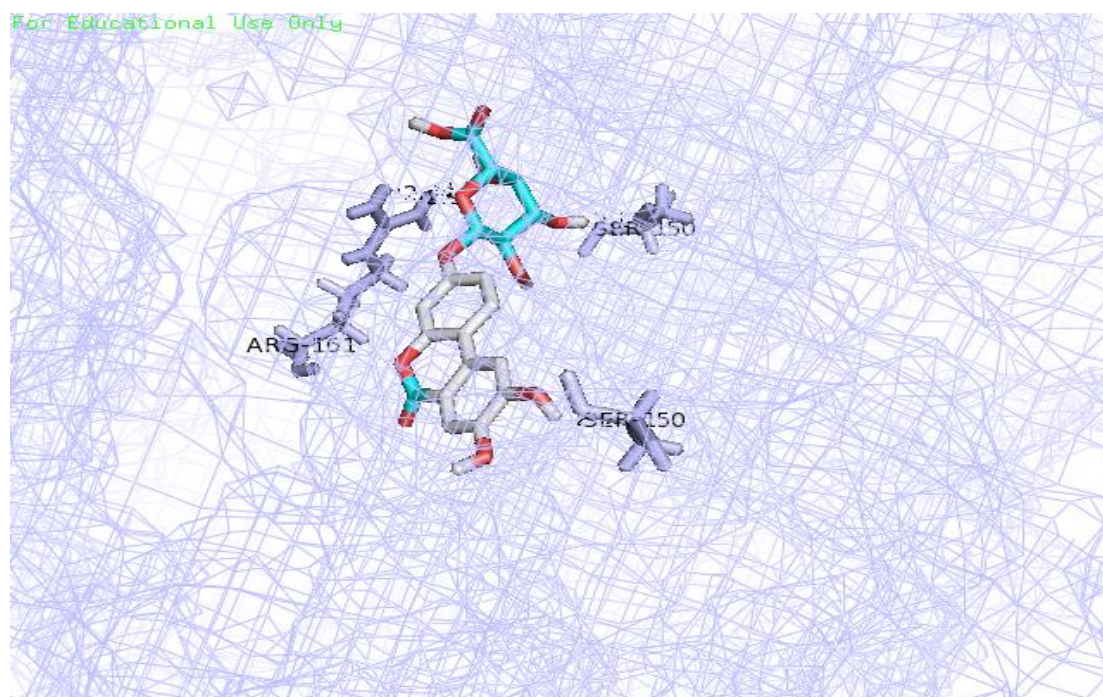
5. Urolithin C 3-glucuronide



For Educational Use Only

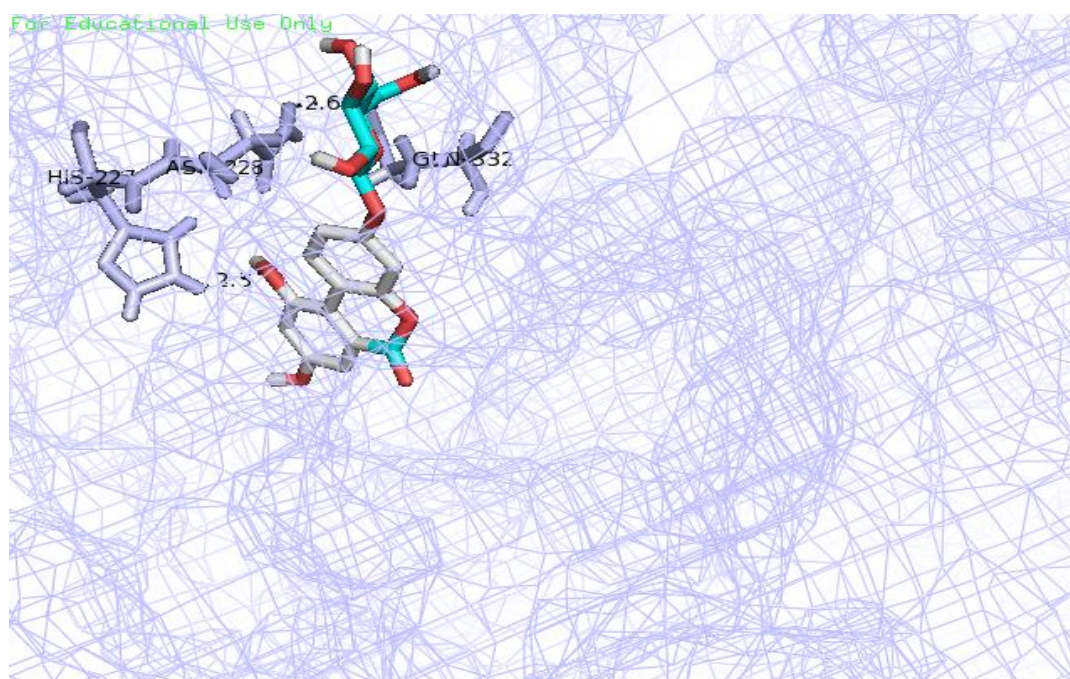
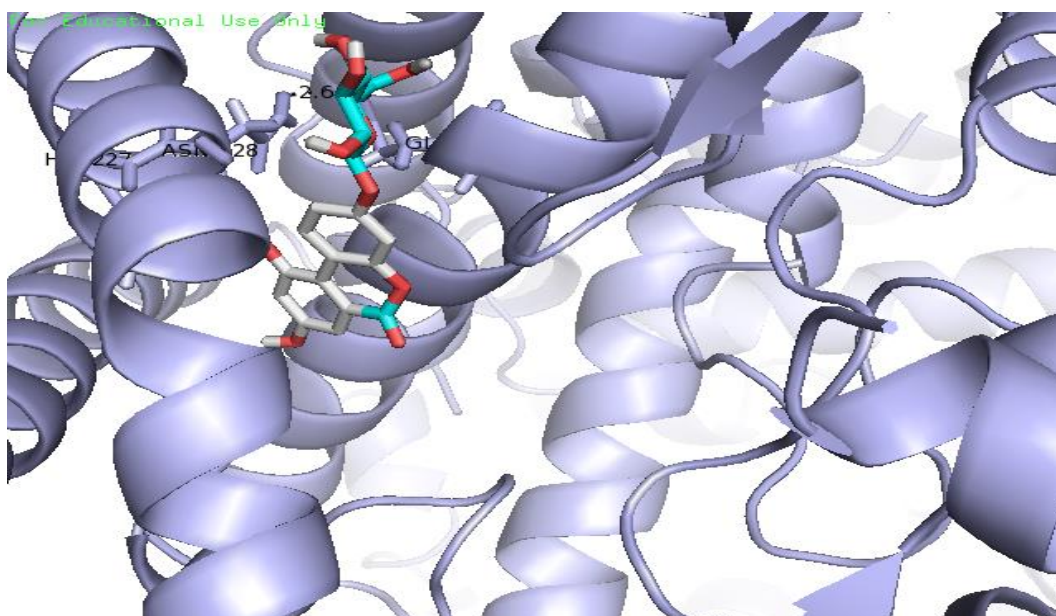
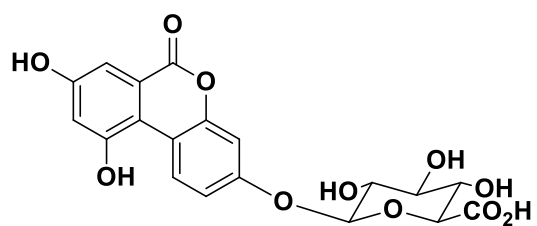


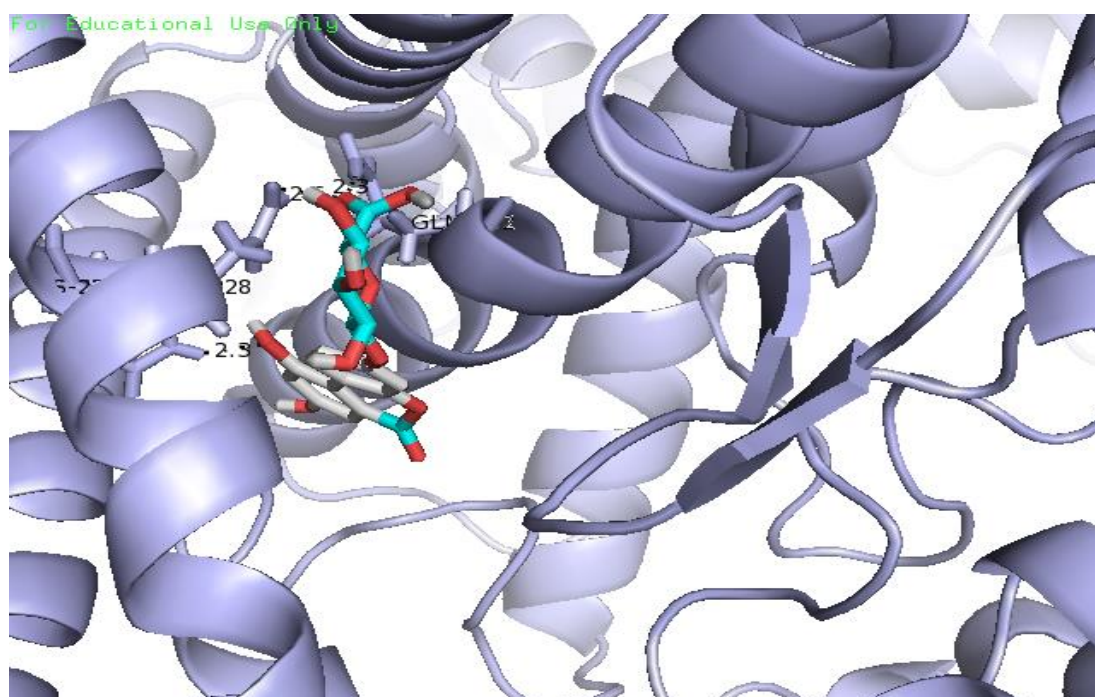
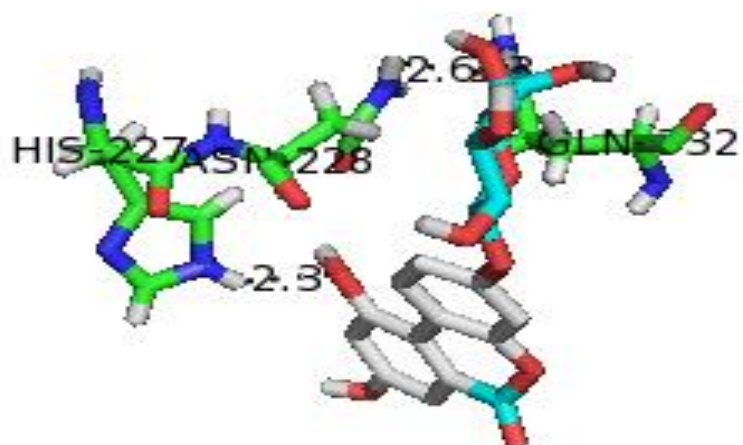
For Educational Use Only



Binding energy [Kcal/mol]	Number of H bonds	Bond distance[Å]	Amino acid residue involved in bonding
-7.7	5	2.1,2.3,2.2,2.1,2.3	ARG-161,SER-150,SER-150

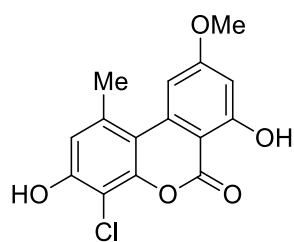
6. Urolithin M 7-Glucuronide



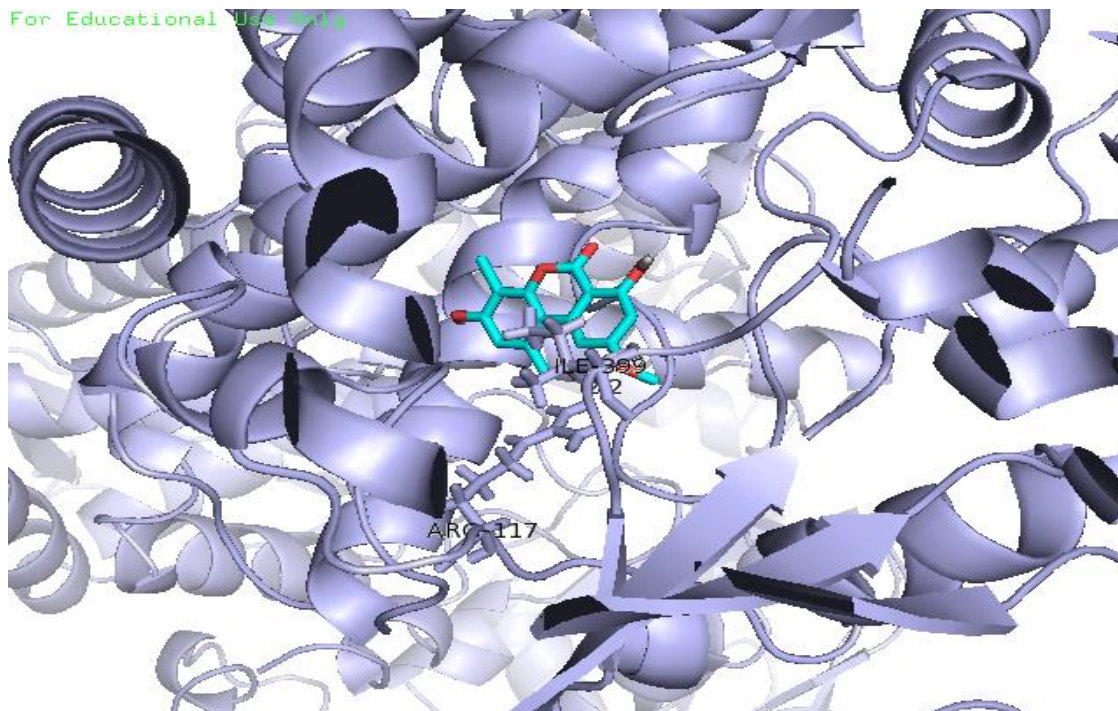


Binding energy [Kcal/mol]	Number of H bonds	Bond distance[Å]	Amino acid residue involved in bonding
-10.6	2	2.3,2.6	HIS-227,GLN-332

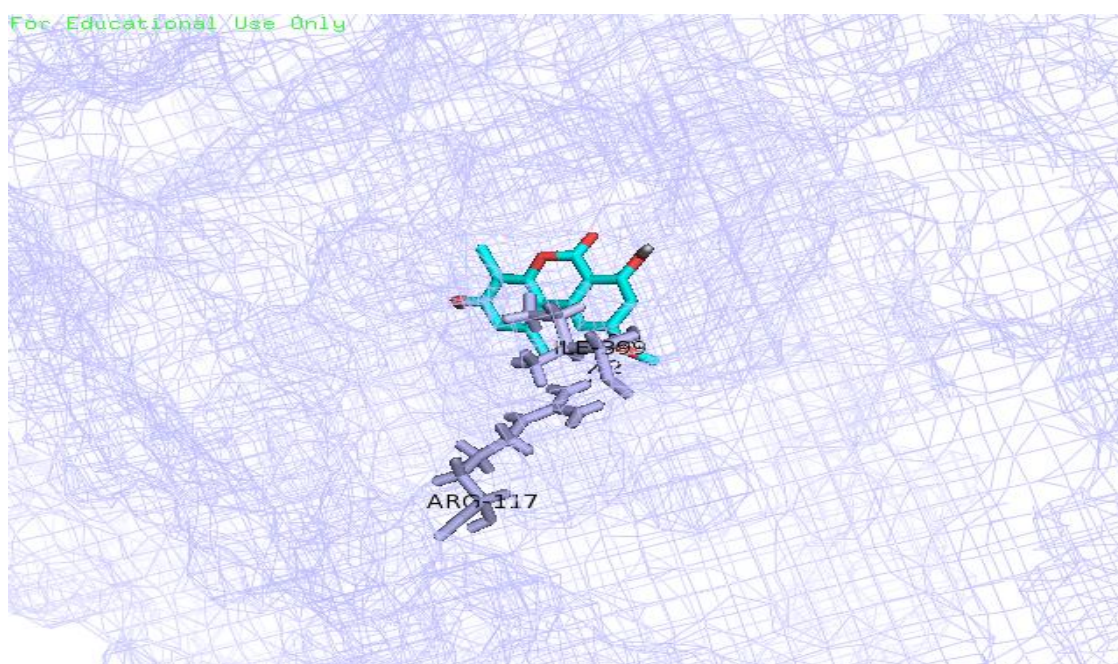
7. Palmariol A



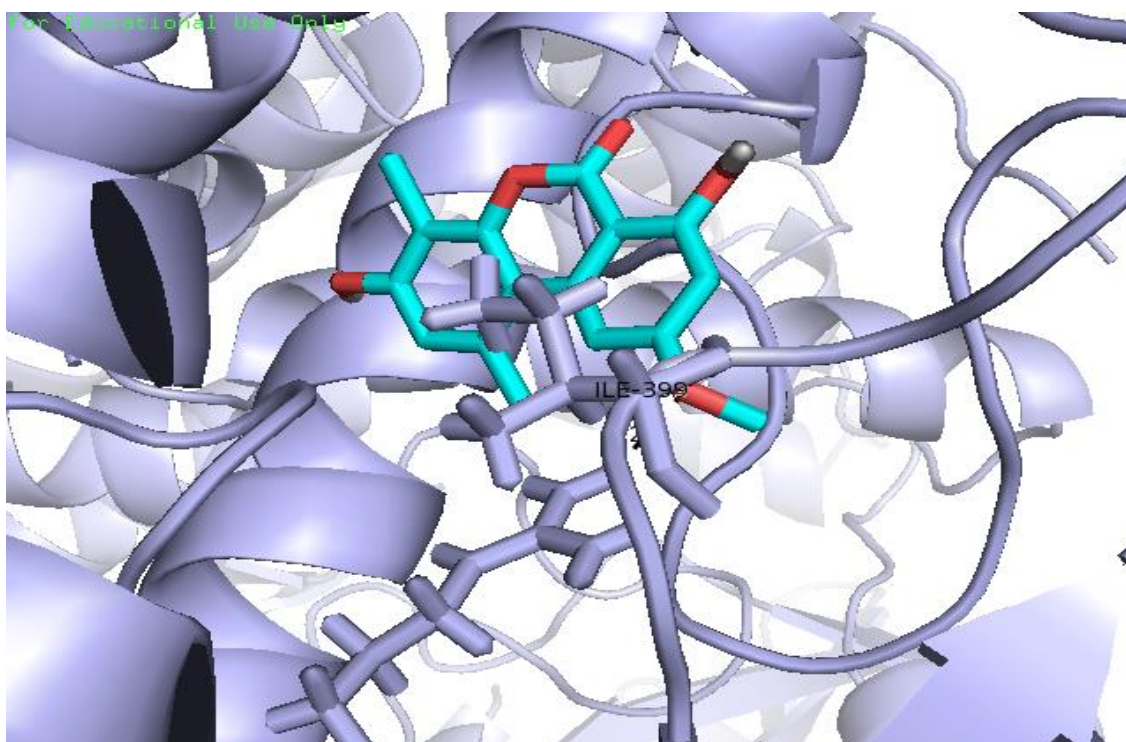
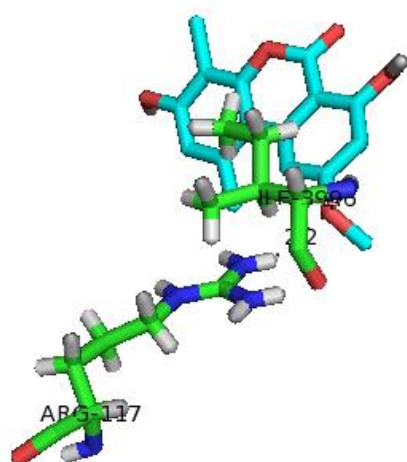
For Educational Use Only



For Educational Use Only

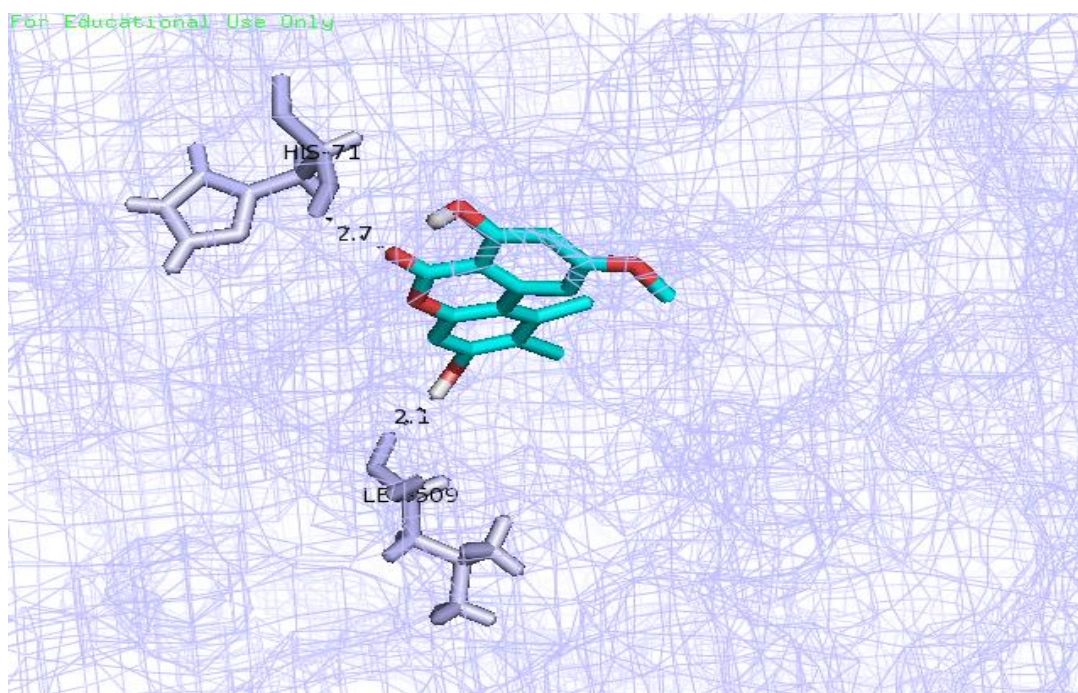
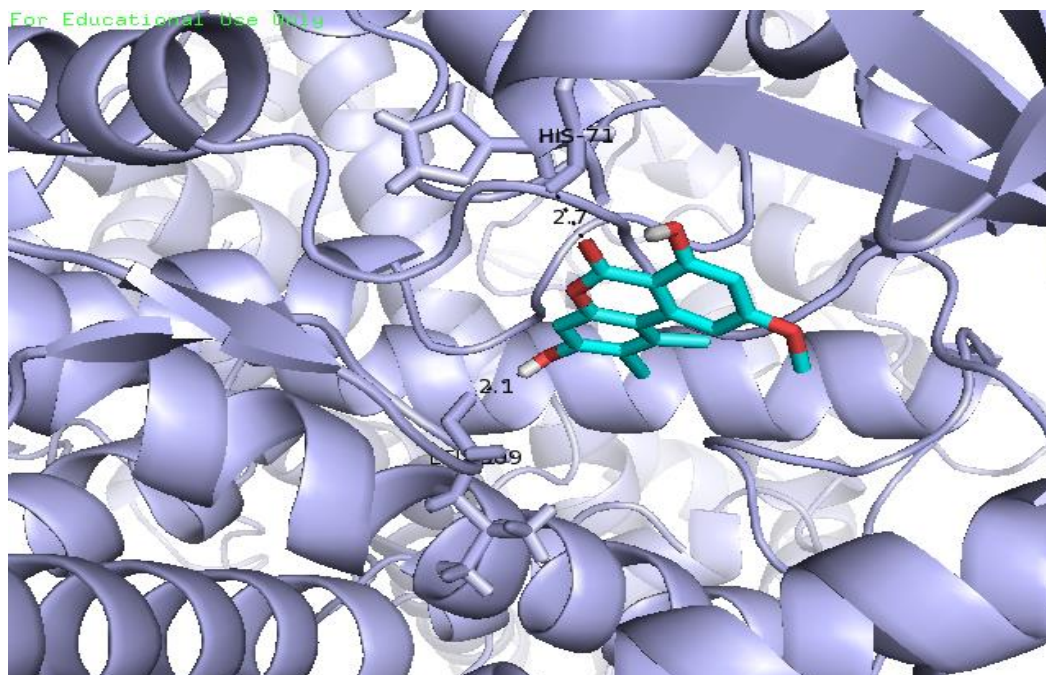
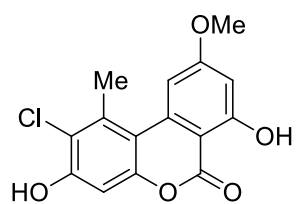


For Educational Use Only

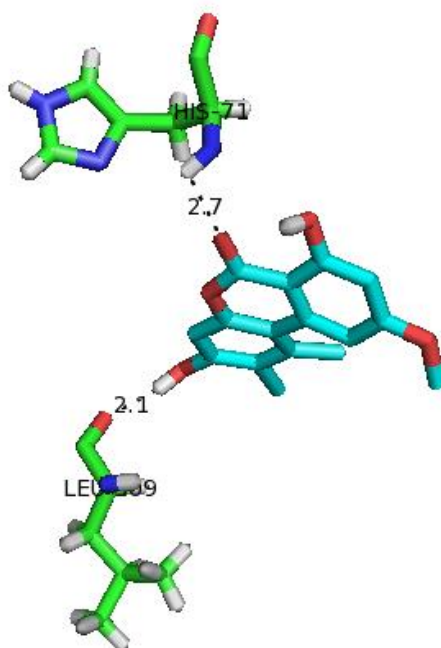


Binding energy [Kcal/mol]	Number of H bonds	Bond distance[Å]	Amino acid residue involved in bonding
-8.2	2	2.2,2.1	ARG-117,ILE-399

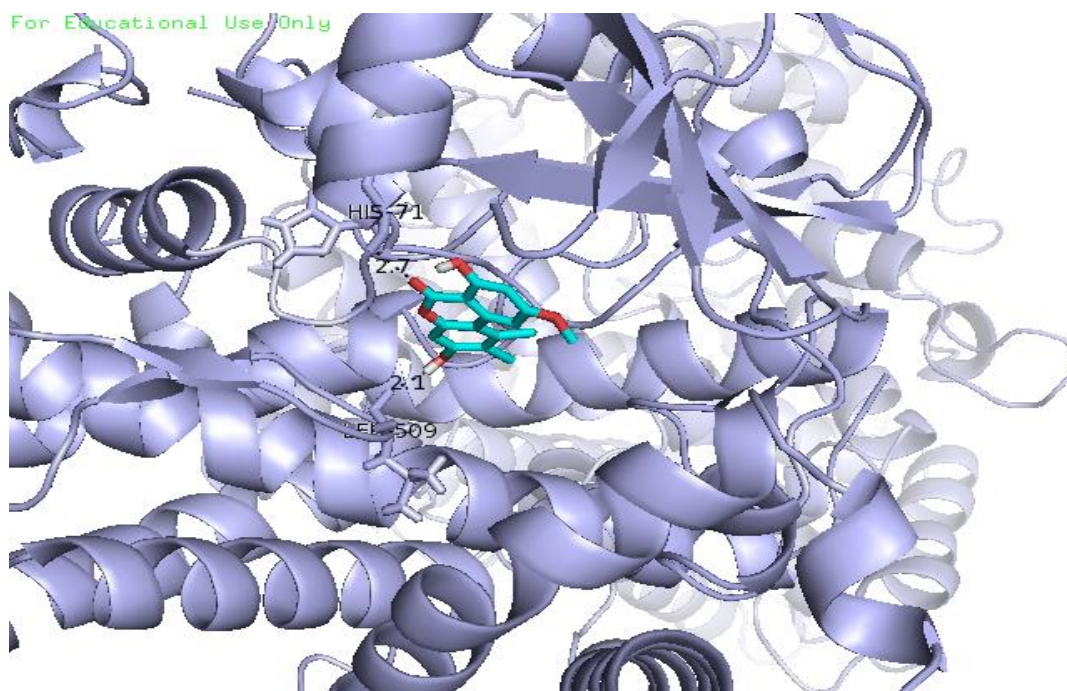
8. Palmariol B



For Educational Use Only

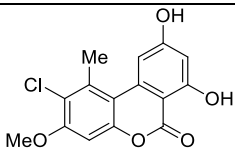
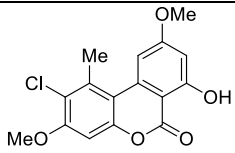
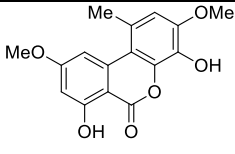
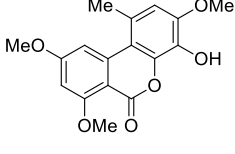
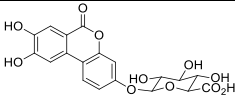
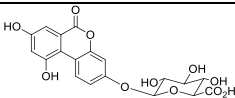
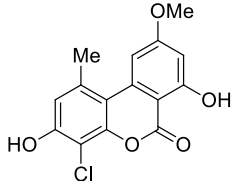
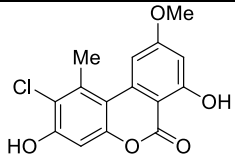


For Educational Use Only



Binding energy [Kcal/mol]	Number of H bonds	Bond distance[Å]	Amino acid residue involved in bonding
-7.3	2	2.1,2.7	LEU-309,HIS-71

4.5 Table 1 . Docking results of synthesized compounds in CYP1B1

Sr no.	Code	Structure	Binding energy [Kcal/mol]	Number of H bonds	Bond distance [Å]	Amino acid residue involved in bonding
1.	Hyalodendriol C		-9.3	3	2.0,2.6, 2.4	SER-127,HIS-227
2.	Graphislactone G		-9.2	1	2.7	HIS-227
3.	Graphislactone A		-7.5	1	2.2	ASN-228
4.	Graphislactone B		-7.1	1	2.5	SER-239
5.	Urolithin 3-C glucuronide		-7.7	5	2.1,2.3, 2.2,2.1, 2.3	ARG-161,SER-150,SER-150
6.	Urolithin M 7-glucuronide		-10.6	2	2.3,2.6	HIS-227,GLN-332
7.	Palmariol A		-8.2	2	2.2,2.1	ARG-117,ILE-399
8.	Palmariol B		-7.3	2	2.1,2.7	LEU-309,HIS-71

4.6 Docking images of synthesized compounds in BCL2 pocket

Docking results of a series of reported compounds in BCL2 protein are shown in Table 2 and the docking images are shown below. The series shows binding energy ranging from -4.8 to -7.6 Kcal/mole. The negative sign of the binding energy attributes to the bound state and hence the values of binding energy are seen for commenting on results. Amongst the series PA shows highest binding energy -8.2 Kcal/mole. The reported inhibitor of BCL2 shows -4.8 Kcal/mole binding energy and one hydrogen bond with histidine molecule. The reported series of molecules shows binding with glycine molecule. All the molecules show at least one hydrogen bond with amino acids in the cavity of the protein. UM shows highest number of hydrogen bonds i.e., 7 which means it is occupying the protein volume completely. PM with highest binding energy shows 4 hydrogen bonds showing hydrophobic interactions with the protein and sitting the pocket correctly. Docking images are shown in three ways, the first one shows ligand and amino acid residue involved in binding, second one shows protein in cartoon view and third one shows the ligand occupying the pocket in the protein. This series shows high occupancy in the cavity of the protein. The ligands penetrate the protein cavity and are stabilized by hydrogen bonds and hydrophobic interactions. BCL2 protein shows a well-defined pocket and the entire series occupies this pocket effectively. This can be seen from the docking images in surface view. Thus, the entire series of reported molecules can act as a good inhibitor of BCL2 protein.

Inhibitor

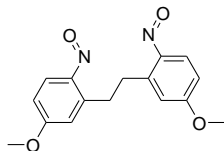
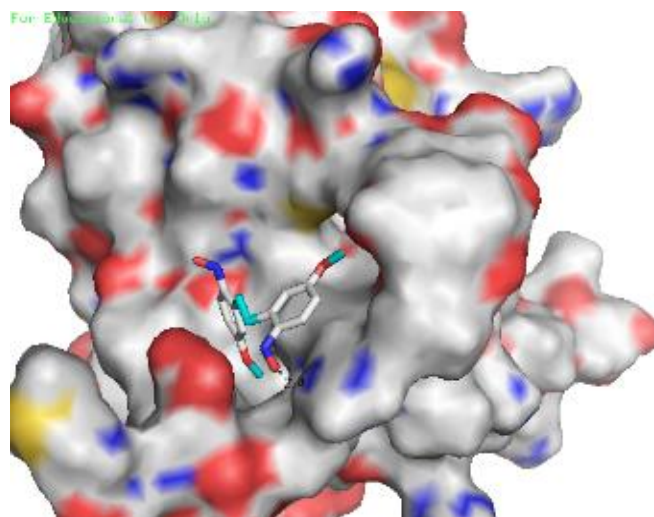
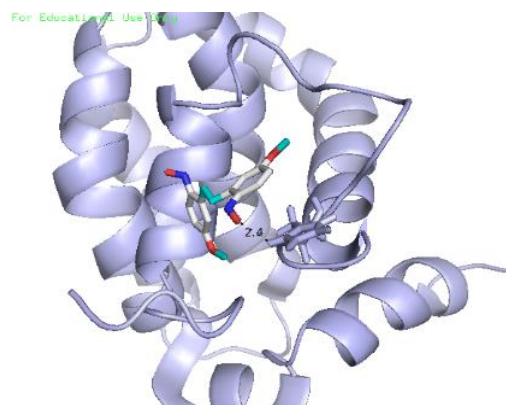
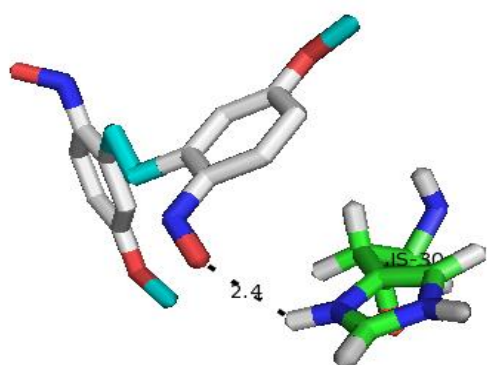
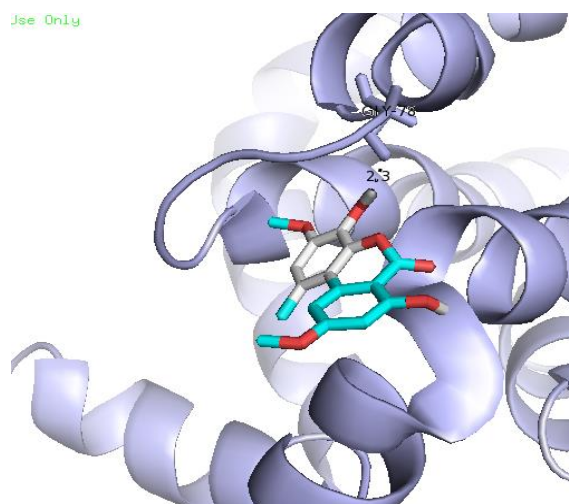
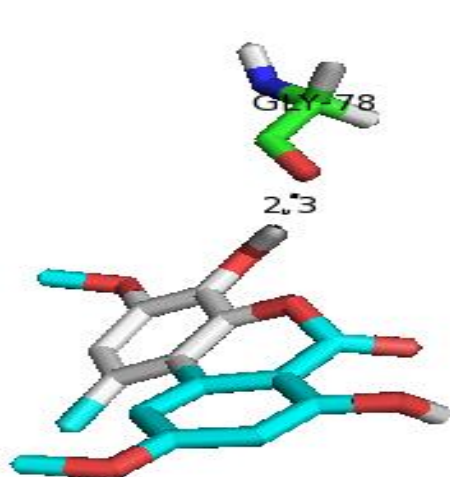
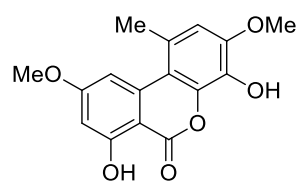


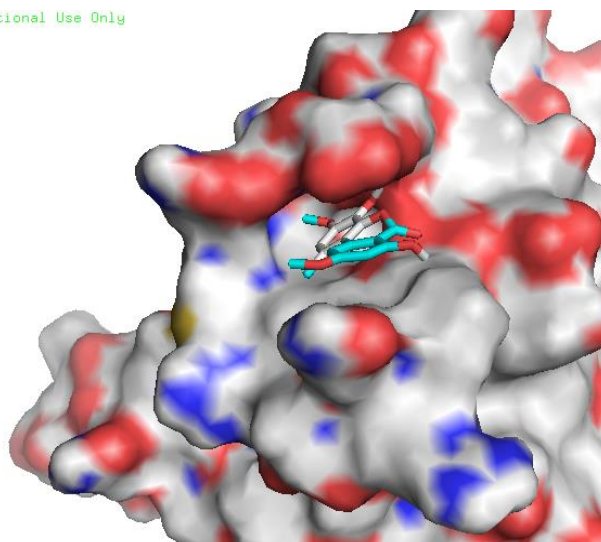
Figure . Structure of standard inhibitor



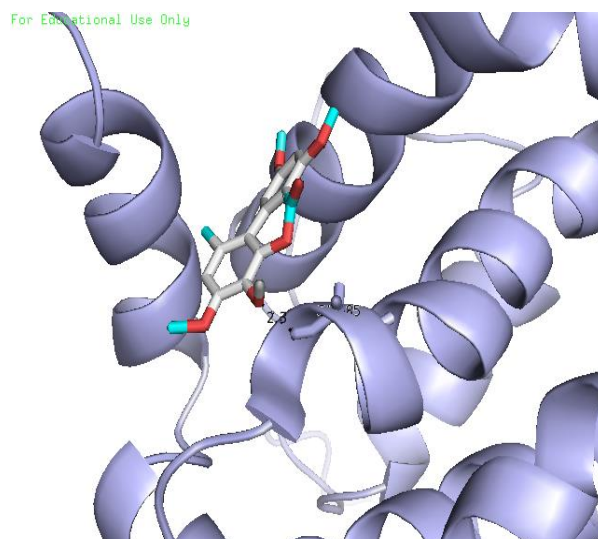
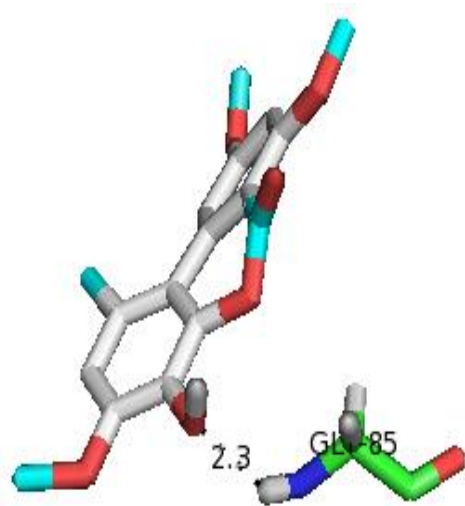
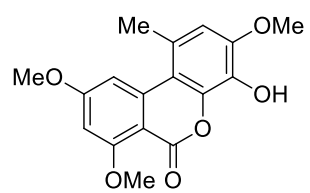
Graphis lactone A



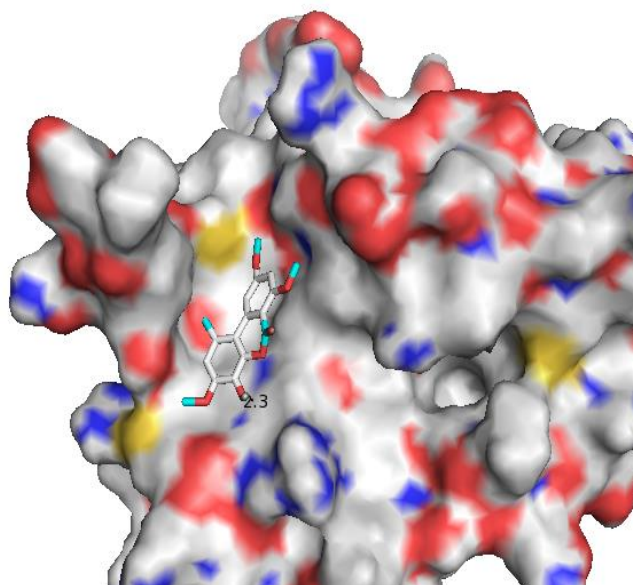
For Educational Use Only



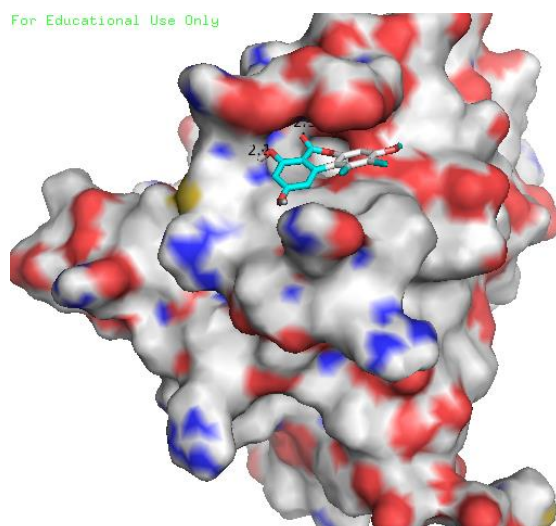
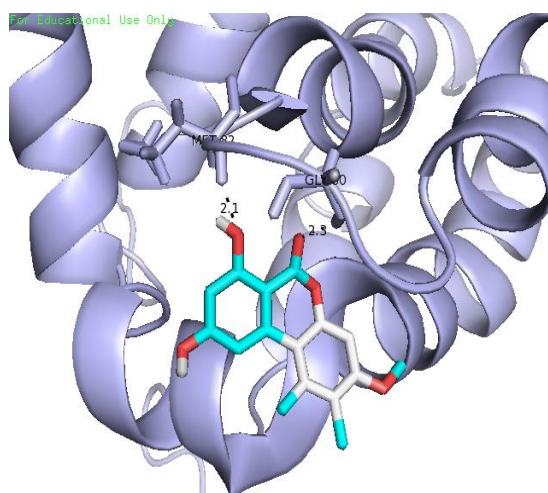
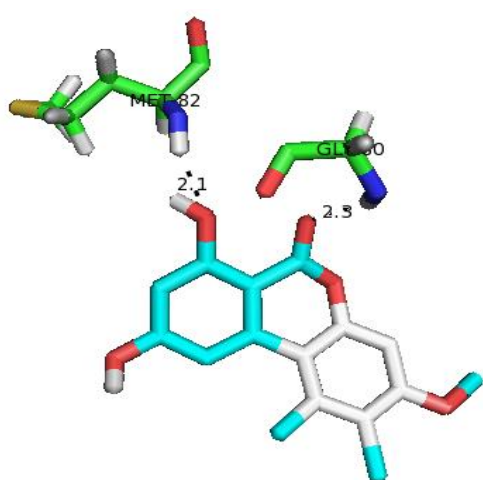
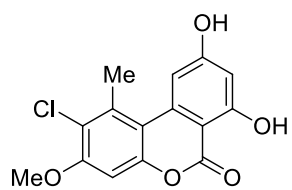
Graphislactone B



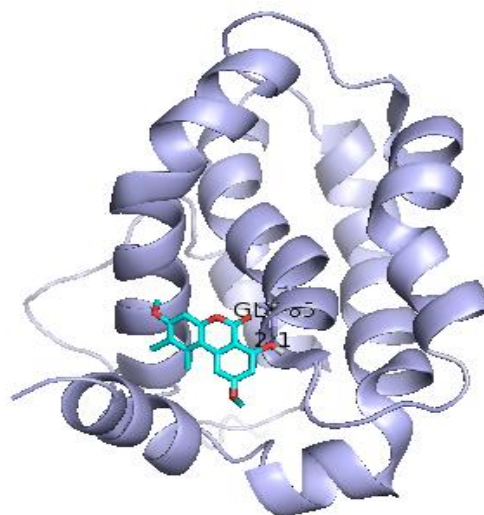
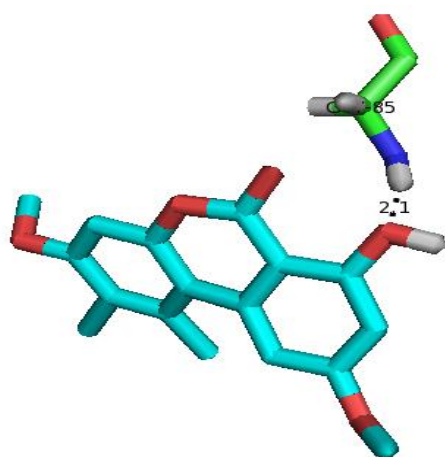
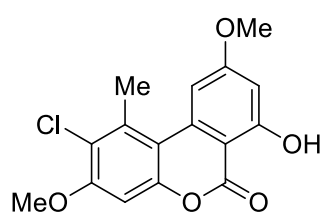
For Educational Use Only



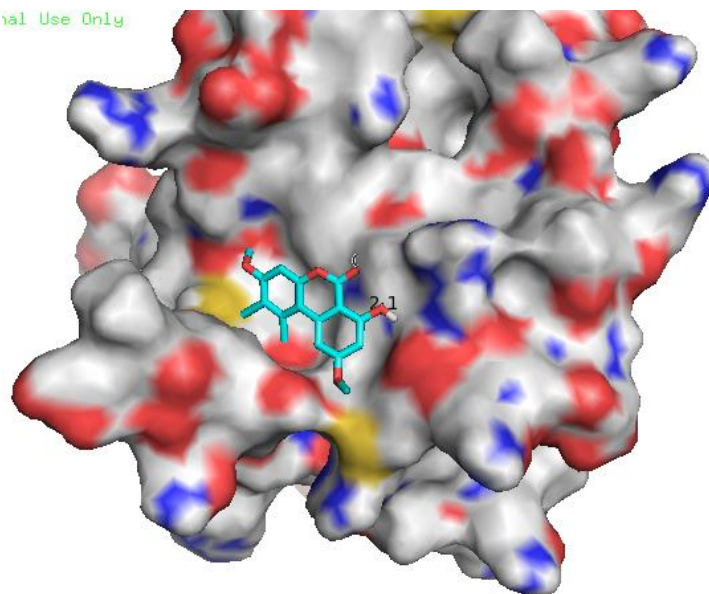
Hyalodendriol C



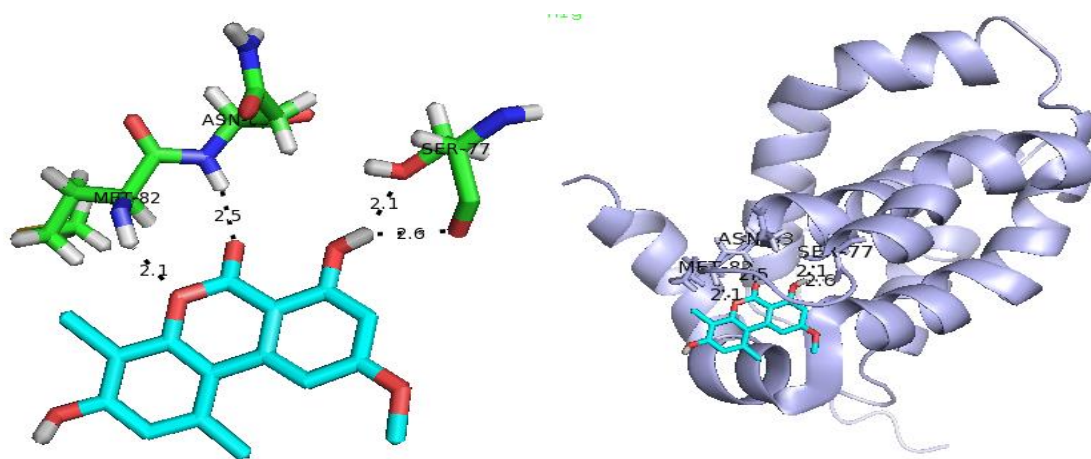
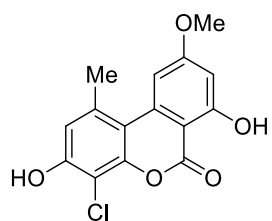
Graphislactone G



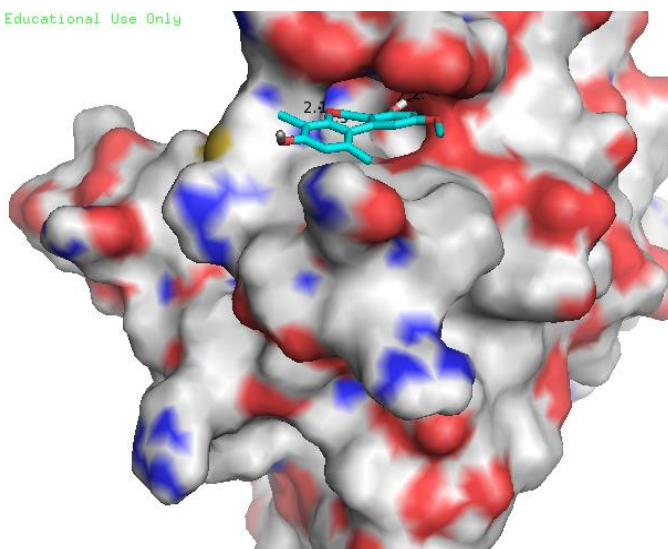
ial Use Only



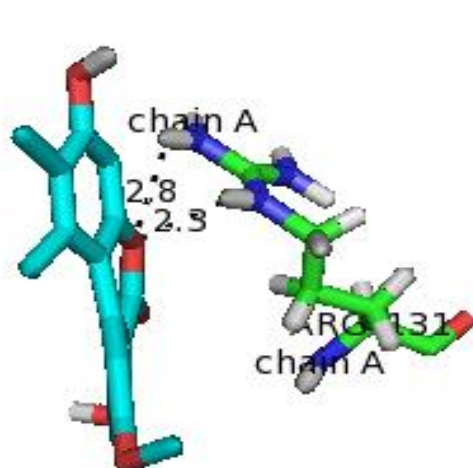
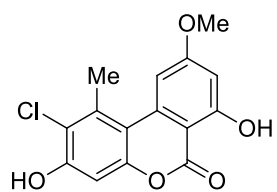
Palmarinol A



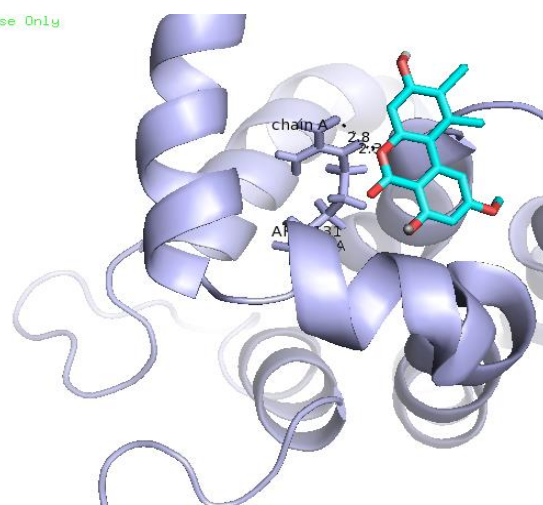
For Educational Use Only



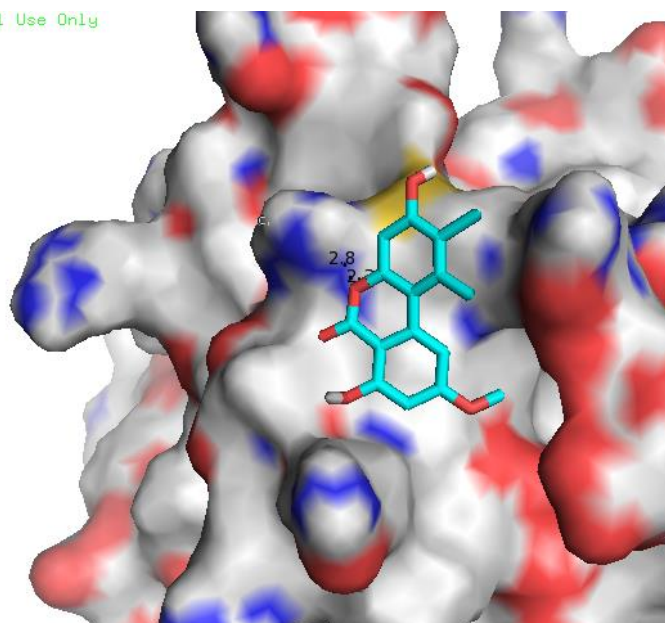
Palmarinol B



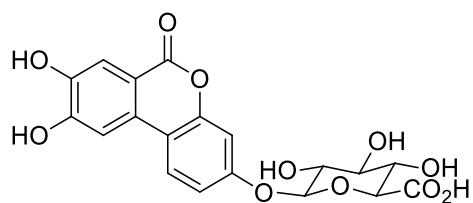
Use Only



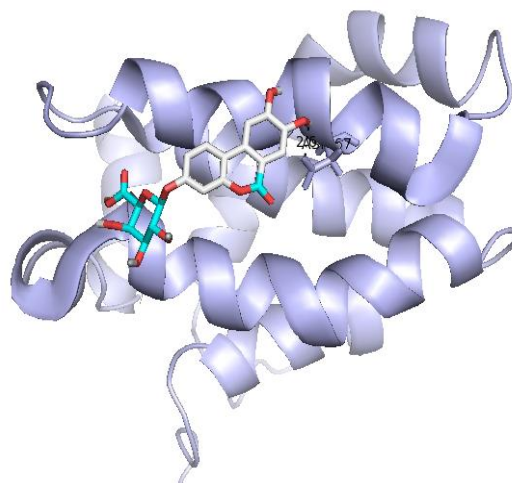
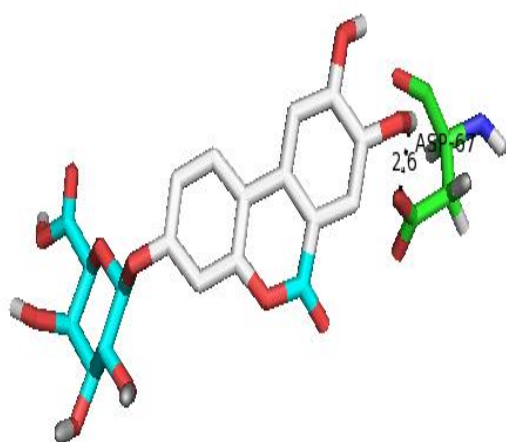
Use Only



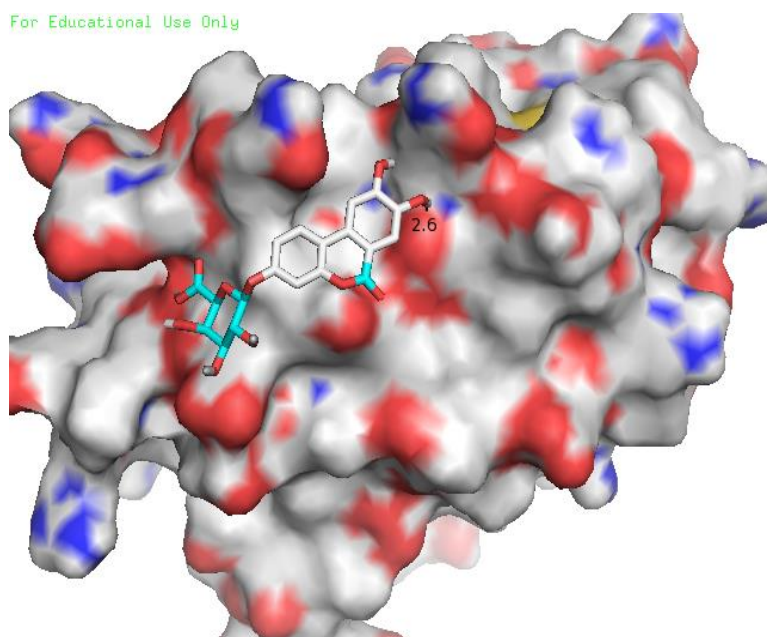
Urolithin C 3-Glucuronide



For Educational Use Only



For Educational Use Only



4.7 Table 2. Docking results of synthesized compounds in BCL2

Sr no.	Code	Binding energy [Kcal/mol]	Number of binding energy	Bond distance[Å]	Amino acid residue involved in bonding
1.	Hyalodendriol C	-7.1	2	2.1,2.3	GLN80, MET82
2.	Graphislactone G	-6.6	1	2.1	GLN85
3.	Graphislactone A	-6.6	1	2.3	GLN87
4.	Graphislactone B	-6.5	1	2.3	GLN85
5.	Urolithin 3-C glucuronide	-4.8	1	2.6	ASP67
6.	Urolithin M 7-glucuronide	-7.6	7	2.2,2.3,2.6,2.3, 2.1,2.6,2.2	GLY126, GLY80, SEB77, GLY78, ARG31
7.	Palmariol A	-8.2	4	2.1,2.5,2.1,2.6	ASN82, MET83, SER77
8.	Palmariol B	-5.3	2	2.8,2.3	ARG131
9.	Standard inhibitor	-4.8	1	2.4	HIS-30

Acknowledgments

First and foremost, I would like to thank Almighty ALLAH for giving me the capability to complete this work and for his continued mercy and blessings upon me. I would like to express my appreciation and special thanks to my supervisor of research, Prof. Hitoshi Abe for giving me the opportunity to work in his lab and for his exceptional supervision, guidance, advice, and support throughout my research. His friendly attitude and kindness allowed me to work in an enjoyable and relaxed environment and his knowledgeable discussions expanded my understanding of research. I would like to thank the other members of my dissertation committee: Prof. Toyooka Naoki and Prof. Ikawa Yoshiya. I would also like to thank my laboratory mates for their friendly behavior and assistance in experiments and learning Japanese. Many technical staff members have helped me along the way, I would like to thank all of them. My colleagues deserve special thanks, Dr. Tanveer Ahmad Mir and Dr. Allah Nawaz for their guidance during my Ph.D. and life in Japan. Last but not the least, my family, their love, and constant support have enabled me to overcome this big task. So, I would like to say thank you from the bottom of my heart to my parents for their love, support at every step of my life, and continuous prayers for my success. I would also like to thank my friends from Pakistan and India for their love, encouragement, best wishes, motivation, and support throughout my Ph.D.

5.1 References

- 1 J Lou, L Fu, Y Peng, and Y L Zhou, *Molecules*, 2013, **18**, 5891.
- 2 T Tanahashi, M Kuroishi, A Kuwahara, N Nagakura, and N Hamada, *Chem. Pharm. Bull.* 1997, **45**, 1183.
- 3 T Tanahashi, Y Takenaka, N Nagakura, and N Hamada, *Phytochemistry*, 2003, **62**, 71.
- 4 Y Shirataki and S Toda, *Nat. Med.* 2001, **55**, 247.
- 5 D Bialonska, S.G Kasimsetty, S.I Khan, and D Ferreira, *J. Agric. Food Chem.*, 2009, **57**, 10181.
- 6 R Gonzalez-Barrio, P Truchado, H Ito, J.C Espin, and F.A Tomas-Barberan, *J. Agric. Food Chem.*, 2011, **59**, 1152.
- 7 J Teske and A Deiters, *Org. Lett.* 2008, **10**, 2195.
- 8 J.P Edwards, S.J West, K.B Marschke, D.E Mais, M.M Gottardis, and T.K Jones, *J. Med. Chem.*, 1998, **41**, 303.
- 9 M.J Coghlan, P Kym, S.W Elmore, A.X Wang, J.R Luly, D Wilcox, M Stashko, C.-W Lin, and J Miner, C. Tyree, *et al. J. Med. Chem.*, 2001, **44**, 2879.
- 10 N Bradburn, R.D Coker, G Blunden, C.H Turner, and T.A Crabb, *Phytochemistry*, 1994, **35**, 665.
- 11 H Hussain, K Krohn, Z Ullah, S Draeger, and B Schulz, *Biochem. Syst. Ecol.*, 2007, **35**, 898.
- 12 J.-C Qin, Y.-M Zhang, L Hu, Y.-T Ma, and J.-M Gao, *Nat. Prod. Commun.*, 2009, **4**, 1473.
- 13 S Wu, Y Chen, Z Li, L Yang, S Li, *Nat. Prod. Res. Dev.*, 2011, **23**, 850.
- 14 H.-W Zhang, W.-Y Huang, Y.-C Song, J.-R Chen, R.-X Tan, *Helv. Chim. Acta.*, 2005, **88**, 2861.
- 15 T Matumoto, T Hosoya, and H Shigemori, *Heterocycles* 2010, **81**, 123.
- 16 W.T.L Sidwell, H Fritz, and C Tamm, *Helv. Chim. Acta.*, 1971, **54**, 207.
- 17 Y.-P Chen, Liu, L.; Zhou, Y.-H.; Wen, J.; Jiang, Y.; Tu, P.-F, *J. Chin. Pharm. Sci.* 2008, **17**, 82.
- 18 S Fang, Y Gu, H Yu, and S Musadillin, *Acta. Bot. Sin.*, 1989, **31**, 382.
- 19 K Ishiguro, M Yamaki, M Kashihara, S Takagi, and K. A Isoi, *Phytochemistry* 1990, **29**, 1010.
- 20 M.I Gil, F.A Tomás-Barberán, B Hess-Pierce, D.M Holcroft, and A.A Kader, *J. Agric. Food Chem.* 2000, **48**, 4581.

- 21 M.A.P Moreno, I.G Alonso, R Martin de Santos, and T.G Lacarra, *Nutr., Hosp.*, 2012, **27**, 1772.
- 22 A.H Aly, R Edrada-Ebel, I.D Indriani, V Wray, W.E.G Muller, F Totzke, U Zirrgiebel, C Schachtele, M.H.G Kubbutat, and W.H Lin, *J., Nat., Prod.*, 2008, **71**, 972.
- 23 F Bensassi, C Gallerne, O Sharaf El Dein, M.R Hajlaoui, H Bacha, C Lemaire, *In Vitro* 2012, **26**, 915.
- 24 S.-J Jeong, N.-Y Kim, D.-H Kim, T.-H Kang, N.-H Ahn, T Miyamoto, R Higuchi, and Y.-C Kim, *Planta. Med.*, 2000, **66**, 76.;
- 25 (a) Z Mao, W Sun, L Fu, H Luo, D Lai, and L Zhou, *Molecules*, 2014, **19**, 5088.; (b) Z Mao, D Lai, X Liu, X Fu, J Meng, A Wang, X Wang, W Sun, Z L Liu, L Zhou, and Y Liu, *Pest. Manag. Sci.*, 2017,**73**, 1478
- 26 B. I. Alo, A. Kandil, P. A. Patil, M. J. Sharp, M. A. Siddiqui, V Snieckus, and P D Josephy, *J. Org. Chem.*, 1991,**56**, 3763
- 27 Y C Song, W Y Huang, C Sun, F W Wang, and R X Tan, *Biol., Pharma., Bull.*, 2005, **28**, 506; (c) T Tanahashi, M Kuroishi, A Kuwahara, N Nagakura, and N Hamada, *Chem. Pharm. Bull.*, 1997,**45**, 1183.
- 28 (a) W-Y Fang, L Ravindar, K P Rakesh, H M Manukumar, C S Shantharam, N S Alharbi, and H-L Qin, A critical review, *Eur., J., Med., Chem.*, 2019,**173**, 117; (b) J Tian, X C Liu, Z L Liu, D Lai, and L Zhou, *Pest. Manag. Sci.*, 2016,**72**, 961.
- 29 K Mori and K Sato, *Tetrahedron*, 1982, **38**, 1221.
- 30 W-w Mao, T-t Wang, H-p Zeng, Z-y Wang, J-p Chen, and J-g Shen, *Bioorg. Med. Chem. Lett.*, 19, **2009**, 4570.
- 31 (a) H Abe, T Fukumoto, Y Takeuchi, and T Harayama, *Heterocycles*, 2007, **74**, 265; (b) K Ahmed, S Enumula, A Pangal, I Jeelani, M Rane, G Mahangade, and V Patel, *Intl., J., Pharm., Biol., Sci.*, 2019, **9**.
- 32 (a) H Mikula, P Skrinjar, B Sohr, D Ellmer, C Hametner, and J Fröhlich, *Tetrahedron*, 2013, **69**, 10322; (b) M Node, T Kajimoto, K Nishide, E Fujita, and K Fuji, *Bull. Inst. Chem.* 1992,**70**, 308.
- 33 M Tanaka, Y Ikeya, H Mitsuhashi, M Maruno, and T Wakamatsu, *Tetrahedron*, 1995, **51**, 11703.
- 34 H Abe, T Fukumoto, Y Horino, T Harayama, and Y Takeuchi, *Heterocycles*, 2010, **82**, 851.
- 35 (a) T Harayama, H Yasuda, T Akiyama, Y Takeuchi, and H Abe, *Chem., Pharm., Bull.*, 48, **2000**, 861; (b) S Takeda, H Abe, Y Takeuchi, and T Harayama, *Tetrahedron*, 2007,**63**, 396; (c) H Abe, K Nishioka, S Takeda, M Arai, Y Takeuchi, and T Harayama, *Tetrahedron Lett.*,

- 2005,**46**, 3197; (d) H Abe, S Takeda, T Fujita, K Nishioka, Y Takeuchi, and T Harayama, *Tetrahedron Lett.*, 2004,**45**, 2327; (e) H Abe, Y Sahara, Y Matsuzaki, Y Takeuchi, and T Harayama, *Tetrahedron Lett.*, 2008,**49**, 605; (f) H Abe and T Harayama, *Heterocycles*, **75**, **2008**, 1305; (g) H Abe, M Arai, K Nishioka, T Kida, K Shioe, Y Takeuchi, and T Harayama, *Heterocycles*, 2008,**76**, 291; (h) K Shioe, Y Takeuchi, T Harayama, and H Abe, *Chem. Pharm. Bull.*, 2010,**58**, 435; (i) H Abe, M Arai, Y Takeuchi, and T Harayama, *Heterocycles*, 2009,**77**, 1409; (j) K Itaya, I Jeelani, and H Abe, Total synthesis of Urolithin Glucuronide *C Heterocycles*, 2021,**103**.
- 36 D M W Anderson and G M Cree, *Carbohydr. Res.*, 1966, **2**, 162.
- 37 H Miyazaki, N Nakamura, T Ito, T Sada, T Oshima, and H Koike, *Chem. Pharm. Bull.*, **37**, **1989**, 2391.
- 38 A Lavecchia, C Di Giovanni, *Curr. Med. Chem.*, 2013, **20**, 2839.
- 39 H Matter, C Sotriffer, Wiley-VCH Verlag GmbH & Co. KGaA, Weinheim, Germany, 2011-319.
- 40 JA Erickson, M Jalaie, DH Robertson, RA Lewis, M Vieth, *J. Med. Chem.*, 2004, **47**, 55.
- 41 E Freire, *Drug Discov. Today*, 2008,**13**, 874.
- 42 HM Kumalo, S Bhakat, ME Soliman, *Molecules*, 2015, **20**, 2000.
- 43 M Wang, Y Yu, C Liang, A Lu, G Zhang, *Int. J. Mol. Sci.*, 2016, **17**, 779.
- 44 J Blaney, *J. Comput. Aided Mol. Des.*, 2012, **26**,14.
- 45 S Mandal, M.N Moudgil, S.K Mandal, *Eur. J. Pharmacol*, 2009, **625**, 100.
- 46 S Urwyler, *Pharmacol. Rev.*, 2011, **63**, 126.
- 47 G.L Wilson, M.A Lill, *Future Med. Chem.*, 2011, **3**, 750.
- 48 Y Fang, *Expert Opin. Drug Discov.*, 2012, **7**, 988.
- 49 A.W Kahsai, K Xiao, S Rajagopal, S Ahn, A.K Shukla, J Sun, T G Oas, Lefkowitz, R.J. *Nat. Chem. Biol.*, 2011, **7**, 700
- 50 B.R Chandrika, J Subramanian, S.D Sharma, *Drug Discov. Today*, 2009, **14**, 400.
- 51 J.D Durrant, J.A McCammon, *Curr. Opin. Pharmacol*, 2010, **10**, 774.
- 52 N Foloppe, R Hubbard, *Curr. Med. Chem.*, 2006, **13**, 3608.
- 53 A.N Jain, *Curr. Protein Pept. Sci.*, 2006, **7**, 420
- 54 M.W Gonzalez, M.G Kann, *PLoS Comput. Biol.*, 2012, **8**, e1002819.
- 55 M.R Arkin, J.A Wells, *Nat. Rev. Drug Discov.*, 2004, **3**, 317.
- 56 I.S Moreira, P.A Fernandes, M.J Ramos, Protein-protein docking dealing with the unknown. *J. Comput. Chem.*, 2010, **31**, 342.
- 57 P. P Jakub, S. Iwona, G.Sebastian, S. Joanna, K. K Anna, *Drug Metab. Dispos.* 2017, **45**,

- 665.
- 58 B. Cerdá, R. Llorach, J. J. Cerón, J. C. Espín, and F. A. Tomás-Barberán, *Eur. J. Nutr.*, 2003, **42**, 28.
- 59 B. Cerdá, J. C. Espín, S. Parra, P. Martínez, and F. A. Tomás-Barberán, *Eur. J. Nutr.*, 2004, **43**, 220.
- 60 N. P. Seeram, S. M. Henning, Y. Zhang, M. Suchard, Z. Li, and D. Heber, *J. Nutr.*, 2006, **136**, 2485.
- 61 B. Cerdá, F. A. Tomás-Barberán, and Espín, *J. Agric. Food Chem.*, 2005, **53**, 235.
- 62 J. A. Giménez-Bastida, A. González-Sarrías, M. Larrosa, F. Tomás-Barberán, J. C. Espín, García, and M. T. Conesa *Mol. Nutr. Food Res.*, 2012, **56**, 796.
- 63 J. C. Espín, R. González-Barrio, B. Cerdá, C. López-Bote, A. I. Rey, and F. A. Tomás-Barberán, *J. Agric. Food Chem.*, 2007, **55**, 10485.
- 64 J. C. Espín, M. Larrosa, M. T. García-Conesa, and F. Tomás-Barberán, *Evid. Based Complement. Alternat. Med.*, 2013, **15**.
- 65 N. P. Seeram, R. N. Schulman, and D. Heber, *pomegranates Ancient Roots to Modern Medicine*, CRC Press, Boca Raton, FL, USA, 2006.
- 66 M. Á. Ávila-Gálvez, J. C. Espín, and A. González-Sarrías, *J. Agric. Food Chem.*, 2018, **66**, 8555.
- 67 M. García-Conesa, M. V. Selma, J. C. Espín, F. A. Tomás-Barberán, *J. Agric. Food Chem.*, 2019, **67**, 11107.
- 68 R. García-Villalba, J. C. Espín, and F. A. Tomás-Barberán, *J. Chromatogr. A.*, 2016, **1428**, 175.
- 69 R. Lucas, D. Alcantara, and J. C. Morales, *Carbohydr. Res.*, 2009, **344**, 1346.
- 70 A. González-Sarrías, V. Miguel, G. Merino, R. Lucas, J. C. Morales, F. Tomás-Barberán, A. I. Álvarez, and J. C. Espín, *J. Agric. Food Chem.*, 2013, **61**, 4359.
- 71 T. Harayama, H. Yasuda, T. Akiyana, Y. Takeuchi, and H. Abe, *Chem. Pharm. Bull.*, 2000, **48**, 864.
- 72 H. Abe, T. Fukumoto, Y. Horino, T. Harayama, and Y. Takeuchi, *Heterocycles* 2010, **82**, 855.
- 73 K. Tahara, H. Yamaga, E. Ghijsens, K. Inukai, J. Adisoejoso, M. O. Blunt, S. D. Feyter, and Y. Tobe, *Nature Chem.*, 2011, **3**, 719.
- 74 W-J. Jiang, K. Ishiuchi, M. Furukawa, Takamiya, T. Kitanaka, and S. Iijima, *Bioorg. Med. Chem.*, 2015, **23**, 6929.
- 75 H. Mikula, P. Skrinjar, B. Sohr, D. Ellmer, C. Hametner, and J. Fröhlich, *Tetrahedron*,

- 2013, **69**, 10322.
- 76 R. Frlan, S. Gobec, and D. Kikelj, *Tetrahedron*, 2007, **63**, 10698
- 77 S. Balamurugan, P. Kannaa, P. Yadupati, and A. Roy, *J. Mol. Struct.*, 2011, **1001**, 124.
- 78 M. Kitamura, S. Takahashi, and T Okauchi, *J. Org. Chem.*, 2015, **80**, 8416.
- 79 S. Chang-Xiao, M. Jean-Francois, C. Chih-Chia, T. Hou-Jen, and H. Ling-Yih, *Chem. Pharm. Bull.*, 2006, **54**, 686.
- 80 K. Maeda, T. Matsukihira, S. Saga, Y. Takeuchi, T. Harayama, Y. Horino, and H. Abe, *Heterocycles*, 2014, **88**, 628
- 81 L. C. Campeau, M. Parisien, A. Jean, K. Fagnou, *J. Am. Chem. Soc.*, 2006, **128**, 590.
- 82 C. D. Garcia, M. de Mendoza, A. A. C. Braga, and A. M. Echavarren, *J. Org. Chem.*, 2007, **129**, 6886.
- 83 W. Pilgrim and P. V. Murphy, *J. Org. Chem.*, 2010, **75**, 6755.
- 84 X.; Lin, Z. San-Yong, S. Xiao-Qiu, H. Li-Li, and Y. Jin-Song, *J. Org. Chem.*, 2010, **75**, 5767.
- 85 Beatriz, S. P J Garcia, G. C. Roser, H. Jordi, A. Ramon, N. Fernando, S. Josep, B. Felix, R. M. Daniel, *Mater. Interfaces*, 2014, **6**, 17625.
- 86 M. Hrast, M. Anderluh, D. Kenz, C. P. Randall, H. Barreteau, A. J. O'Neill, D. Blanot, S. Gobec, *Eur., Jou., of Med., Chem.*, 2014, **73**, 96.
- 87 H. Miyazaki, N. Nakamura, T. Ito, T. Sada, T. Oshima, and H. Koike, *Chem. Pharm. Bull.*, 1989, **37**, 2397.
- 88 M. Bednarski and S. Danishefsky, *J. Am. Chem. Soc.* 1986, **108**, 7067.

List of Publications

1. **Ishtiaq Jeelani***, Katsunori Itaya, and Hitoshi Abe, Total Synthesis of Hyalodendriol C, *Heterocycles*, 102, **2021**, DOI: 10.3987/COM-21-14480 (**Published 14th May 2021**)
2. Katsunori Itaya, **Ishtiaq Jeelani**, and Hitoshi Abe*, Total synthesis of Urolithin C 3-Glucuronide, *Heterocycles*, 103, DOI: 10.3987/COM-20-S(K)51. 8 (**Published 28th January 2021**)
3. Hitoshi Abe,* **Ishtiaq Jeelani**, Atsuro Yonoki, Haruka Imai, and Yoshikazu Horino, Synthesis of Chloro-substituted 6*H*-Dibenzo[*b,d*]pyran-6-one Natural Products, Graphislactone G, and Palmariols A and B, *Chem Pharm. Bull.* (**Accepted in Chemical and Pharmaceutical Bulletin on 30 April, Ref. No. MS21-00316R1**)
4. **Ishtiaq Jeelani*** Katsunori Itaya, and Hitoshi Abe, Total synthesis of biologically active natural products with 6*H*-Dibenzo[*b,d*]pyran-6-one using Palladium-catalyzed biaryl coupling reactions, *Abstract* ISBN: 978-93-90214-28-0, 8th World Conference on Pharmaceutical Science and Drug Manufacturing, 17-18 April, Bangkok, Thailand.